

PL-01

Analysis of the Heme Structural Factors to Control Oxygen Affinity of Myoglobin: Application to Design Myoglobin-Based Oxygen Carrier

Saburo NEYA

Department of Physical Chemistry, Graduate School of Pharmaceutical Sciences, Chiba University, Chuoh-Inohana, Chiba 260-8676

Artificial oxygen carrier is an important complement for the blood transfusion medicine. We have been exploring the myoglobin (Mb)-based O₂ carrier by perturbing the factors associated with heme prosthetic group. Our strategies to design the O₂ carrier were as follows:

1. Releasing the heme-globin contacts Since the heme in Mb is surrounded by many globin groups, weakening of the heme-globin contacts is expected to destabilize the heme conformation to affect the oxygen affinity. We found that small hemes dynamically rotate about the iron-histidine bond with a rate of ca. 1,000 s⁻¹ [1, 2]. However, O₂ affinities of the two Mbs bearing rotating and static hemes were almost the same. The results demonstrate that the loose heme-globin contacts in the heme pocket are not always essential for the O₂ binding.

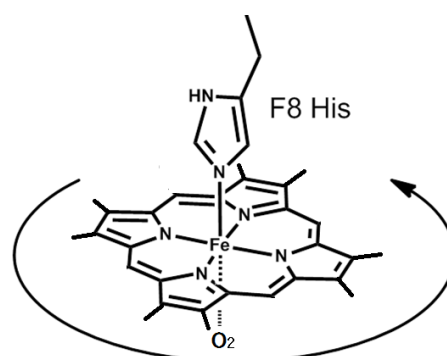


Fig. 1 Heme rotation in Mb heme pocket.

2. Heme shape modification Heme is a cyclic tetrapyrrole with a square molecular shape. When the square structure was altered to rectangular, trapezoid or irregular tetragon, the oxygen affinity of the reconstituted Mbs changed over more than 10⁶-fold. Especially, two corrrhycene-substituted Mbs with $P_{50} = 37$ and 7 mmHg showed O₂ delivery ability comparable that of red blood cell [2].

3. Cobalt substitution When the heme iron in Mb is replaced with cobalt, the resulting Mb exhibits a much lower affinity than native Mb. The oxygen delivery by protoheme Co(II)Mb with $P_{50} = 50$ mmHg was found to be 23% which is comparable with that of Hb. Owing to the disability to bind CO, Co(II)Mb has a merit not to remove the physiological concentration of CO, which serves as an *in-vivo* messenger, produced by heme oxygenase [3].

In conclusion, the oxygen affinity of Mb is readily controlled by the heme shape modification and the cobalt substitution. Several resulting Mbs exhibit good O₂ delivery capacity. These observations demonstrate the potential utility of Mb to create new artificial oxygen-carriers.

[1] *J. Biol. Chem.* **1987**, 262, 6725-6728; *J. Biol. Chem.* **1993**, 268, 8935-8942.

[2] *Molecules* **2013**, 18, 31680-3182.

[3] *Inorg. Chem.* **2013**, 52, 7387-7393; *Artificial Organs* **2014**, in press

For half a century, it has been known that cytochrome *c* (cyt *c*) forms polymers, but the polymerization mechanism remained unknown. We found that horse cyt *c* forms polymers by successive domain swapping, where the C-terminal helix is displaced from its original position in the monomer and Met-heme coordination is perturbed significantly.¹ In the crystal structures of dimeric and trimeric horse cyt *c*, the C-terminal helices were replaced by the corresponding domain of other cyt *c* molecules and Met80 was dissociated from the heme. Cyanide ion bound to the heme iron of dimeric horse cyt *c*.² The peroxidase activity of horse cyt *c* was enhanced by its dimerization, where its Compound III (oxy-form) and Compound I (oxoferryl porphyrin cation radical) species were detected in the reactions with hydrogen peroxide and *m*-chloroperbenzoic acid, respectively.³ We also found that domain-swapped oligomeric cyt *c* is produced during refolding from its guanidinium ion-induced unfolded state at high protein concentration and low temperature.⁴ Domain-swapped oligomeric cyt *c* interacted more strongly with anionic phospholipid-containing vesicles and the outer membrane of HeLa cells, compared to the monomer.⁵ Oligomeric cyt *c* induced a lateral phase separation of lipids in vesicles, leading to membrane disruption. Oligomeric cyt *c* also induced morphological changes in HeLa cells. However, the structural and thermodynamic properties of dimeric *Hydrogenobacter thermophilus* (HT) cytochrome *c*₅₅₂ (cyt *c*₅₅₂) were different from those of dimeric horse cyt *c*, although both proteins belong to the cyt *c* superfamily. Dimeric HT cyt *c*₅₅₂ exhibited a domain-swapped structure, where the N-terminal α -helix together with the heme was exchanged between protomers.⁶ Since a relatively strong H-bond network was formed at the loop around the heme-coordinating Met, the C-terminal α -helix did not dissociate from the rest of the protein in dimeric HT cyt *c*₅₅₂. We also found that myoglobin (Mb) forms a domain-swapped dimer with two extended α -helices.⁷ Each new long α -helix was formed by the E and F helices and the EF-loop of the original monomer, and as a result the proximal and distal histidines of the heme originated from different protomers. The changes in the structure and properties of cyt *c* and Mb by domain swapping will be discussed.

1. S. Hirota, Y. Hattori, S. Nagao, M. Takeda, H. Komori, H. Kamikubo, S. Wang, I. Takahashi, S. Negi, Y. Sugiura, M. Kataoka, and Y. Higuchi, *Proc. Natl. Acad. Sci. U.S.A.* **2010**, *107*, 12854.
2. A. D. Nugraheni, S. Nagao, S. Yanagisawa, T. Ogura, and S. Hirota, *J. Biol. Inorg. Chem.* **2013**, *18*, 383.
3. Z. Wang, T. Matsuo, S. Nagao, and S. Hirota, *Org. Biomol. Chem.* **2011**, *9*, 4766.
4. P. P. Parui, M. S. Deshpande, S. Nagao, H. Kamikubo, H. Komori, Y. Higuchi, M. Kataoka, and S. Hirota, *Biochemistry* **2013**, *52*, 8732.
5. S. Junedi, K. Yasuhara, S. Nagao, J. Kikuchi, and S. Hirota, *ChemBioChem* **2014**, *15*, 517.
6. Y. Hayashi, S. Nagao, H. Osuka, H. Komori, Y. Higuchi, and S. Hirota, *Biochemistry* **2012**, *51*, 8608.
7. S. Nagao, H. Osuka, T. Yamada, T. Uni, Y. Shomura, K. Imai, Y. Higuchi, and S. Hirota, *Dalton Trans.* **2012**, *41*, 11378.

PL-03

Production and Applications of Radioisotopes at RIKEN RI Beam Factory

Hiromitsu HABA

Nishina Center for Accelerator-Based Science, RIKEN, Wako, Saitama 351-0198, Japan

Due to its high sensitivity, the radioactive tracer technique has been successfully applied for investigations of the behavior of elements in the fields of chemistry, biology, medicine, engineering, and environmental sciences. We have been developing production technologies of radiotracers for application studies at RIKEN RI Beam Factory (RIBF) [1]. With 14-MeV proton, 24-MeV deuteron, and 50-MeV alpha beams from AVF cyclotron (AVF), we presently produce about 50 radiotracers from ^7Be to ^{211}At . Among them, ^{65}Zn , ^{109}Cd , and ^{88}Y are delivered to Japan Radioisotope Association for fee-based distribution to the general public in Japan. On the other hand, radionuclides of a large number of elements are simultaneously produced from metallic targets such as ^{nat}Ti , ^{nat}Ag , and ^{197}Au irradiated with a 135-MeV $\text{nucl.}^{-1} \text{ }^{14}\text{N}$ beam from RIKEN Ring Cyclotron [2]. These multitracers are also supplied to universities and institutes for collaborative researches.

Chemical characterization of newly-discovered superheavy elements (SHEs, atomic number $Z \geq 104$) is an extremely interesting and challenging subject in modern nuclear and radiochemistry. We have been developing a gas-jet transport system at the focal plane of the gas-filled recoil ion separator GARIS at RIKEN Linear ACcelerator (RILAC) to start up SHE chemistry at RIBF [3,4]. This system is a promising approach for exploring new frontiers in SHE chemistry: (i) the background radioactivities of unwanted reaction products are strongly suppressed, (ii) the intense beam is absent in the gas-jet chamber and hence high gas-jet efficiency is achieved, and (iii) the beam-free condition also allows for investigations of new chemical systems. Recently, the isotopes of element 104 (^{261}Rf), 105 (^{262}Db), and 106 (^{265}Sg) were successfully extracted to a chemistry laboratory, and their decay properties were investigated in detail with the rotating wheel apparatus for α/SF spectrometry (SF: Spontaneous Fission) [5,6]. Rapid single-atom chemistry apparatuses are under development in collaboration with nuclear chemists around the world, and soon chemical properties of new elements will be investigated [7].

Since the Fukushima Dai-ichi nuclear power plant accident in 2011, we have contributed to radioactivity measurements of soils, air dusts, foods, etc., and to developments of decontamination technologies and a low-cost radiation detector. In the symposium, the one-year monitoring of airborne radionuclides in Wako after the accident [8] will be also introduced.

References

- [1] H. Haba and S. Enomoto, *RIKEN Accel. Prog. Rep.* **2005**, 38, 105.
- [2] S. Enomoto and H. Haba, *Isotope News* **2008**, 12, 9 (in Japanese).
- [3] H. Haba *et al.*, *J. Nucl. Radiochem. Sci.* **2007**, 8, 55; **2008**, 9, 27.
- [4] H. Haba *et al.*, *Eur. Phys. J. D* **2007**, 45, 81.
- [5] H. Haba *et al.*, *Chem. Lett.* **2009**, 38, 426.
- [6] H. Haba *et al.*, *Phys. Rev. C* **2011**, 83, 034602; **2012**, 85, 024611; **2014**, 89, 024618.
- [7] H. Haba, *Isotope News* **2012**, No. 702, 2 (in Japanese).
- [8] H. Haba *et al.*, *Geochem. J.* **2012**, 46, 271.

O-01

Preparation and Characterization of Oxo-sulfido- and Oxo-selenido-molybdenum(VI) Complexes Possessing a Ene-1,2-dithiolate Ligand and Their Atom Transfer Reactivity

Hideki SUGIMOTO¹, Susumu TATEMOTO¹, Kazuo TOYOTA², and Shinobu ITOH¹

¹Department of Material and Life Science, Graduate School of Engineering, Osaka University, Suita 565-0879. ²Department of Chemistry, Graduate School of Science, Osaka City University, Osaka 558-8585

The active sites of the molybdenum hydroxylases are featured by mononuclear isostructural oxo-sulfido- or oxo-selenido-molybdenum(VI) centre ($\text{Mo}^{\text{VI}}\text{O}(\text{S})$ or $\text{Mo}^{\text{VI}}\text{O}(\text{Se})$) coordinated with a dithiolene (ene-1,2-dithiolate) unit.¹ Replacement of the sulfide and selenide groups with an oxo group ($\text{Mo}^{\text{VI}}\text{O}_2$) makes the enzymes inactive.¹ In the modelling studies of the molybdenum enzymes, however, isostructural $\text{Mo}^{\text{VI}}\text{O}_2$, $\text{Mo}^{\text{VI}}\text{O}(\text{S})$, and $\text{Mo}^{\text{VI}}\text{O}(\text{Se})$ model complexes having an identical molybdenum(VI)-dithiolene framework have yet to be reported.² Here, we succeed in preparation of a series of $[\text{Mo}^{\text{VI}}\text{O}_2\text{L}_2]^{2-}$ (**1^O**), $[\text{Mo}^{\text{VI}}\text{O}(\text{S})\text{L}_2]^{2-}$ (**1^S**), and $[\text{Mo}^{\text{VI}}\text{O}(\text{Se})\text{L}_2]^{2-}$ (**1^{Se}**, L = 1,2-dicarbomethoxyethylene-1,2-dithiolate). The spectroscopic properties and their atom transfer reactivity are described.³

The oxo-silylalcholato-molybdenum(VI) complex coordinated with L, $(\text{Et}_4\text{N})[\text{Mo}^{\text{VI}}\text{O}(\text{OSiBuPh}_2)\text{L}_2]$ (**2**), was converted to **1^O** in the presence of OH^- (Et_4NOH) in CH_3CN at room temperature. On the other hand, the treatments with SH^- (Et_4NSH) and SeH^- (Et_4NSeH) below $-20\text{ }^\circ\text{C}$ and $-60\text{ }^\circ\text{C}$, respectively, in a dry argon atmosphere resulted in the formations targeted complexes. The complexes were characterized by UV-vis, resonance Raman, and ESI-mass spectra, and elemental analysis. The crystal structure of **1^O** was also determined. The DFT calculations at (U)B3LYP level of theory showed the Mo=S bond length of 2.21 Å for **1^S** and the Mo=Se bond distance of 2.36 Å for **1^{Se}** and that the bond dissociation energy (kcal mol^{-1}) of $\text{Mo}^{\text{VI}}=\text{E}$ decreases as the E atom goes from O (88 kcal mol^{-1}) to S (47) and to Se (35). An atom transfer reaction from **1^{S/Se}** to triphenylphosphine was investigated to show that they gave $\text{Ph}_3\text{P}=\text{S}$ and $\text{Ph}_3\text{P}=\text{Se}$ in nearly quantitative yields at $-40\text{ }^\circ\text{C}$ and at $-80\text{ }^\circ\text{C}$, respectively. Kinetic study for the atom transfer reactions indicated that the selenium atom transfer is significantly faster than the sulfur atom transfer by ca. 10^4 times. On the other hand, oxygen atom transfer from **1^O** to Ph_3P hardly proceeded at room temperature.

1. R. Hille, J. Hall, P. Basu, *Chem. Rev.* **2014**, *114*, 3963.
2. H. Sugimoto, H. Tsukube, *Chem. Soc. Rev.* **2008**, *37*, 2609.
3. H. Sugimoto, S. Tatemoto, K. Toyota, K. Ashikari, M. Kubo, T. Ogura, S. Itoh, *Chem. Commun.* **2013**, *49*, 4358.

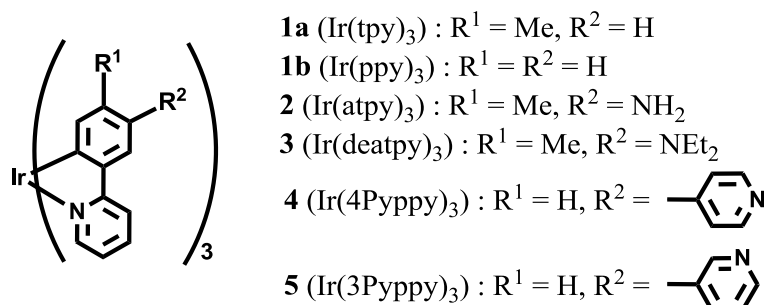
O-02

Photochemical Properties and Cell Death-Inducing Activity of Cyclometalated Iridium Complexes Having Basic Groups

Shin AOKI^{1,2}, Yosuke HISAMATSU^{1,2}, Akihiro NAKAGAWA¹, Aya KANDO¹, Masahiro KOHNO³

¹Faculty of Pharmaceutical Sciences, Tokyo University of Science, 2641 Yamazaki, Noda 278-8510. ²Center for Technologies against Cancer, Tokyo University of Science, Noda 278-8510. ³Graduate School of Bioscience and Biotechnology, Tokyo Institute of Technology, 4259 Nagatsuta-Cho, Midori-ku, Yokohama 226-8503.

Cyclometalated iridium (Ir) complexes are promising material candidates in the production of organic light-emitting diodes (OLEDs) and biological probes, due to their excellent luminescence properties.¹ Recently, we have found the regioselective halogenation, nitration, formylation, and acylation of Ir(tpy)₃ (**1a**) and Ir(ppy)₃ (**1b**) (tpy = 2-(4'-tolyl)pyridine and ppy = 2-phenylpyridine).² The tris(5'-amino) derivative of **1a**, Ir(atpy)₃ (**2**), exhibits a weak red colored emission at 600 nm and it changes to green upon protonation. Recently, tris(*N,N*-diethylamino) (**3**)³ and tris(pyridyl) Ir complexes (**4** and **5**)⁴ were synthesized from **1a** or **1b** as new luminescence pH sensors. Interestingly, **3** exhibits a weak red-colored emission at basic pH and strong green emission at acidic pH,³ while the emission of **4** and **5** exhibit green emission at basic pH and red emission upon protonation.⁴ Staining studies and photoinduced cell death of HeLa-S3 cells with **3~5** was also conducted.^{3,4} In this presentation, these results be reported.



Scheme 1. The structures of cyclometalated Ir complexes synthesized in this work.

1) (a) R. C. Evans, P. Douglas, C. J. Winscom, *Coord. Chem. Rev.* **2006**, 250, 2093. (b) L. Flamigni, A. Barbieri, C. Sabatini, B. Ventura, F. Barigelletti, *Top. Curr. Chem.* **2007**, 281, 143. (c) Y. You, W. Nam, *Chem. Soc. Rev.* **2012**, 41, 7061.

2) (a) S. Aoki, Y. Matsuo, S. Ogura, H. Ohwada, Y. Hisamatsu, S. Moromizato, M. Shiro, M. Kitamura, *Inorg. Chem.* **2011**, 50, 806. (b) Y. Hisamatsu, S. Aoki, *Eur. J. Inorg. Chem.* **2011**, 5360.

3) S. Moromizato, Y. Hisamatsu, T. Suzuki, Y. Matsuo, R. Abe, S. Aoki, *Inorg. Chem.* **2012**, 51, 12697.

4) A. Nakagawa, Y. Hisamatsu, S. Moromizato, M. Kohno, S. Aoki, *Inorg. Chem.* **2014**, 53, 409.

O-03

Synthesis and Chemical Properties of Heme Alcoholate Complexes and Mn Heme Thiolate Complex

Yoshinori SHIRAKAWA, Yuki NIWA, Nobuki KATO, Naoki UMEZAWA, Tsunehiko HIGUCHI

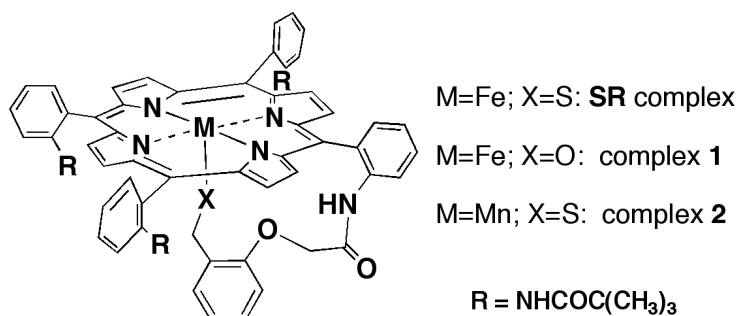
*Graduate School of Pharmaceutical Sciences, Nagoya City University,
Tanabe-dori, Mizuho-ku, Nagoya 467-8603, Japan*

Cytochrome P450 plays a central role in drug metabolism and steroid biosynthesis. Among heme enzymes, cytochrome P450 and NO synthase (NOS) have strong oxidizing ability and unusual structure, in that their heme iron has thiolate coordination. We previously succeeded in synthesizing the first synthetic heme thiolate (**SR** complex)¹ which retains thiolate coordination during catalytic oxidation and found several remarkable axial ligand effects on catalytic oxidation. However, alcoholate and selenolate ligand, which are belonged to chalcogen group same as thiolate, have not ever been examined for researching such relative effect of axial ligand by us and other investigators.

Now we prepared the first stable and isolable heme alcoholate **1** and manganese heme thiolate **2** in order to investigate the effect of elemental substitution on **SR** complex on spectroscopic and catalytic properties. We obtained UV-Vis spectra, FT-IR and EPR spectra of these complexes. The N-O stretching mode of complex **1-NO** was 60 cm⁻¹ higher than that of **SR-NO** and 38 cm⁻¹ lower than that of an alcohol-ligated heme². Complex **1** had 0.2 V higher E_{1/2} (Fe(II)/Fe(III)) than that of **SR** complex. Both two results indicate that electron donative ability of alcoholate is much less than that of thiolate. Catalytic activity of **1** was much lower than that of **SR** on the oxidation of 2,4,6-tri-*tert*-butyl-phenol with perphenylacetic acid.

Electronic absorption spectra of **2** (Mn^{III}) showed λ_{max} of Soret band at 434 nm which is much shorter than that of usual Mn porphyrin (e.g. Mn *meso*-tetraphenylporphyrin chloride (Mn(TPP)Cl): 470 nm).

Catalytic activity of complex **2** on the oxidation of 2,4,6-tri-*tert*-butylphenol with perphenylacetic acid was comparable to that of **SR**.



References

- (1) a) Higuchi, T.; Uzu, S.; Hirobe, M. *J. Am. Chem. Soc.* **1990**, *112*, 7051 – 7053; b) Higuchi, T.; Shimada, K.; Maruyama, N.; Hirobe, M. *J. Am. Chem. Soc.* **1993**, *115*, 7551 – 7552; c) Urano, Y.; Higuchi, T.; Hirobe, M.; Nagano, T. *J. Am. Chem. Soc.* **1997**, *119*, 12008 – 12009; d) Suzuki, N.; Higuchi, T.; Urano, Y.; Kikuchi, K.; Uekusa, H.; Ohashi, Y.; Uchida, T.; Kitagawa, T.; Nagano, T. *J. Am. Chem. Soc.* **1999**, *121*, 11571 – 11572; e) Ohno, T.; Suzuki, N.; Dokoh, T.; Urano, Y.; Kikuchi, K.; Hirobe, M.; Higuchi, T.; Nagano, T. *J. Inorg. Biochem.* **2000**, *82*, 123 – 125; f) Suzuki, N.; Higuchi, T.; Nagano, T. *J. Am. Chem. Soc.* **2002**, *124*, 9622 – 9628; g) Yamane, T.; Makino, K.; Umezawa, N.; Kato, N.; Higuchi, T. *Angew. Chem. Int. Ed.* **2008**, *47*, 6438-6440
- (2) Yi, G.-B.; Chen, L.; Khan, M. A.; Richter-Addo, G. B. *Inorg. Chem.* **1997**, *36*, 3876.

O-04

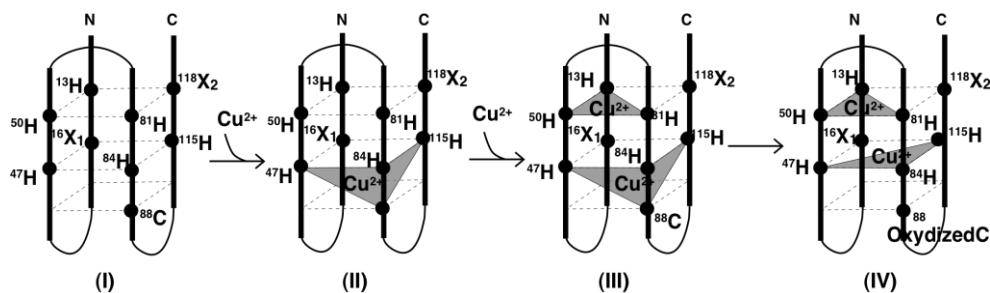
Creation of the Type 3 Copper Site in the 4-Helical Bundle Protein Using a Transient Cys-Cu²⁺ Linkage

Masato ANBE¹, Daigo SHIGA¹, Yu TAKANO², Haruki NAKAMURA², and Toshiki TANAKA¹

¹Department of Material Science, Nagoya Institute of Technology, Aichi 466-8555. ²Institute for Protein Research, Osaka University, Osaka 565-0871

A 30% of natural proteins contain metal ions that are responsible for their functions. Hence, metal ion binding designs in the proteins were recently vigorously increased using, in particular, α -helical bundle proteins. Only a few examples of the binuclear sites were so far reported. We have reported the design of type 1 blue copper protein, AM2C, using the four helical bundle protein. Then the design was further applied to create the purple copper protein, bi-AM2C, which include the two Cu²⁺ ions forming a Cu₂S₂ diamond cluster. The type 3 copper proteins, tyrosinase and hemocyanin, have two Cu²⁺ ions coordinated to three His residues bridged by two oxygens. During preparing the purple copper protein, we hit upon that the Cys residue could participate in determination of the binding position of the Cu²⁺ ion. Hence, we carried out to provide the two Cu²⁺ binding sites in vicinity using Cys-Cu²⁺ interaction as a transient linkage.

To analyze the role of the Cys residues, we created a mutant protein, which had His residues instead of the Cys residues in bi-AM2C. This protein was found to bind only one Cu²⁺ ion, implying the importance of the Cys residue for two Cu²⁺ bindings. Then, we made a strategy using a transient Cys-Cu²⁺ linkage for the two Cu²⁺ binding site in vicinity, as shown below. The protein, prepared by protein expression in *E. coli*, exhibited a typical α -helical structure. The metal bindings were analyzed by UV-vis and EPR spectra. Addition of one eq. of Cu²⁺ to the protein gave a yellowish color with maxima at 424 and 615 nm. EPR analysis gave a small A//. The both indicated the formation of the Cu²⁺-S(Cys) linkage. Addition of another one eq. of Cu²⁺ gave the similar UV-vis spectra with maxima at 422 and 600 nm, while EPR showed another new signals indicating the Cu²⁺-N(His) linkages. Following the auto-oxidation of the Cys residue after 6 hr, the solution disappeared the color with no UV-vis spectra above 400 nm, and gave only EPR signals showing the Cu²⁺-N(His) linkages. The ICP analysis of this complex gave 1.65 eq. of Cu²⁺ bound for one protein. The complex was oxidized by H₂O₂, however, it showed the similar EPR spectrum. The UV-vis spectrum had a shoulder around 300 nm. In conclusion, we succeeded in providing the two Cu²⁺ binding sites in vicinity, but the oxidation was hampered by the steric hindrance between the two Cu²⁺.



D. Shiga *et al.*, *J. Am. Chem. Soc.* **2010**, *132*, 18191.

D. Shiga *et al.*, *Biochemistry* **2012**, *51*, 7901.

O-05

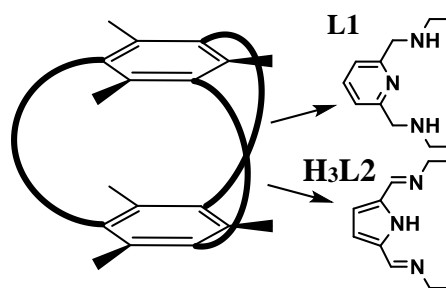
Syntheses of Model Compounds Mimicking Asymmetric Multi-metallic Active Sites in the Protein Cavities

Yasuhiro FUNAHASHI^{1,3}, Kojiro NAGATA¹, Yuya IWASAKI², Kosuke TANGE¹, Kensuke FUKUI², Tsubasa HATANAKA¹, Tomohiko INOMATA², Tomohiro OZAWA², and Hideki MASUDA²

¹Graduate School of Science, Osaka University, Toyonaka 560-0043.

²Graduate School of Engineering, Nagoya Institute of Technology, Nagoya 466-8555. ³PRESTO-JST

In the biological systems, the active site of metalloproteins frequently form asymmetric metal clusters having non-equivalent metal centers. Multicopper oxidases (**MCOs**), such as ascorbate oxidase, laccase, and ceruloplasmin, catalyze substrate oxidation coupled with reducing dioxygen to water. At the active site for dioxygen reduction, triangular copper centers are comprised of one type II copper center and one pair of type III copper centers¹. In photosystem II (**PSII**) of chloroplasts, the oxygen evolving complex (**OEC**) oxidizes water to dioxygen, driven by light energy. The **OEC** consists of a CaMn₄ cluster, the whole structure of which resembles a distorted chair, with the asymmetric CaMn₃O₄ cubane, formed in the protein environments². From these points of view, biomimetic model studies on these active metal sites of **MCOs** and **OEC**, require a new synthetic strategy of synthesizing asymmetric and heterometallic multinuclear core structures.



Cryptand type ligands.

Therefore, in order to construct a biomimetic tricopper system of **MCO**, we synthesized multicopper complexes with a mesitylene-capped cryptand, **L1** and **H₃L₂**, with bis(aminomethyl)pyridyl and bis(imino)pyrrolyl spacers, respectively. A series of tricopper complexes, [Cu₃(**L1**)(Cl)₃], [Cu₂Cu^{II}(**L1**)(Cl)₃]⁺, and [Cu₂Cu^{II}(**L1**)(Cl)₄(H₂O)]²⁺ were synthesized and structurally characterized by X-ray crystallographic analyses. The asymmetric tricopper core structures are constructed by assembling copper ions inside the cage cavity. Varied in the different oxidation states, the coordination structures are changed, however, three copper centers are maintained in the cavity without decomposition. The electrochemical behaviors reflected on reversible changes of the tricopper core and ligand-shell structures. Interestingly, the mixed valence tricopper(I/II) complex, [Cu₂Cu^{II}(**L1**)(Cl)₃]⁺ exhibited that the electron spin is localized on one planar 4-coordinate copper(II) center by strong correlation between the electronic state and coordination geometries in the ligand-shell environments of **L1**. In a fully oxidized tricopper(II) complex, [Cu^{II}₃(**L2**)(OH)₄]⁻, the electron spin is also localized on one copper(II) center, and the other two copper(II) centers form bis(μ-hydroxo) core with strong anti-ferromagnetic interaction. This magnetoructural properties are quite similar to those of triangular Type II and Type III copper(II) centers in **MCOs**.

Furthermore, we also succeeded in synthesizing a heterometallic sodium(I) trimanganese(II) complex, [Na^IMn^{II}₃(OH)₃(OEt)], containing a Mn₃Na cubane structure analogous to **OEC**. We concluded that the heterometallic core formed due to size-selective incorporation into **L2**.

1. E. I. Solomon, U. M. Sundaram, T. E. Machonkin, *Chem. Rev.*, **1996**, 96, 2563.
2. Y. Umena, K. Kawakami, J.-R. Shen, N. Kamiya, *Nature* **2011**, 473, 55.

O-06

Regulation of Axial/Rhombic Structure in Blue Copper Protein, Pseudoazurin Met16 Variants

Takahide YAMAGUCHI¹, Akiko TAKASHINA¹, Kana GUNJI¹, Sayaka ASAMURA¹, Junko YANO², Vittal K. YACHANDRA², Robert K. SZILAGYI³ and Takamitsu KOHZUMA¹

¹Graduate School of Science and Engineering, Ibaraki University, Ibaraki 310-8512. ²Lawrence Berkeley National Laboratory, Berkeley, CA 94720, USA. ³Department of Chemistry and Biochemistry, Montana State University, Bozeman, MT, USA.

Pseudoazurin (PAz) functions as an electron donor to nitrite reductase utilizing Type 1 copper site [1]. The spectroscopic and electrochemical properties of PAz are significantly affected by the mutation of Met16 located at the second coordination sphere of Type 1 copper site [2]. The EPR spectra demonstrated the population of “axial” and “rhombic” site are influenced by the interaction with mutated amino acid at Met16 position [3, 4].

The X-ray crystal structure of WT PAz demonstrated the copper atom occupies dual position at the active site. It is very interesting that the occupancy for each copper position were greatly consistent with the axial/rhombic components, which were estimated from EPR [3, 4]. The geometric and electronic structures of Type 1 copper sites in PAz Met16 variants were probed by multi-edge X-ray absorption spectroscopic (XAS) measurements. X-ray absorption near edge structure (XANES) at the Cu K-edge showed the higher Cu effective nuclear charge as indication of more localized electron on Cu²⁺ atom in the axial site. The extended X-ray absorption fine structure (EXAFS) was used to obtain Cu-ligand distances including Cu-S_{Met} (2.48 Å), Cu-S_{Cys} (2.16 Å), and average Cu-N_{His} (1.95 Å) for the pure rhombic site of Met16Val. The Cu-S_{Cys} bond is characterized by S K-edge XANES in WT, Met16Phe and Met16Val variants to have 38±8 %, 39±6 % and 30±10% S covalency, respectively.

In order to extend the experimental results beyond local structural information, a 89 atoms computational model was generated from the 1.35 Å resolution structure of WT PAz. DFT calculations were carried out using a systematic series of hybrid density functionals. The optimization of Cu-ligand distances with keeping the α - and β -C atoms positions fixed allowed for the understanding of the origins of experimental Cu-L distances from EXAFS and atomic spin densities from XANES using validated electronic structural methods [5]. Comparison of the WT and Met16Ile variant of PAz with the pure rhombic site [6] enabled us to expand the scope of our investigations toward the non-covalent outer sphere environment and generate realistic structural models for the axial and rhombic sites. Differences in these models generated an experimentally hypothesis regarding protein dynamics involving the 16th amino acid in regulating geometric and electronic structure of the Type 1 Cu site.

Reference

- [1]. Averill, B. A. *Chem. Rev.* **1996**, *96*, 2951-2964
- [2]. Kohzuma, T. *et al. J. Inorg Chem.* **2010**, *104*, 250-260
- [3]. Kohzuma, T. *et al. J. Biol. Inorg. Chem.* **2007**, *12*, 165-173
- [4]. Gast, P. *et al. J. Inorg. Biochem.* **2014**, *In Press*
- [5]. Szilagy, R. K and Solomon, E. I. *Curr. Opin. Chem. Biol.* **2002**, *6*, 250-258
- [6]. Kohzuma, T. *et al. unpublished result*

O-07

The Application of a Cytochrome P450 Complex Eluted from Encapsulated Biomaterials to the Catalysis of Enantioselective Oxidation (SanCat-S/-R)

Hiroyuki NAGAOKA

Sanyo Shokuhin Co., Ltd. R & D, 555-4 Asakura, Maebashi, Gunma 371-0811, Japan

A membrane-bound enzyme (ME: i.e., a Cytochrome P450 Complex) eluted from encapsulated pea protein (PP) under aeration is applicable for the kinetic resolutions of turnover: the each enantiomer of *rac*-1-(6-methoxy naphthalen-2-yl)ethanol (*rac*-1) can be selectively synthesized (>99% ee; ~50% chemical yield), utilizing two types of biomaterials: (1) A PEG (1000/4000 = 2/1)-aggregated ME (SanCat-S: synthesizing highly enantiopure *R*-(-)-1) and (2) a glutaraldehyde (GA)/a PEG (4000)-coated ME (SanCat-R: synthesizing *S*-(+)-1 (*S*-naproxen precursor)), which are placed on the market: WAKO Code No. 355-34211 (1g), 351-34213 (5g), respectively.¹⁾

Cytochrome P450 enzymes are found in all organisms, and compared with bacteria P450 and animal P450 (~20 and 60 different forms, respectively), plants make several forms because they synthesize unusual pigments and exotic toxins to protect themselves; It has been reported that an oxygen-driven cytochrome P450 enzyme (Cyt-P450, a HBP) that depends on oxygen instead of a redox cofactor as a detoxification system catalyzes hydroxylation, epoxidation, and dehalogenation, generating a reactive oxygen species via an iron electron-transfer system. Thus, the development of a new method for the purification and characterization of a new plant-P450 system may be enabled. Both reactions (SanCat-S -R) occur in the absence of an added cofactor (e.g., NAD(P)) in aqueous media. The specific activities of SanCat-S and SanCat-R were determined to be 0.8 ± 0.03 mU (Mean \pm SD)/(mg·min) and 0.6 ± 0.02 mU (Mean \pm SD)/(mg·min), respectively, and the species exact nature engaged in the key reaction was consistent with that of a heme binding protein (HBP) based on an N-terminal sequence comparison, which showed 93% similarity with a 20.853 kDa hemophore HasA gene product [*Pseudomonas fluorescens Pf-5*, a plant commensal bacterium]. The PP-HBP can be regenerated via successive asymmetric catalytic event using an incorporated iron electron-transfer system in the presence of oxygen—a process seemingly similar to that utilized by oxygen-driven cytochrome P450 enzyme (Cyt-P450: cysteine- $\text{Fe}^{2+} + \text{O}_2 \rightarrow \text{Fe}^{3+}-\text{O}-\text{O}- \rightarrow \text{Fe}^{4+} = \text{O}$ (oxidizing *rac*-1, -2) $\rightarrow \text{Fe}^{2+} + \text{H}_2\text{O}$). Compared with bacteria and animal, plants make several (a few hundred) forms; thus, the new plant-HBP system similar to a Cyt-P450 is enabled as a member of cytochrome P450 family.²⁻³⁾ The use of a raw biomaterial as a ME-catalytic system with an incorporated redox cofactor for asymmetric oxidation overcomes the apparent difficulties in working with pure dehydrogenase enzyme/redox cofactor systems for biotransformation.

References:

- 1) H. Nagaoka, K. Udagawa and K. Kirimura, *Biotechnol. Prog.* **2012**, 28, 953.
- 2) H. Nagaoka, *ACS Catal.* **2014**, 4, 553.
- 3) H. Nagaoka, *RSC Adv.* **2014**, 4 (31), 16333.

Tatsuya FUNAI¹, Junko NAKAMURA¹, Yuki MIYAZAKI¹, Risa KIRIU¹, Osamu NAKAGAWA¹, Shun-ichi WADA¹, Akira ONO², and Hidehito URATA¹

¹Osaka University of Pharmaceutical Sciences, Osaka 569-1094. ²Faculty of Engineering, Kanagawa University, Yokohama 221-8686.

Metal ions, such as Hg^{II} and Ag^I ions, were found to coordinate to mismatched base pairs. The metal ion coordination significantly raises the melting temperatures (T_m values) of duplex DNAs containing thymine-thymine (T-T) and cytosine-cytosine (C-C) base pair mismatches. The stabilization of the duplex DNAs was due to the formation of metal-mediated base pairs, such as T-Hg^{II}-T and C-Ag^I-C base pairs.^{1,2}

We focused on the biological relevance of metal-mediated base pairs, which are comprised of non-hydrogen-bonding metal-chelating bonds. We tested the metal-mediated base pairs as a substrate for DNA polymerases and discovered that in the presence of Hg^{II} ions, the Klenow fragment (KF) incorporates dTTP into the site opposite thymine in a template strand and make a phosphodiester bond to elongate the primer strand.³ In the presence of Ag^I ions, however, KF incorporated dATP not dCTP into the site opposite cytosine in a template strand.⁴ This result is quite unexpected because Ag^I ions are known to specifically stabilize duplexes containing a C-C mismatched base pair.²

Furthermore, we extensively investigated the Ag^I-mediated primer extension reaction by using 3'→5' exonuclease activity-deficient KF (KF exo-). The enzyme incorporates dTTP as well as dATP into the site opposite cytosine in templates depending on the upstream sequence of the incorporation site. However, the enzyme did not incorporate dCTP into the same site at all under the same conditions. The use of large amounts of the enzyme and a higher concentration of dCTP allowed the incorporation of dCTP into the site opposite cytosine in some templates depending on the upstream sequence of the incorporation site. Thus, the comparative susceptibility of dNTPs to the reaction was shown to be dATP > dTTP ≫ dCTP.⁵

The stability of the metal-mediated base pairs is not always important for recognition by DNA polymerases, and the shapes and/or net charges of the metal-mediated base pairs may be important in replication reaction by DNA polymerases.

References

1. Y. Miyake, *et al.*, *J. Am. Chem. Soc.*, **2006**, 128, 2172.
2. A. Ono, *et al.*, *Chem. Commun.*, **2008**, 4825.
3. H. Urata, *et al.*, *Angew. Chem. Int. Ed.*, **2010**, 49, 6516.
4. T. Funai, *et al.*, *Angew. Chem. Int. Ed.*, **2012**, 51, 6464.
5. T. Funai, *et al.*, *Angew. Chem. Int. Ed.*, in press.

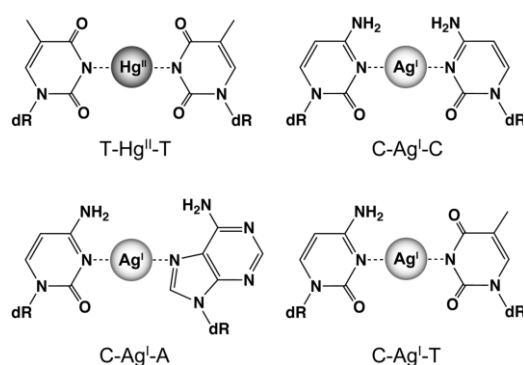


Fig. 1 Structures of metal-mediated base pairs.

Development of the *Myo*-Inositol-Hexakisphosphate Metal Complexes for Elimination of Radionuclides from the Body

Kazuma OGAWA, Sumi KADONO, Tadahisa FUKUDA, Tatsuto KIWADA, and Akira ODANI

Graduate School of Medical Sciences, Kanazawa University, Kanazawa 920-1192.

The radioactive nuclides have leaked into the surrounding environment from the Fukushima Daiichi Nuclear Power Plant resulting from the Great East Japan Earthquake on 11 March 2011. In these radionuclides, ^{137}Cs ($T_{1/2} = 30.1$ y) and ^{90}Sr ($T_{1/2} = 29.1$ y), which are water-soluble radionuclides and have long half-life, contaminated aquatic ecosystems and food products. Moreover, as ^{137}Cs and ^{90}Sr are concentrated in muscle and bone, respectively, ^{137}Cs and ^{90}Sr could be considered harmful to human.

Myo-inositol-hexakisphosphate (IP6) (Fig. 1), which is a compound contained in grain, beans, and oil seeds, has a great ability for complexation with metals. IP6 forms insoluble complexes with La and Zn. We supposed that La-IP6 and Zn-IP6 promote elimination of ^{137}Cs and ^{90}Sr from body by adsorption of La-IP6 and Zn-IP6 with ^{137}Cs and ^{90}Sr in the gastrointestinal tract, and evaluated adsorptive capacity of La-IP6 and Zn-IP6 to ^{137}Cs and ^{90}Sr *in vitro* and *in vivo*. In this study, ^{85}Sr was used instead of ^{90}Sr as ^{85}Sr emits gamma ray.

To evaluate stability of La-IP6 and Zn-IP6 complexes, La-IP6 solution and Zn-IP6 solution (pH 1.2) were incubated for 6 hours. After incubation, 94.0% of La-IP6 and 85.8% of Zn-IP6 were intact, respectively. In *in vitro* binding assay of La-IP6 and Zn-IP6 complexes to ^{137}Cs and ^{85}Sr , La-IP6 and Zn-IP6 adsorbed ^{137}Cs and ^{85}Sr . The adsorption capacity Zn-IP6 to ^{137}Cs and ^{85}Sr is greater than that of La-IP6.

To evaluate usefulness of Zn-IP6 *in vivo*, Zn-IP6 was administrated to mice after intravenous injection of ^{137}Cs . However, the biodistribution of ^{137}Cs was almost same between Zn-IP6 treated group and non-treated control group. When ^{85}Sr was orally administrated to mice with pretreatment of Zn-IP6, ^{85}Sr showed lower accumulation in the femur and blood compared to non-treated control group. Consequently, this result suggested the pretreatment of Zn-IP6 suppressed the absorption of ^{85}Sr from the gastrointestinal tract.

In conclusion, the pretreatment of Zn-IP6 could decrease absorbed radiation dose after ^{90}Sr intake.

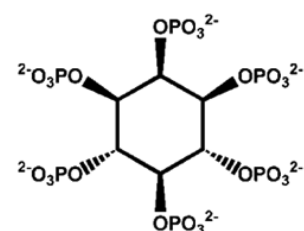


Fig. 1. Structure of *myo*-inositol-hexakisphosphate (IP6)

O-10

The Linkage Structure between D-Penicillamine and RGD Peptide (Pen-X-RGD) Significantly Affects Formation and Biodistribution of ^{99m}Tc -labeled bis(Pen-X-RGD) Complexes

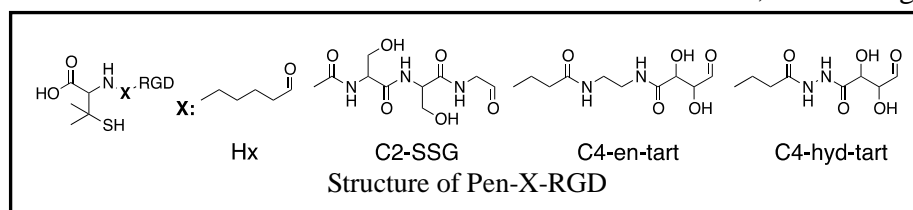
Tomoya UEHARA, Hiroyuki TATEISHI, Yoshihito HAYASHI, Hirofumi HANAOKA, and Yasushi ARANO

Department of Molecular Imaging and Radiotherapy, Graduate School of Pharmaceutical Sciences, Chiba University, Chiba 260-8675

Technetium-99m (^{99m}Tc) is an ideal radionuclide for diagnostic nuclear medicine and molecular imaging, due to an emission of a gamma ray suitable to external imaging (140 keV) with a half life of 6 h and its availability from $^{99}\text{Mo}/^{99m}\text{Tc}$ generator. ^{99m}Tc -labeled compounds are usually prepared by reacting ^{99m}Tc with a large excess of ligand to ensure high radiochemical yields under sterile conditions in short reaction time, and are administered to subjects without purification. The presence of a large amount of unlabeled ligand, however, impairs target accumulation of the ^{99m}Tc -labeled compounds by competing for a target molecule. To overcome the dilemma, we have developed a way to prepare divalent ^{99m}Tc -labeled compounds by reacting ^{99m}Tc with monovalent ligands (D-penicillamine-conjugated RGD peptide via hexanoic acid) that form ^{99m}Tc complexes at the ^{99m}Tc to ligand ratio of 1:2 ($^{99m}\text{Tc}(\text{Pen-Hx-RGD})_2$). $^{99m}\text{Tc}(\text{Pen-Hx-RGD})_2$ provided clear SPECT images of tumors in the presence of excess ligand. However, non-specific accumulations were also observed in the liver and intestine.

In this study, to reduce hepatobiliary excretion of the ^{99m}Tc -labeled compound, the linkage structure of Pen-Hx-RGD was changed from Hx to methyamide-Ser-Ser-Gly (C2-SSG), butylamido-ethyl-amido-tartarate (C4-en-tart) or butyl-hydrazido tart (C4-hyd-tart) to prepare Pen-C2-SSG-RGD, Pen-C4-en-tart-RGD or Pen-C4-hyd-tart-RGD (Figure). ^{99m}Tc complexation reaction and biodistribution of $^{99m}\text{Tc}(\text{Pen-X-RGD})_2$ (X = C2-SSG, C4-en-tart and C4-hyd-tart) were compared.

All the three new ^{99m}Tc -labeled compounds possessed lipophilicity significantly lower than that of $^{99m}\text{Tc}(\text{Pen-Hx-RGD})_2$. When injected into mice, all the three ^{99m}Tc labeled compounds also exhibited lower accumulation in the liver and intestine compared with $^{99m}\text{Tc}(\text{Pen-Hx-RGD})_2$. However, significant differences were observed in the ^{99m}Tc complexation reactions. Both Pen-C2-SSG-RGD and Pen-C4-en-tart-RGD generated ^{99m}Tc -complexes of ^{99m}Tc to ligand ratios of 1:1 (5- or 7-membered ring structure) at ligand concentration lower than 10^{-4} M. $^{99m}\text{Tc}(\text{Pen-C4-hyd-tart-RGD})_2$, on the other hand, was obtained with radiochemical yield over 95% at ligand concentration of 10^{-4} M. These results indicated that the interposition of linkages with high hydrophilicity facilitated renal excretion of the resulting ^{99m}Tc -labeled bis(Pen-X-RGD) $_2$ complexes. In addition, the presence of nitrogen atoms or hydroxyl groups in the linkage impaired the formation of ^{99m}Tc -labeled bis(Pen-X-RGD), due to the formation of intramolecular coordination. Thus, the linkage structure should be designed to satisfy the two criteria.



O-11

Role of Carnosine in the Neurodegenerative Processes Induced by Zinc

Dai MIZUNO, Ayumi SUGA, and Masahiro KAWAHARA

Department of Bio-Analytical Chemistry, Musashino University, Tokyo 202-8585.

Zinc (Zn) is abundantly present in the brain and has important roles in the processes of memory formation. However, excess Zn secreted after transient global ischemia is toxic and central to the pathogenesis of vascular type of dementia. We have investigated the molecular mechanism of Zn-induced neurotoxicity using GT1-7 cells (immortalized hypothalamic neurons), which are more susceptible to Zn compared to other neuronal cells. The exposure to Zn induced the elevation of intracellular Ca^{2+} levels. The Ca^{2+} channel blockers attenuated Zn-induced neuronal death. Our analysis using the DNA microarray revealed that expressions of several genes, such as metal-related genes (metallothionein, zinc transporter 1 (ZnT-1)), endoplasmic reticulum (ER)-stress related genes (GADD34, GADD45, p8), calcium-related genes (activity-related cytoskeleton protein (Arc)) were increased after Zn exposure. We also developed a rapid and convenient screening system for compounds which protect neurons from Zn neurotoxicity, and searched such compounds among various fishes or agricultural products. Among tested, we found carnosine (β -alanyl histidine) in the eel muscle attenuated Zn-induced neuronal death. Carnosine is an endogenous dipeptide abundantly present in the muscles and in the olfactory bulb in the brain. It reportedly has various beneficial characteristics such as anti-oxidant activity, anti-crosslinking activity, anti-fatigue activity, *etc.* Carnosine also has the ability to chelate Zn and other metals. However, our analysis using RT-PCR revealed that carnosine did not inhibit Zn-induced upregulation of metallothionein or ZnT-1. Thus, it is possible that the chelating ability of carnosine did not influence the Zn influx into the cells. Meanwhile, the existence of carnosine significantly inhibited Zn-induced expressions of ER-stress related genes such as GADD34 or GADD45. Increasing evidence suggests that ER stress, the unfolded protein response, is implicated in the pathogenesis of various neurodegenerative diseases including Alzheimer's disease, Parkinson's disease, prion diseases, and ischemia. Considering that dantrolene, which prevents ER stress by inhibiting Ca^{2+} release from ER, attenuated Zn-induced neurotoxicity, it is possible that the pathway related to ER stress may be implicated in Zn-induced neurotoxicity and in the pathogenesis of vascular type of dementia. Furthermore, we have demonstrated that carnosine did not influence toxicity induced by other metals such as Cd^{2+} , but attenuated the death of GT1-7 cells caused by thapsigargin or tunicamycin, both are inducers of ER stress. We and other researchers reported that carnosine inhibits the neuronal death induced by prion protein fragment and attenuates the accumulation of Alzheimer's β -amyloid protein. Therefore, it is possible that carnosine not only attenuates Zn-induced neuronal death but protects from other neurodegenerative by inhibiting some pathways related to ER stress.

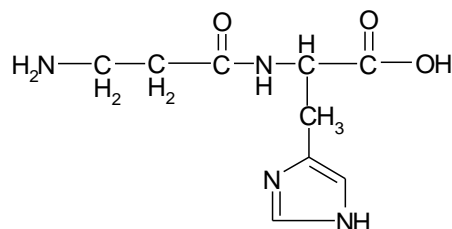


Fig. 1 Structure of carnosine

Zn²⁺ Signaling in Dentate Granule Cells Is Necessary for LTP Maintenance and Memory Recall

Atsushi TAKEDA, Tatsuya MINAMINO, Hiroaki FUJII, Masatoshi NAKAMURA, Shunsuke TAKADA, and Haruna TAMANO

Department of Neurophysiology, School of Pharmaceutical Sciences, University of Shizuoka, 52-1 Yada, Suruga-ku, Shizuoka 422-8526

Brain zinc homeostasis is strictly controlled under healthy condition, indicating the importance of zinc homeostasis in physiological function in the brain. Zinc is relatively concentrated in the hippocampus. The hippocampus is required for memory for a limited period of time after learning. Learning and memory have been closely linked to strengthening of synaptic connections between neurons, i.e., synaptic plasticity, within the dentate gyrus–CA3–CA1 trisynaptic circuit of the hippocampus. The trisynaptic circuit, i.e., perforant pathway–dentate granule cells, mossy fiber–CA3 pyramidal cells, Schaffer collateral–CA1 pyramidal cells, is glutamatergic. A subclass of glutamatergic neurons is stained by Timm's sulfide-silver method, which predominantly stains zinc in the presynaptic vesicles. Vesicular zinc plays a role for synaptic Zn²⁺ signaling and may be involved in learning and memory. We have reported the real-time relationship between in vivo dentate gyrus LTP and recognition memory by focusing on the loss and/or blockade of Zn²⁺ signaling with zinc chelators in the dentate gyrus; intracellular Zn²⁺ signaling in the dentate gyrus is required for object recognition memory, probably via dentate gyrus LTP expression. In the present study, the real-time relationship between the extinction of maintained LTP and the extinction of recognition memory was examined focusing on the loss of Zn²⁺ signaling with zinc chelators in the dentate gyrus. Maintained dentate gyrus LTP was erased by the transient loss of Zn²⁺ signaling in the dentate gyrus. The irreversible erasure was rescued not only by amelioration of the loss of Zn²⁺ signaling, but also by pretreatment with Jasplakinolide, a stabilizer of F-actin. It is likely that synaptic Zn²⁺ is involved in the formation of F-actin and is required for LTP maintenance in the dentate gyrus. Simultaneously, acquired space recognition memory was affected by the loss of Zn²⁺ signaling, but not by pretreatment with Jasplakinolide prior to the loss of Zn²⁺ signaling. The present study indicates that the extinction of acquired memory coincides with the extinction of maintained LTP under the transient loss of Zn²⁺ signaling in the dentate gyrus. It is likely that dentate gyrus LTP maintenance is real-timely linked to the retention of space recognition memory.

O-13

Development of Low- Molecular- Weight Fluorescent Zn²⁺ Probe Based on 2,2'-Bipyridine

Masayori HAGIMORI¹, Naoko MIZUYAMA², Yoshinori TOMINAGA³, Hideo SAJI⁴, and Takahiro MUKAI¹

¹Department of Biophysical Chemistry, Kobe Pharmaceutical University, Kobe 658-8558. ²Department of Clinical Trial Management, Foundation for Biomedical Research and Innovation, Kobe 650-0047. ³Department of Environmental Materials Chemistry, Nagasaki University, Nagasaki 852-8521. ⁴Department of Patho-Functional Bioanalysis, Kyoto University, Kyoto 606-8501

Zinc plays an important role in many biochemical processes, including gene expression, apoptosis, enzyme regulation, immune responses, and neurotransmission. Zn²⁺ is present in living cells over a wide range of concentrations varying from nanomolar to millimolar. Living systems contain two forms of Zn²⁺. The first form is tightly chelated with proteins, also known as metalloproteins. The other is the free or chelatable form. Although most of the Zn²⁺ exists in the chelated form, the latter form is also believed to play an important role in biological systems. It is known that free or chelatable Zn²⁺ is released in response to cellular signaling. In the mammalian central nervous system, free or chelatable Zn²⁺ ions are colocalized with glutamate in the presynaptic vesicles of the hippocampus. Although a large amount of work has contributed to the understanding of the roles played by Zn²⁺ in physiology, particularly in the field of neurochemistry, the role of free or chelatable Zn²⁺ in human health and diseases remains largely unexplored.

Fluorescent probes have attracted attention as optical materials for biosensing because of their high sensitivity. A variety of fluorescent Zn²⁺ probes based on quinoline, BF₂-chelated dipyrromethene, fluorescein, etc. have been developed, and they can provide useful information about zinc biology. However, most of the fluorescent probes presented so far possess a fluorescent core and a separate moiety for binding to Zn²⁺ within the molecule; therefore, the molecular weight is usually large and the molecules are hydrophobic. As a result, applications of such molecules in biological systems often face difficulties because of their low solubility in aqueous media. In a previous study, we reported the water-soluble and small-molecular-weight fluorescent Zn²⁺ probes based on pyridine-pyridone.¹ This core structure acts as the chelating functionality for Zn²⁺, as well as the fluorescent part within this single molecule. Moreover, we revealed that small modifications of pyridine-pyridone brought about a marked improvement in properties such as the affinity toward Zn²⁺ and aqueous solubility.² Herein, we developed low-molecular-weight fluorescent probes based on 2,2'-bipyridine for visualizing Zn²⁺ in living cells. New probes incorporating pyridylalkylamine showed high affinity toward Zn²⁺ and aqueous solubility. In addition, fluorescence microscopy imaging showed that these probes could be used for detecting Zn²⁺ in living cells.

1. M. Hagimori, N. Mizuyama, Y. Yamaguchi, H. Saji, and Y. Tominaga, *Talanta* **2011**, *83*, 1730.

2. M. Hagimori, T. Uto, N. Mizuyama, T. Temma, Y. Yamaguchi, Y. Tominaga, and H. Saji, *Sens. Act. B.* **2013**, *181*, 823.

O-14

Increase in Intracellular Copper Concentration and Changes in Expression of Copper-Regulating Genes During Differentiation of PC12 Cells into Neurons

Maki TOKUMOTO¹, Aya TEJIMA¹, Naohiro HATAKEYAMA¹, Siyuan WU², Tsutomu ISHIKAWA², Noriyuki SUZUKI², Yasumi ANAN¹, and Yasumitsu OGRA¹

¹Laboratory of Chemical Toxicology and Environmental Health, Showa Pharmaceutical University, Machida, Tokyo 194-8543. ²Graduate School of Pharmaceutical Sciences, Chiba University, Chuo, Chiba 260-8675

Some neurodegenerative diseases such as Alzheimer's disease, amyotrophic lateral sclerosis and prion diseases, are a result of the disturbance of copper (Cu) homeostasis, although it remains unclear whether the disturbance of Cu homeostasis has aberrant effects on neurons. In this study, we investigated Cu metabolism specifically in neurons in terms of changes in the intracellular Cu concentration and the expression of Cu-regulating genes, such as Cu transporters and metallothioneins (MTs), before and after the differentiation of rat pheochromocytoma cells (PC12 cells) into neurons. Naive PC12 cells generated neurites after treatment with 50 ng/mL nerve growth factor (NGF) for six days. In addition to this morphological change, the expression of NeuN protein, a neuron biomarker, was observed in the NGF-treated cells. Hence, the naive PC12 cells were able to differentiate under the conditions we adopted. After the differentiation, Cu and Zn imaging with fluorescent probes revealed an increase in intracellular Cu concentration. The concentrations of other essential metals such as iron and manganese, which were determined by an inductively coupled plasma mass spectrometer (ICP-MS), were not altered. The mRNA expression of the Cu influx transporter, Ctr1, was decreased after the differentiation, and the differentiated cells acquired tolerance to Cu and cisplatin, another substrate of Ctr1. In addition, the expression of MT-3, a brain-specific isoform, was increased, contrary to the decreased expression of MT-1 and MT-2. These results suggested that the differentiation of PC12 cells into neurons induced MT-3 expression, thereby resulting in intracellular Cu accumulation. The decrease in Ctr1 expression was assumed to be a response aimed at abolishing the physiological accumulation of Cu after the differentiation.

O-15

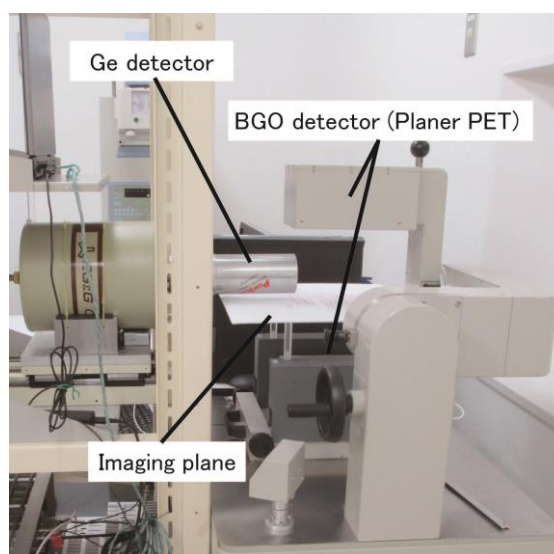
Multiple Probe Positron Emission Tomography Applied for Biometal Imaging

Tomonori FUKUCHI¹, Takahisa HANADA², Hiromitsu HABA³,
Yasuyoshi WATANABE¹, and Shuichi ENOMOTO^{1,2}

¹RIKEN Center for Life Science Technologies, Kobe 650-0047.

²Graduate School of Medicine, Dentistry and Pharmaceutical Sciences, Okayama University, Okayama 700-8530. ³RIKEN Nishina Center for Accelerator-Based Science, Wako 351-0198.

Positron Emission Tomography (PET) represents today essential role in nuclear medicine, due to its ability to provide quantitative bio-distribution of a molecular probe. Using metal radionuclide as imaging probe, PET is also useful for research of biometal dynamics. However, PET works only for single probe, because positron-electron annihilation results in two 511-keV photons irrespective of radionuclides. In order to overcome this limitation, we have been developing Polychrome-PET (P-PET) for multiple molecular simultaneous imaging. The P-PET identifies different probes by detection of the de-excitation γ -ray emitted after the positron. Candidate metal radionuclides for the P-PET are the following: ^{22}Na , ^{48}V , ^{52}Mn , ^{60}Cu , etc. For the P-PET, we expect various new applications not only medical use but also biometal research, such as analysis of the time sequence of multiple biometal, analysis of additional dosage of the same biometal, correlation between drug and biometal, etc. For a feasibility study of the P-PET, we have been performing computer simulations and experimental studies. In the simulations, a Monte Carlo based simulator Gate (Geant4 Application for Tomographic Emission) [1] was used. A PET system with additional 32 germanium semiconductor γ -ray detectors (Ge detector), which provide about 10% of γ -ray detection efficiency, gives practical images of multiple probes. For experimental study, we have been developed a planer type PET system [2] integrated with a Ge detector as shown in Figure. Using this prototype system, we successfully produce multiple probe images. In this report, we discuss specific applications of biometal dynamics by means of multiple probe images obtained by the P-PET.



Prototype P-PET system

- [1] D. Strul *et al.*, "GATE (Geant4 Application for Tomographic Emission): a PET/SPECT general-purpose simulation platform", Nucl. Phys. B (Proc. Suppl.) 125 (2003) 75-79.
[2] H. Uchida *et al.*, "A compact planar positron imaging system", Nucl. Inst. and Meth. A 516 (2004) 564-574.

O-16

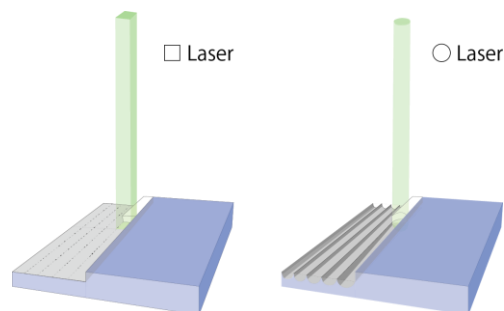
Multi-Range Imaging Mass Spectrometry Using Laser Ablation-ICP-Mass Spectrometry

Takafumi HIRATA, Kentaro HATTORI, Seiya OHARA

Laboratry for Planetary Sciences, Kyoto University, Kitashirakawa Oiwakecho, Kyoto 606-8502, Japan

Plasma ion source mass spectrometer coupled with the laser ablation sample introduction technique (LA-ICPMS) has now become the most sensitive and user-friendly analytical tool to derive elemental and isotopic distribution among the different phases or minerals. Moreover, in the LA-ICPMS technique, atomization and ionization of the analytes were independently carried out from the sampling (i.e., post ionization technique), and therefore, the sampling and ionization conditions could be separately optimized. The post ionization technique results in the smaller contribution of the matrix effect, which could be the major source of analytical error. Furthermore, for the LA-ICPMS technique, sample was located under the atmospheric pressure sample cell, and laser induced sample aerosols were carried into the ICP ion source using a He carrier gas. This suggests that no evacuation of the sample housing is required, and therefore, biological cell or tissue samples (i.e., wet samples) can be directly subsidized to elemental imaging analysis, obviating the drying or freezing procedure for the analysis. The LA-ICPMS technique has further advantages of imaging analysis for samples with various sizes, ranging from 10 microns to >10 mm. Because of high capability for quantitative imaging of ultratrace-elements, together with high analytical capability to measure large-sized samples, the LA-ICPMS technique has blossomed to become the key analytical technique for the imaging analysis of trace-elements and isotopes. This is very important to obtain elemental and isotopic images for not only biological samples, but also various rock or minerals.

We have developed new calibration technique for the elemental imaging for trace-elements in biochemical samples using a soft laser ablation-inductively coupled plasma-mass spectrometry (SLA-ICPMS) technique. With finely controlled laser fluence, only the spliced biochemical samples (1 μ m thickness) were preferentially and totally ablated, whereas no laser ablation could be made for the glass substrate. This can minimize the changes in the resulting sampling volume (depth), possibly caused by the heterogeneity in matrix composition, hardness or color of the sample. Under the preferential and total ablation conditions, volume of the sample ablated can be well defined, and therefore, concentrations of the analytes could be calibrated based on the signal intensity data and the volume of the sample and standard. Combination of the LA-ICPMS technique and the preferential and total ablation achieved by the soft ablation protocol can become a powerful method for studying the metabolism of the trace-elements. In this study, we have developed new laser ablation technique for the imaging of the trace-elements in various solid samples. Details of the analytical procedure and capabilities will be described in this presentation.



DNA Interaction, Photocleavage, and Cytotoxicity of Heterodinuclear Ruthenium(II)–Platinum(II) Complexes as Photochemotherapeutic Agents

Takakazu YANO, Misaki NAKAI, Yasuo NAKABAYASHI

Department of Chemistry and Materials Engineering, Kansai University,
3-3-35 Yamate-cho, Suita, Osaka 546-8680

Cisplatin (*cis*-[PtCl₂(NH₃)₂]) has been one of the leading anticancer drug for near 30 years. However, cisplatin has several drawbacks such as toxicity and drug resistance. Ru(II)-polypyridine complexes were proposed as potential antitumor substances with non-covalent interactions and available for photodynamic therapy (PDT). In this study, we have synthesized heterodinuclear Ru(II)-Pt(II) (**1** – **6**) and mononuclear Ru(II) (**7** and **8**) complexes, and evaluated DNA photocleavage ability. The interactions of these complexes with DNA have been investigated by spectroscopic (UV-vis, fluorescence, ESR) and agarose gel electrophoretic methods. In addition, the cytotoxicity of **1** – **8** was also determined using the MTT assay in Hela cell lines. All the complexes can photocleave pBR322 DNA with visible light radiation (xenon lamp, 300 W) through both ·OH and ¹O₂ (**1** – **6**) and ¹O₂ (**7**, **8**) generation mechanisms [1]. The DNA photocleavage ability of **1** – **6** is higher than that of **7** and **8**. Furthermore, in the series of **1** – **6** DNA photocleavage ability of **1** – **3** (R = H) is higher than that of **4** – **6** (R = *tert*-Bu). **1** and **4** (X = Cl⁻) can bind covalently to DNA through the dissociation of Cl⁻ in low Cl⁻ concentration (0 – 15 mM). On the other hand, **2**, **3**, **5** and **6** interact with DNA by non-covalent mode. **1** – **6** exhibit higher cytotoxicity compared to **7** and **8**. Moreover, **4** – **6** are found to be more cytotoxic than **1** – **3**, that is, **4** – **6** may be expected to be applied to antitumor drugs that reduce the drawbacks and increase their effects.

Reference

1. F. Gao, H. Chao, F. Zhou, X. Chen, Y.-F. Wei, L.-N. Ji, *J. Inorg. Biochem.*, **2008**, *102*, 1050-1059.

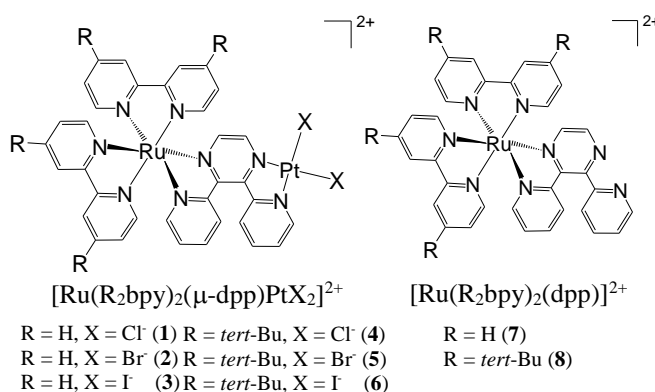


Fig. 1. Structures of heterodinuclear Ru(II)-Pt(II) and mononuclear Ru(II) complexes in this study.

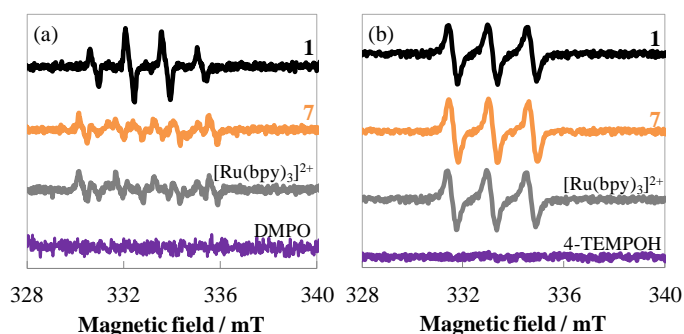


Fig. 2. ESR spectra of DMPO (a) in 5 mM Tris-HCl / 50 mM NaCl (pH 7.5) and 4-TEMPOH (b) in DMF in the absence or presence of **1**, **7** and [Ru(bpy)₃]²⁺ irradiated 300 W xenon lamp for 1 h.

DMPO : 5, 5-dimethyl-1-pyrroline N-oxide

4-TEMPOH : 2, 2, 6, 6-tetramethyl-4-piperidinol

P-02

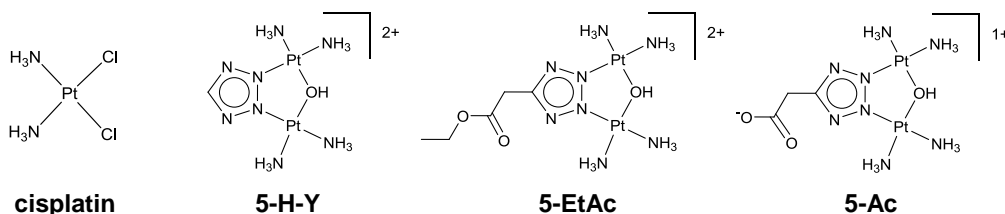
Structure-Activity Relationship Study, DNA Binding Ability, and Cellular Uptake of Anticancer Tetrazolato-Bridged Dinuclear Platinum(II) Complexes

Masako UEMURA¹, Miyuu HOSHIYAMA¹, Ayako FURUKAWA¹, Yoshihiro HIGUCHI¹, and Seiji KOMEDA¹

¹Faculty of Pharmaceutical Sciences, Suzuka University of Medical Sciences, Mie 513-8670.

The series of tetrazolato-bridged dinuclear platinum(II) complexes (tetrazolato-bridged complexes) [$\{cis\text{-Pt}(\text{NH}_3)_2\}_2(\mu\text{-OH})(\mu\text{-5-R-tetrazolato-N2,N3})\}^{n+}$], is known to circumvent cross-resistance to cisplatin and to be one of the most promising next-generation drug candidates for the treatment of cancers that are difficult to cure. We reported that **5-H-Y** (R = H, n = 2), the most effective derivative, provides both coordinative and non-coordinative interactions with DNA, the latter of which seems to cause DNA compaction very efficiently. This suggests that the non-coordinative interaction, which is not observed for cisplatin, is also involved in the anticancer mechanism. To find out in which process, cellular uptake or DNA binding, tetrazolato-bridged complexes and cisplatin behave differently from each other, we have made a couple of quantitative evaluations of the amount of coordinative Pt—DNA adducts formed on calf thymus (CT) DNA and of cellular accumulation, as well as cytotoxicity study.

Cisplatin resulted to yield more coordinative DNA adducts than **5-H-Y**, suggesting that the cytotoxicity of tetrazolato-bridged complexes is determined not only by binding ability but also other factors, such as non-coordinative DNA binding ability. The cellular uptake study was also performed for cisplatin, **5-H-Y** and other tetrazolato-bridged complexes of **5-EtAc** (R = CH₂COOCH₂CH₃, n = 2) and **5-Ac** (R = CH₂COO⁻, n = 1) combined with their cytotoxicity assays. Each of cisplatin, **5-H-Y**, **5-EtAc** and **5-Ac** (1 μM) was added to cisplatin-resistant L1210 mouse leukemia cells (L1210R), and the cellular Pt concentration was quantitated using ICP-MS. There was a certain correlation between the cellular Pt concentration and the cytotoxicity. For instance, **5-Ac**, which exhibits no cytotoxicity, was hardly taken into L1210R, although it is the most powerful DNA compactor among tetrazolato-bridged complexes ever reported. Interpretation of structure-activity relationship combined with DNA binding ability and cellular uptake will be presented.



P-03*

Aromatic Ring Stacking in Anthracene Containing 4N Coordinated Pt(II) Complexes and Their Antitumor Effect

Yasuko YAMAGA, Yuki MATSUOKA, Tatsuto KIWADA, Kazuma OGAWA, and Akira ODANI

Graduate School of Medical Sciences, Kanazawa University, Kanazawa 920-1192

Cisplatin $(\text{NH}_3)_2\text{PtCl}_2$, a typical Platinum drug, coordinated DNA guanine N7 and formed Pt(II)-coordinated DNA-HMG protein adduct, which could not be recognized by the repaired DNA enzyme and resultant apoptosis of the cell was induced. We hypothesized that this adduct was the form of cisplatin anticancer activity and synthesized 4N coordinated Pt(II) complexes as the model complexes of cisplatin binding DNA-HMG adduct, Pt(Ar)(AtX) (Fig.1), where Ar : substituted phenanthroline (R-phen), AtX : anthracene (At) containing diamine, and found the excellent antitumor effect of Pt(MP)(AtC3) (MP=5-methyl-1,10-phenanthroline, AtC3=N-9-anthracenyl-trimethylenediamine). To explore the aromatic ring stacking-biological activity relationship, we studied the properties of Pt(II) complexes involving new AtX.

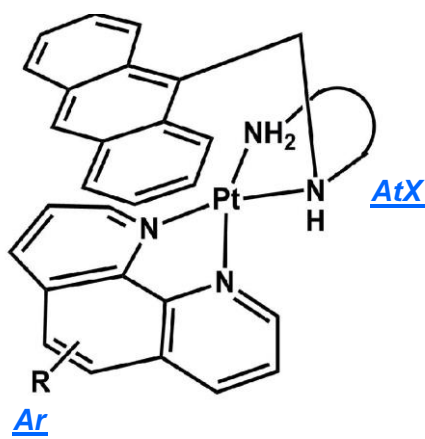


Fig 1. Pt(Ar)(AtX)

in vitro cytotoxicity of the Pt complexes. One of possible way to explain the relation between the stacking and the antitumor activity may be the lipophilicity which was evaluated by log P(octanol/water) to be lipophilic in high activity complexes.

The distribution of Pt in mouse was studied to characterize the Pt complex. These indicated the specific stacking structure plays an important role in anticancer effect.

The IC₅₀ (50% inhibition concentration of cell growth) of Pt(MP)(AtX) in 39 human cell lines showed the antitumor activity order : AtC3 > new AtX. The relation was hold in Pt(DMP) complexes (DMP =5,6-dimethyl-phen). The aromatic ring stacking between Pt-phen and side chain At was studied by H-1 NMR upfield shifts due to face-to-face aromatic ring stacking. The At ring inside the chelate ring of Pt-phen was indicated the H-1 upfield shifts in the following order: AtC3 > new AtX. This was same as antitumor activity and the aromatic ring stacking was important on

P-04

Cytotoxicity of Pt(IV) Complexes Against Cisplatin-Resistant Human Ovarian Cancer Cell –Potential Role of Reactive Oxygen Species–

Takamitsu SHIMIZU, Takao TOBE, Karin SHIMIZU, Miki MOTOYAMA, Yoshinori OKAMOTO, Koji UEDA, and Narolekao KOJIMA

Faculty of Pharmacy, Meijo University, Nagoya 468-8503

Some of platinum(IV) [Pt(IV)] complexes have been under developed as anti-cancer prodrugs. The prodrugs are to be converted to Pt(II) complexes by biological reductants before accessing cell nucleus, thereby generating the Pt(II)-DNA binding, an anti-cancer entity. Pt(IV) complexes show less adverse effects (such as renal toxicity) due in part to their lower reactivity with biological molecules as compared to a representative Pt(II) drug, cisplatin. Importantly, Pt(IV) complexes are still active against cisplatin-resistant cancer cells. In this study, we found that there was no difference in the intracellular distribution (influx/efflux pattern, intracellular transport, and subsequent DNA platination) between *cis*-Pt(IV) and cisplatin. However, *cis*-Pt(IV) was active against cisplatin-resistant cancer cells, and damaged DNA, generating 8-oxodG. Here, we discuss on the involvement of 8-oxodG and the detail of the *cis*-Pt(IV) action mechanism.

Cytotoxicity was evaluated by live-cell fluorescence staining method against human ovarian cancer cell lines (A2780) and its cisplatin-resistant subline (A2780cis). Pt-DNA-crosslink formation was also studied by agarose gel electrophoresis, where the crosslink was quantified by the decrease of ethidium bromide staining of DNA. Intracellular influx/efflux patterns and DNA platination amount were quantified using ICP-MS. Amount of 8-oxo-7,8-dihidro-2'-deoxyguanosine (8-oxodG), a biomarker for DNA oxidation, was determined by HPLC-ECD.

Cisplatin completely failed to decrease the survival of A2780cis at a concentration that killed A2780, whereas *cis*-Pt(IV) exerted cytotoxicity in both cell lines. The Pt-DNA-crosslink formation assay showed the platinum binding to DNA only in the presence of reductants such as glutathione (GSH) or ascorbic acid (AsA), indicating that Pt(IV) was reduced to Pt(II). However, it is also known that excess amount of GSH turns to break the Pt-DNA binding and suppresses the 8-oxodG induced by *cis*-Pt(IV). In contrast, AsA increased the 8-oxodG induction by *cis*-Pt(IV). On the other hands, cisplatin didn't induce the 8-oxodG with or without these reductants. Thus, oxidative DNA damage induced by *cis*-Pt(IV) could be one of the resistant-overcoming mechanisms. Furthermore, intracellular accumulation of Pt in the presence of *cis*-Pt(IV) was decreased by overloading a Cu(II) transporter CTR1 with Cu(II), whereas the cytotoxicity was not suppressed under such conditions. From these results, it is indicated that *cis*-Pt(IV) influxed by a pathway different from CTR1 induces oxidative DNA damage in A2780cis during the intracellular Pt(IV) oxidation processes.

P-05*

Development of Cytotoxic Manganese Complexes and Their Photocaged Derivatives by Using Nitric Oxide

Yuji IWAMOTO, Masahito KODERA, and Yutaka HITOMI

Department of Molecular Chemistry and Biochemistry, Faculty of Science and Engineering, Doshisha University, 1-3 Miyakodani, Tatara 610-0321 Kyoto

Most of anti-cancer agents have potential side-effects due to their low selectivity. Photodynamic therapy (PDT) can partly solve this problem because PDT utilizes nontoxic compounds that become or release bioactive molecules to targeted cancer cells upon selective exposure to light.

We have developed manganese(II) complexes, $[\text{Mn}(\text{dpaq}^{\text{R}})]\text{ClO}_4$ (**Chart 1**), supported by pentadentate monoamido ligands that show superoxide dismutase (SOD) activity comparable to a well-known SOD mimic, EUK-134, and further discovered that $[\text{Mn}(\text{dpaq}^{\text{NO}_2, \text{ester}})]\text{ClO}_4$ is more cytotoxic with IC_{50} (concentration that produces a 50% inhibitory effect) value of $12.4 \pm 0.2 \mu\text{M}$ against HeLa cells, than the clinically used anti-cancer agent, cisplatin. In this study, we will discuss the cytotoxic mechanism of $[\text{Mn}(\text{dpaq}^{\text{R}})]\text{ClO}_4$ and also report a new strategy to develop photo-caged cytotoxic compounds by using nitric oxide (NO).

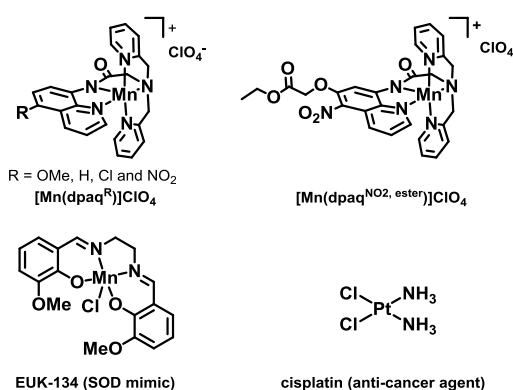


Chart 1 Chemical structures of manganese-based SOD mimics and cisplatin.

First, we found that both glutathione (GSH) and 2,7-dichlorodihydrofluorescein (DCFH) were significantly oxidized in the presence of $[\text{Mn}(\text{dpaq}^{\text{R}})]\text{ClO}_4$ under air, suggesting that $[\text{Mn}(\text{dpaq}^{\text{R}})]\text{ClO}_4$ may release reactive oxygen species (ROS) such as H_2O_2 via reductive dioxygen activation, while they are SOD mimics. Next, we tried to detect H_2O_2 , which should be formed as a result of the reductive dioxygen activation, by the means of the HRP/Amplex Red coupled assay, but found no detection of H_2O_2 . These results indicate another possibility that $[\text{Mn}(\text{dpaq}^{\text{R}})]\text{ClO}_4$ should produce some metal-based oxidants capable of oxidizing GSH and DCFH.

Recently we reported that the NO adducts of $[\text{Mn}(\text{dpaq}^{\text{R}})]\text{ClO}_4$, $[\text{Mn}(\text{NO})(\text{dpaq}^{\text{R}})]\text{ClO}_4$, are capable of releasing nitric oxide in a controlled manner by near-IR light irradiation^[1]. We expected that the NO adducts should show lower cytotoxicity because of lacking in a labile coordination site required for reductive dioxygen activation to produce ROS or metal-based oxidants, and become photocaged derivatives of the parent cytotoxic complexes $[\text{Mn}(\text{dpaq}^{\text{R}})]\text{ClO}_4$. As expected, we found that $[\text{Mn}(\text{NO})(\text{dpaq}^{\text{R}})]\text{ClO}_4$ showed low cytotoxicity with IC_{50} values of ca. $100 \mu\text{M}$ against HeLa cells in the dark, but became cytotoxic after light irradiation ($[\text{Mn}(\text{NO})(\text{dpaq}^{\text{NO}_2, \text{ester}})]\text{ClO}_4$: $\text{IC}_{50} = 17 \pm 1 \mu\text{M}$ against HeLa cells). Thus, the current study suggest that the NO adducts will be promising unique PDT reagents.

Reference

[1] Y. Hitomi, Y. Iwamoto, M. Kodera, *Dalton Trans.*, **2014**, 43, 2161-2167.

P-06*

Hetero- and Homobimetallic Complexes Having $M^{II}-(\mu-OH)-M^{III/II}$ Cores ($M^{II}M^{III/II} = MnMn, MnFe, FeFe$): Preparation, Characterization, and Reactivity

Yohei SANO^{1,2}, and A. S. BOROVIK¹

¹Department of Chemistry, University of California–Irvine, Irvine, California 92697-2025, United States

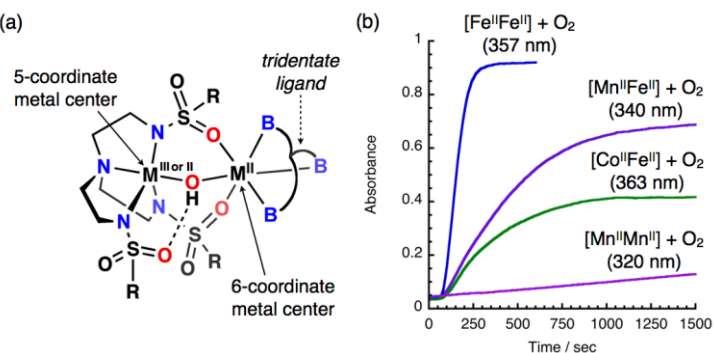
²Department of Applied Chemistry, Faculty of Engineering, Osaka University, Suita, Osaka 565-0871, Japan

The active site of several proteins contain bimetallic cores that are necessary for function, especially in the binding and activation of dioxygen. For example, bimetallic cores have been implicated in the function of hemerythrin, methane monooxygenase, the ribonucleotide reductases, and manganese catalases. The functional requirements of these metalloproteins often necessitates that one or both of the metal centers is coordinatively unsaturated to ensure the binding of small molecules and substrates.

Metal complexes with the tetradentate sulfonamido-based tripodal ($[MST]^{3-}$) has been reported recently and showed that the ligand enforces a 5-coordinate geometry around the metal center.^{1,2} It was discovered that the $[MST]^{3-}$ ligand is also capable of binding a second metal ion to the sulfonamido oxygen atoms, allowing formation of discrete heterobimetallic complexes. In the initial reports, the heterobimetallic complexes contained one transition metal ion and one Group 2 metal ion. To extend this approach, hetero- and homobimetallic complexes containing two transition metal ions were prepared, $[TMTACN \supset M^{II}-(\mu-OH)-M^{III/II}MST]^{+ \text{ or } 0}$ ($M^{II}M^{III/II} = MnMn, MnFe, \text{ and } FeFe$), (**Figure 1a**).³ The bimetallic complexes with $[M^{II}(\mu-OH)M^{III}]$ or $[M^{II}(\mu-OH)M^{II}]$ cores were characterized by various spectroscopies and their molecular structures are determined by X-ray analysis – all methods are consistent with one metal center being 5-coordinate metal center, having N_4O primary coordination sphere with distorted trigonal-bipyramidal geometry. The other metal ion was a 6-coordinate metal center, having N_3O_3 primary coordination sphere with a distorted octahedral geometry. (a) Preliminary functional studies revealed that when the $[M^{II}(\mu-OH)M^{II}]$ systems were treated with dioxygen, new species are formed that are distinct from the original $[M^{II}(\mu-OH)M^{II}]$ systems (**Figure 1b**).

Figure 1. (a) Our bimetallic complexes

$[TMTACN \supset M^{II}-(\mu-OH)-M^{III/II}MST]^{+ \text{ or } 0}$ with unsymmetrical ligand system, and (b) reactivity data for the reaction of $[M^{II}M^{II}]$ ($MnMn, MnFe, FeFe, CoFe$) core and O_2 .



(1) Park, Y. J.; Ziller, J. W.; Borovik, A. S. *J. Am. Chem. Soc.* **2011**, *133*, 9258–9261.

(2) Park, Y. J.; Cook, S. A.; Sickerman, N. S.; Sano, Y.; Ziller, J. W.; Borovik, A. S. *Chem. Sci.* **2013**, *4*, 717–726.

(3) Sano, Y.; Weitz, A. C.; Ziller, J. W.; Hendrich, M. P.; Borovik, A. S. *Inorg. Chem.* **2013**, *52*, 10229–10231.

P-07*

Novel Dinitrogen Iron Complex with Cyclopentane-Bridged Iminophosphine Ligand

Tatsuya SUZUKI¹, Michael D FRYZUK², and Hideki MASUDA¹

¹*Department of Frontier Materials, Graduate School of Engineering, Nagoya Institute of Technology, Gokiso, Showa, Nagoya 466-8555, Japan.*

²*Department of Chemistry, The University of British Columbia, 2036 Main Mall, Vancouver, BC, Canada, V6T 1Z1*

FeMo cofactor (FeMoco), which is the active center of nitrogenase enzyme that converts N₂ into NH₃, has iron ions surrounded with sulfur rich environment.¹ The mechanistic study on nitrogen fixation by nitrogenase enzymes has suggested that the sulfur atom plays a role as a proton donor in the reaction. Thus, it is necessary to supply protons. So, we designed cyclopentane-bridged iminophosphine ligand as a proton donor group. The cyclopentane-bridged iminophosphine group has been involved in equilibrium between the imine/enamine tautomers and easily deprotonated to produce an anionic enamine form.² This behavior is thought to give some protons to the dinitrogen molecule through the reaction. In this study, we synthesized and characterized novel iron complexes using cyclopentane-bridged iminophosphine ligands.

We prepared *N*-(2-diisopropylphosphino-phenyl)-*P,P*-diisopropyl-*P*-(2-(2,6-diisopropylphenylamino)cyclopent-1-enyl)phosphoramine ligand having 2-diisopropylphosphino-phenyl a cyclopentane-bridged iminophosphine groups (**HNpNPⁱPr**). The iron complex with **NpNPⁱPr**, [Fe(**NpNPⁱPr**)Br], was prepared and characterized. Stirring a THF solution of [Fe(**NpNPⁱPr**)Br] with 1 equiv of KC₈ for overnight under the dinitrogen atmosphere gave [Fe(**NpNPⁱPr**)₂(μ-N₂)] as a dark brown solid, whose structure was determined by X-ray crystal structure analysis (Fig. 1). Here, we report the synthesis, crystal structure and characterization of [Fe(**NpNPⁱPr**)₂(μ-N₂)].

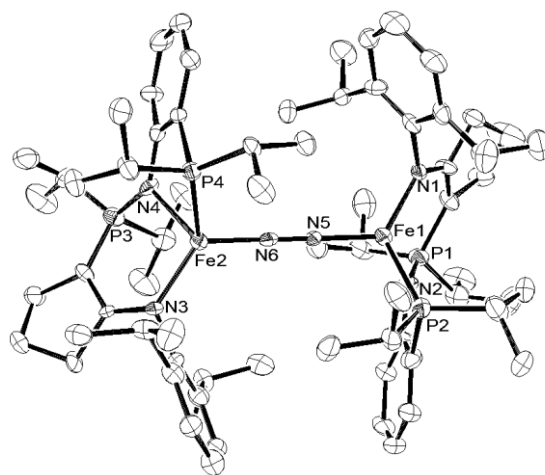


Fig. 1 Crystal structure of [Fe(**NpNPⁱPr**)₂(μ-N₂)].

[1] O. Einsle, F. A. Tezcan, S. L. A. Andrade,

B. Schmid, M. Yoshida, J. B. Howard, and D. C. Rees, *Science*, **2002**, 297, 1696.

[2] T. C. Wambach, J. M. Ahn, B. O. Patrick, and M. D. Fryzuk, *Organometallics* **2013**, 32, 4431.

P-08*

Development of Nitrile Hydration Catalyst Using Cobalt Complex with Water Activation Site

Hiroki ANDO, Tomohiko INOMATA, Tomohiro OZAWA, and Hideki MASUDA

Graduate School of Engineering, Nagoya Institute of Technology, Nagoya 466-8555.

Nitrile hydratase (NHase) is an enzyme that catalyzes hydration of nitrile compounds to the corresponding amides. NHase is a metalloenzyme with an active site octahedral Fe^{III} or Co^{III} ion. The active site structure of NHases has three cysteine sulfurs and two deprotonated peptide amide nitrogens as donor atoms,^[1] which is dramatically different from the active site of usually known nonheme iron enzymes. The nitrile hydration reaction using NHase applied for industrial production of acrylamide from acrylonitrile.^[2] This process is more advantageous than the production method used before because of its less by-products. On the other hand, the enzymatic method is known to show a deactivation by temperature rising and excessive production of acrylamide in the reaction media. Therefore, in this study, development of a new artificial catalyst that contains a concept of the NHase hydration reaction has been tried. Recently, it is suggested that a coordinated nitrile molecule was attacked by a water molecule nearby the active site activated by sulfenate oxygen as a base.^[3] We designed a new metal complex (CoL_{Py}) with pyridyl group as a base for water activation (Figure 1). To center metal, we chose cobalt as well as NHase.

X-ray crystal analysis of $\text{Co}^{\text{II}}\text{L}_{\text{Py}}$ clarified that the Co^{II} center had a pseudo-octahedral geometry (Figure 2). The pyridyl nitrogen also coordinated to the Co^{II} center to form four-membered $\kappa^2\text{N,S}$ -chelate rings. The small S1-Co-N2 angle (65.6°) made us expect the easy release of the pyridyl group from Co^{II} center. In this presentation, synthesis and characterization of the cobalt complex will be discussed.

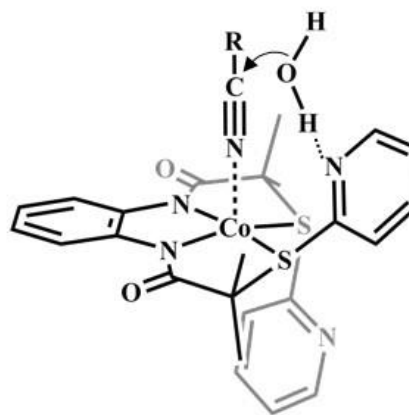


Figure 1. Expected nitrile hydration reaction by CoL_{Py}

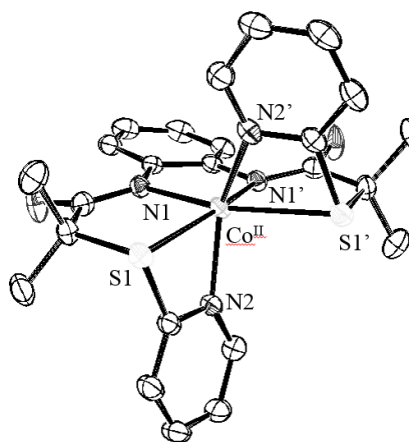


Figure 2. Crystal structure of $\text{Co}^{\text{II}}\text{L}_{\text{Py}}$

[1] S. Nagashima, M. Nakasako, D. Naoshi, M. Tsujimura, K. Takio, M. Odaka, M. Yohda, N. Kamiya, I. Endo, *Nat. Struct. Biol.* **1998**, 5, 347.

[2] M. Kobayashi, S. Shimizu, *Nat. Biotechnol.* **1998**, 16, 733.

[3] K. Hashimoto, H. Suzuki, K. Taniguchi, T. Noguchi, M. Yohda, M. Odaka, *J. Biol. Chem.* **2008**, 283, 36617.

P-09*

Preparation and Characterization of Dicopper Complex as an Active Site Model of pMMO

Tatsuya OCHIAI, Tomohiko INOMATA, Tomohiro OZAWA, and Hideki MASUDA

Department of Frontier Materials, Nagoya Institute of Technology, Gokiso-cho, Showa-ku, Nagoya 466-8555, Japan

Particulate methane monooxygenase (pMMO) catalyzes the oxidation of methane to methanol under ambient conditions. The active site of pMMO contains dicopper center, each of which is surrounded with different coordination environments. Considering the structural features and strong oxidation ability of pMMO, $(\mu\text{-oxo})\text{Cu}^{\text{II}}\text{Cu}^{\text{III}}$ species is one of the most dominant active species for the enzymatic methane oxidation^[1].

We have studied the preparation and characterization of a novel asymmetric dicopper complex as the active intermediate for methane oxidation. Unique dicopper complex with different coordination environments, $[\text{Cu}^{\text{II}}_3(\text{L1})(\mu\text{-PhCOO})]$ (**1**) (**L1** = *N*-(3-(bis(pyridin-2-yl methyl)amino) -2-hydroxypropyl) -3,5-di-*tert*-butyl-2-hydroxybenzamide), was prepared from the reaction of **H₃L1**, $\text{Cu}^{\text{II}}(\text{PhCOO})_2$, and NaH in DMF. The single crystal of **1** was obtained from MeCN solution. X-ray structure of complex **1** (Figure 1) revealed an asymmetric dicopper(II) complex. The Cu(1) and Cu(2) ions are coordinated in a five-coordinate trigonal-bipyramidal and in a four-coordinate square-planar geometries, respectively. The Cu(1)···Cu(2) distance is 3.099(1) Å and Cu(1)–O(1)–Cu(2) angle is 104.69(13) °.

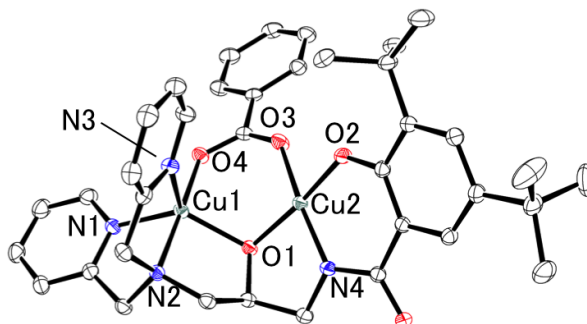


Figure 1. ORTEP view of Complex 1, showing 30 % probability thermal ellipsoids.

ESR measurement of complex **1** at 77 K in CH_2Cl_2 exhibited a spectrum typical for square-planar copper(II) complex; $g_{\parallel} = 2.243$, $g_{\perp} = 2.054$, $A_{\parallel} = 193$ G. CV measurement gave irreversible waves with an oxidation wave assignable to copper(III/II) process at $E_{\text{pa}} = 0.22$ V vs. Fc/Fc^+ . Furthermore the electrochemical behavior of complex **1** was studied using spectropotentiostatic technique. Significant increase in absorption band was observed in the range of 350–400 nm (ϵ 3545 $\text{M}^{-1} \text{cm}^{-1}$) after oxidation at 0.22 V vs. Fc/Fc^+ . The intense bands in this region is assignable to some charge transfer transitions. We have concluded that the resultant species is the novel mixed-valence dicopper(II,III) complex as an active site model of pMMO.

[1] R. L. Lieberman and A. C. Rosenzweig, *Nature* **2005**, 434, 177.

¹Graduate School of Science and Technology, Shizuoka University, 836 Ohya, Suruga-ku, Shizuoka 422-8529. ²Green Chemistry Research Division, Research Institute of Green Science and Technology, Shizuoka University, 836 Ohya, Suruga-ku, Shizuoka 422-8529.

Proximal and distal histidine residues provide the coordination environment for stable O₂ fixation at the heme site of hemoglobin (Hb) and myoglobin (Mb), while proximal and distal-polar residues create a reaction environment for O–O bond activation at the heme sites of some metalloenzymes such as cytochrome *c* peroxidase (CcP), cytochrome P450, and heme oxygenase (HO). For activation of the O–O bond by these residues, the so-called “push–pull” mechanism has been proposed. This is a cooperative effect by electron donation from the proximal residue at the fifth site (push effect) and associations from distal-polar residues to the coordinating substrate (pull effect).

We have recently designed a new porphyrin ligand, amtp, that has an amide group at the *ortho*-position of a phenyl group of tetraphenylporphyrin (TPP) to mimic the microenvironment created by a distal-polar residue observed in the heme-containing metalloproteins. In this paper, we show the details of the unique conversions of [Co^{II}(amtp)] (**1**) to new Co(III) complexes bearing an acyclic pentapyrrole-type ligand (**2**),^[2] lpp, and a porphodimethene-type ligand (**3**),^[3] ampord, under air in the presence of nitrogen bases. The amide groups and additions of nitrogen bases are necessary for the conversion, indicating that this system mimics the “push–pull” mechanism.

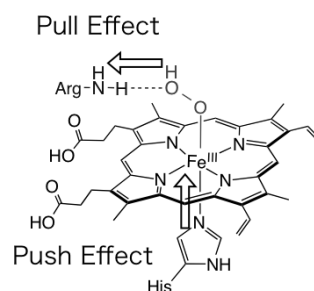
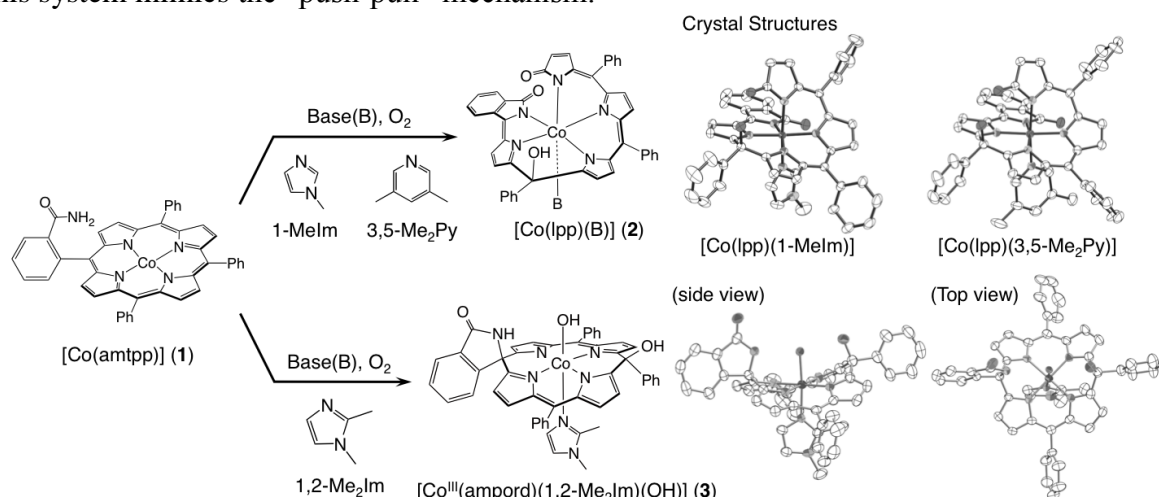


Figure 1. “Push–Pull” mechanism proposed for O–O activation.^[1]



Scheme 1. Conversion of **1** to **2** and **3** by reaction with O₂ in the presence of nitrogen bases.

[1] (a) J. H. Dawson, *Science*, **1988**, *240*, 433. (b) M. Sono, M. P. Roach, E. D. Coulter, J. H. Dawson, *Chem. Rev.*, **1996**, *96*, 2841.

[2] K. Yamanishi, M. Miyazawa, T. Yairi, S. Sakai, N. Nishina, Y. Kobori, M. Kondo, F. Uchida, *Angew. Chem. Int. Ed.* **2011**, *50*, 6583.

[3] K. Yamanishi, T. Yairi, K. Suzuki, M. Kondo, *Chem. Commun.*, **2013**, *49*, 9296.

Syntheses and Structures of Iron – Amideporphyrin

Masashi OKAHISA¹, Kana SHIBATA², Katsunori YAMANISHI¹, Keisuke SUZUKI¹, and Mitsuru KONDO³,

¹Graduate School of Science and Technology, Shizuoka University, Shizuoka 422-8529 ²Department of Chemistry, Faculty of Science, Shizuoka 422-8529 ³Green Chemistry Research Division, Research Institute of Green Science and Technology, Shizuoka 422-8529

Proximal and distal-polar residues create a reaction environment for O–O bond activation at the heme sites of some metalloenzymes such as cytochrome c peroxidase (CcP), cytochrome P450 (CYPs), and heme oxygenase (HO) [1, 2]. HO activates O₂ at the active site, and then hydroxylates the *meso*-carbon of heme, yielding hydroxy heme in the initial step. For activation of the O–O bond at the active sites, the so-called “push–pull” mechanism has been proposed. This is a cooperative effect by electron donation from the proximal residue at the fifth site (push effect) and associations from distal-polar residues to the coordinating substrate (pull effect). We have designed a new porphyrin ligand, amtp, which has an amide group at the ortho-position of a phenyl group of tetraphenylporphyrin (TPP) to mimic the microenvironment created by a distal-polar residue observed in the heme-containing metalloproteins. In a recent report, we have shown that [Co^{II}(amtp)] converted to new Co(III) complexes bearing an acyclic pentapyrrole-type ligand by activation of O₂ at the Co site in the presence of axial ligands [3].

In this work, we succeeded in the syntheses of iron complexes with amtp. Reaction of FeCl₂ with H₂amtp under air yielded [Fe^{III}(amtp)Cl]. Treatments of this compound with excess 1-methylimidazole (1-MeIm) provided [Fe^{III}(amtp)(1-MeIm)₂]Cl. This compound was successfully reduced to the [Fe^{II}(amtp)(1-MeIm)₂] by treatment with Cp₂Co. When 1-vinylimidazole (1-VinylIm) or 3,5-dimethylpyridine (3,5-Me₂py) were used instead of 1-MeIm, [Fe^{II}(amtp)B₂] (B = 1-VinylIm, 3,5-Me₂py) were isolated. Structures of Compounds **1**, **2**, and **3** were characterized by single crystal X-ray diffraction studies. The syntheses, structures and properties of the Fe-amtp compounds are described.

- [1] Poulos T. L. in *The Porphyrin Handbook*, ed. Kadish K. M., Smith, K. M. and Guilard, R., Academic Press, San Diego, 2000, vol. 4, pp. 189–218.
- [2] Meunier B., in *Comprehensive Coordination Chemistry II*, ed. Que L. and Tolman W. B. Elsevier, Oxford, 2004, vol. 8, pp. 261–280.
- [3] Yamanishi K., Miyazawa M., Yairi T., Sakai S., Nishina N., Kobori Y., Kondo M., and Uchida F., *Angew. Chem., Int. Ed.*, 2011, 50, 6583–6586.

P-12*

Direct Electrochemical Study on Electron Transport from Cytochrome *c* to Cytochrome *cd*₁-Type Nitrite Reductase from a Halophilic Denitrifier *Halomonas Halodenitrificans*

Kumiko TACHIBANA, Yuki TAKAHASHI, Kunishige KATAOKA, Daisuke SEO, and Takeshi SAKURAI

Graduate School of Natural Science and Technology, Kanazawa University, Kakuma, Kanazawa 920-1192

Denitrification is an anaerobic respiration process to obtain energy during the conversion from nitrate to nitrogen via nitrite, nitric oxide, and nitrous oxide, and concerns in the global nitrogen cycle. It has been considered that a cytochrome in the periplasm functions as a common electron donor to the soluble and membrane-bound enzymes involved in denitrification, nitrate reductase, nitrite reductase, nitric oxide reductase, and nitrous oxide reductase.

From the soluble fraction of *Halomonas halodenitrificans* we isolated three cytochromes as potential electron donors towards the enzymes involved in denitrification, and characterized them as C-type cytochromes. One of cytochromes with the split α band in the reduced form (12KDa cytochrome) exhibited electrochemical communications with an Au electrode modified with 4,4'-dithiodipyridine, while other cytochromes with molecular masses of 24 kDa and 44kDa did not show good electrochemical response. The formal potential of the 12kDa cytochrome was 220 mV (vs. NHE) with ca. 30 mV shift depending on pH.

We also isolated the cytochrome *cd*₁ type-nitrite reductase, the homodimer of 73 kDa molecular mass protomer from the soluble fraction. Nitrite reductase maximally exhibited the enzymatic activity at pH 6 in a considerably narrow range of pH, 4-8. The enzymatic activity was not dependent on NaCl concentration. It was impossible to perform electrochemistry of nitrite reductase using any electrode irrespective of the presence or absence of nitrite. However, the electric current for 12 KDa cytochrome was increased in the presence of nitrite reductase, and increased further when nitrite was added. This indicates that electrons are supplied to nitrite reductase via 12 KDa cytochrome from the modified Au electrode, and substrate is catalytically reacted. To support this, the electric current for 12kDa cytochrome increased with increasing nitrite reductase concentration. Accordingly, a direct electrochemical system of nitrite reductase has been constructed with the assistance of 12kDa cytochrome as the effective mediator of electron.

Further, we obtained nitric oxide reductase from the inner membrane of *H. halodenitrificans*. However, direct electrochemistry of nitric oxide reductase was impossible. No electrochemical response of 12kDa cytochrome was also observed in the presence of n-dodecyl- β -D-maltoside utilized to solubilize nitric oxide reductase, of which use making difficult to construct the electrochemical system of nitric oxide reductase. Irrespective of this, it has been ascertained spectrophotometrically that the 12kDa cytochrome is best able to transfer electrons to nitric oxide reductase among three soluble cytochromes.

As a conclusion, the 12kDa cytochrome is the natural common electron donor towards the denitrification enzymes, the cytochrome *cd*₁ type nitrite reductase and nitric oxide reductase in *H. halodenitrificans*.

P-13*

Cu, Zn, Ca Transport in Serum Revealed by Quaternary Human Serum Albumin Complex Formation

Keiko SEKIMOTO, Mio KAMEI, Tsuguno KATSUNO, Tatsuto KIWADA, Kazuma OGAWA, and Akira ODANI

Graduate School of Medical Sciences, Kanazawa University, Kanazawa 920-1192

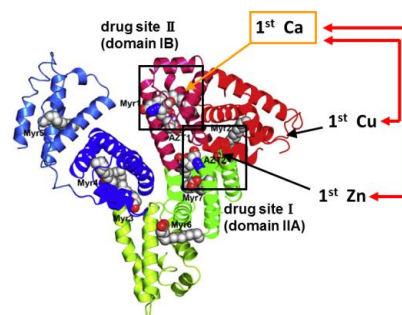
Human serum albumin (HSA) is a major carrier protein of metal ions and drugs in serum. There were many studies about drug-drug interaction on HSA, however, there is no report about metal-metal interactions on HSA. Here we reported equilibrium study of quaternary Cu(II)-Zn(II)-Ca(II)-HSA systems by pH method.

pH titrations were carried out 50 μ M a:b:c:d Cu-Zn-Ca-HSA systems at 25 $^{\circ}$ C, and I=0.1(KCl). The results were analyzed as multi-equilibria and β pqr were calculated by the least-squares treatment using Hyperquad[1]: $p\text{Cu}+q\text{Zn}+r\text{Ca}+s\text{HSA}+t\text{H} = \text{Cu}_p\text{Zn}_q\text{Ca}_r(\text{HSA})_s\text{H}_t$ β pqrst = $[\text{Cu}_p\text{Zn}_q\text{Ca}_r(\text{HSA})_s\text{H}_t]/([\text{Cu}]^p[\text{Zn}]^q[\text{Ca}]^r[\text{HSA}]^s[\text{H}]^t)$ The stability constants β is the physical constant and was used for complex/adduct formation simulation by HySS.

In binary metal(II)-HSA system 1st Cu bound HSA with 2deprotonation(-2H⁺) and 1st Zn and 1st Ca bound HSA without deprotonation. The simulation based on β pqrst at pH 7.4 and 0.6 mM 1:1 X-HSA showed X-HSA complex was major. This also showed that under [X] in serum ([Cu]=20 μ M, [Zn]=15 μ M, [Ca]=2.5mM) Ca-HSA was major, but Cu-HSA, Zn-HSA were rare. Considering ternary Cu-Zn-HSA, Zn-Ca-HSA, Ca-Cu-HSA systems, in serum condition both Cu-Ca-HSA and Zn-Ca-HSA complexes formed because ternary X-Y-HSA complex formations were preferable to binary X-HSA and Y-HSA formations. After taking into the quaternary complex for the simulation, the simulated complex formation showed the quaternary Cu-Zn-Ca-HSA complex was major as Cu and Zn carriers. This revealed that Cu and Zn were transported together by Ca-HSA though there was 30-40 fold Cu and Zn free Ca-HSA. Such a concerted binding in Cu-Zn-Ca-HSA complex was explained by the postulated stability constant $\Delta\log K$ defined in the equilibrium $x\text{Cu-HSA-H}_n + y\text{Zn-HSA-H}_n + z\text{Ca-HSA-H}_n \rightleftharpoons \text{Cu}_x\text{-Zn}_y\text{-Ca}_z\text{-HSA-H}_n + (x+y+z-1)\text{HSA-H}_n$.

The cooperative binding of Cu and Zn to Ca-HSA may be due to the helix-helix interaction in HSA where the metal ions bind between the helix and facilitate the helix-helix interaction such as the hydrogen bond and the electrostatic interaction to form stable HSA.

[1] P. Gans, A. Sabatini and A. Vacca, *Talanta*, **43**, 1739-1753(1996).



human serum albumin (HSA)

P-14*

Relationship between Heme Mobility and Ligand Binding in Neuroglobin

Takeyuki MURAKAMI¹, Hirohumi TSUJINO¹, Eri MASUDA¹,
Akane HIDAHA¹, Taku YAMASHITA^{1,2}, and Tadayuki UNO¹

¹ Graduate School of Pharmaceutical Sciences, Osaka University

² School of Pharmacy and Pharmaceutical Sciences, Mukogawa Women's University

Neuroglobin (Ngb) was discovered in 2000 as the third member of the globin family in vertebrates. Ngb is expressed in nerve tissues, mainly in the brain and the retina. Like other globin proteins such as hemoglobin (Hb) and myoglobin (Mb), Ngb can reversibly bind small ligands such as cyanide and oxygen (O₂) to the heme iron in the ferric and ferrous states. However, the physiological role of Ngb as an O₂ binder or a transporter should be denied because of its low concentration in the brain. On the other hand, it has been suggested from *in vivo* and *in vitro* studies that Ngb plays a neuro-protective role against reactive oxygen species (ROS). Over-expression of Ngb leads to the recovery from stroke, and hence it is considered that Ngb scavenges ROS and reduces ischemic infraction. However, true physiological role of Ngb remains still uncertain.

Ngb has two structural features: one is “heme slide” induced by ligand binding to the heme, and the other is an intramolecular disulfide bond. From an X-ray crystal structural analysis, it was shown that the heme slides deeply into the internal protein cavity upon the binding of carbon monoxide (CO). On the other hand, Ngb has three cysteine residues and forms a disulfide bond between Cys46 and Cys55 in response to the redox state in the cells. Although these structural features are unique to Ngb, their roles for the Ngb function have not been clarified yet.

In order to reveal the mechanism of heme slide, we focused on Phe106 that locates closely to the heme and shifts its position by the CO binding. We prepared some mutants (F106V, F106L, and F106W) and examined their ligand binding affinities. We employed cyanide (CN⁻) and CO ligands which have relatively high affinity to ferric and ferrous heme, respectively, and evaluated their dissociation constants (*K_d*) by UV-visible titration method. We found that the ligand affinity depended on the bulkiness of the residue at 106 in both ferric and ferrous Ngbs, suggesting that this position greatly affects the degree of heme slide. On the other hand, we prepared another series of mutants in which each cysteine is substituted by a serine (C46S, C55S, and C120S), and studied the effects of disulfide bond on the ligand binding property. We found that C46S and C55S mutants show lower ligand affinity than WT and C120S Ngbs, and hence the formation of disulfide bond between Cys46 and Cys55 is crucial for the regulation of ligand binding in Ngb. Since physiological role of Ngb should be closely linked to the oxygen binding, our results suggest strongly that the heme slide, as well as the disulfide bond, play key roles in regulating Ngb functionality.

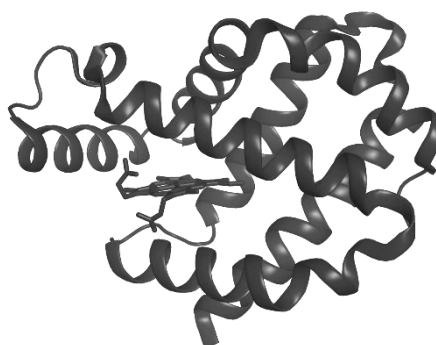


Fig. 1. Crystal structure of human Ngb (pdb: 4MPM).

The Effect of Cytochrome b5 on Peroxynitrite Generation and Tyrosine Nitration

Ryota YANASAKA¹, Hirofumi TSUJINO¹, Shumpei HANAI¹, Taku YAMASHITA^{1,2}, and Tadayuki UNO¹

¹*Graduate School of Pharmaceutical Sciences, Osaka University*

²*School of Pharmacy and Pharmaceutical Sciences, Mukogawa Women's University*

Cytochrome b5 (Cgb) was discovered in 2001 as the fourth member of the vertebrate globin family. Cgb is a hexa-coordinated heme protein with a molecular weight of 21-kDa, and is ubiquitously expressed in various organs. Although some possibilities about Cgb's function have been proposed by previous studies, the physiological role of Cgb is still uncertain. It has been suggested, however, that the function would be closely related to oxygen. It is because Cgb can bind diatomic gases such as oxygen at the heme iron as other globins (hemoglobin, myoglobin and neuroglobin), and Cgb is up-regulated under hypoxia at ischemia and reperfusion injury. It has also been suggested that Cgb might play a role of protecting cells against reactive oxygen species (ROS). Peroxynitrite, which is one of the ROS, is generated from nitric oxide (NO) and superoxide anion *in vivo*, and causes various oxidative stresses, such as tyrosine nitration of proteins. Because NO and superoxide levels increase under ischemia and reperfusion injury, we postulated that Cgb might protect cells by inhibiting tyrosine nitration to 3-nitrotyrosine. In this study, we investigated the effect of Cgb on the tyrosine nitration and peroxynitrite generation in the presence of NO and superoxide anion *in vitro*.

SIN-1 is a reagent which produces NO and superoxide anion simultaneously to afford peroxynitrite in a solution. In this study, SIN-1 was used for the tyrosine nitration, and the produced amount of 3-nitrotyrosine was determined by HPLC. We found that Cgb inhibits the nitration reaction in a dose-dependent manner, although bovine serum albumin (BSA), a negative control, does not. In order to reveal the inhibition mechanism, we further studied the effect of Cgb on the peroxynitrite generation from SIN-1. DCDHF (2',7'-dichlorofluorescein diacetate) was used to detect and quantify peroxynitrite. DCDHF reacts with peroxynitrite and the product can be detected by absorbance at 500 nm. We found again that peroxynitrite generation was inhibited by Cgb but not by BSA. These results suggest that the inhibition of tyrosine nitration by Cgb is attributed to the inhibition of peroxynitrite generation from SIN-1. Some previous studies, however, suggested that Cgb could promote peroxynitrite generation when a large amount of NO was supplied. Therefore, Cgb would modulate peroxynitrite generation and tyrosine nitration, depending on the solution condition.

In conclusion, we focused on the effect of Cgb on the tyrosine nitration, and we could show that Cgb inhibits the nitration reaction by suppressing the amount of peroxynitrite generation from SIN-1. Because tyrosine nitration of signal-transducing proteins regulates cell apoptosis and/or survival, our results suggest strongly that Cgb plays a key role in cytoprotection against oxidative stress at ischemia and reperfusion injury by inhibiting tyrosine nitration. Cgb would modulate peroxynitrite generation and protein tyrosine nitration in response to the levels of NO and superoxide anion in the cells.

P-16*

Effect of SNPs on the Drug Metabolism of CYP2D6 ~ Corrections for P420 Content ~

Yuri NARIKIYO¹, Chiaki HORII¹, Mayu YAMADA¹, Hirofumi TSUJINO¹, Taku YAMASHITA^{1,2}, and Tadayuki UNO¹

¹Graduate School of Pharmaceutical Sciences, Osaka University

²School of Pharmacy and Pharmaceutical Sciences, Mukogawa Women's University

The cytochrome P450s (CYPs) constitute a superfamily of heme-containing enzymes that catalyze metabolism of a wide variety of substrates. In human, CYP2D6 is one of the most important isoforms because it is involved in the metabolism of approximately 30% of currently marketed drugs, although its expression level amounts to only 2% of all hepatic CYPs. In addition, CYP2D6 gene is reported to show a number of single nucleotide polymorphisms (SNPs) which result in four phenotypes; ultra-rapid, extensive, intermediate, and poor metabolizers. Because the SNP mutation induces inter-individual difference in drug effect, its understanding is essential to rationally develop and safely use any drugs.

When we purified several CYP2D6 variants with our *E. coli* expression system, we recognized that the variants were unstable, and the amount of P420 increased relative to that in WT. Because P420 is an inactive form of CYP, its content should affect the drug metabolism significantly. Therefore, we first prepared WT CYP2D6 which contained various amounts of artificial P420, and studied the effects of P420 on the metabolic activity. UV-visible difference spectroscopy was used to estimate the P420 content, and metabolic activity for imipramine was evaluated by HPLC technique. As a result, we found that the activity (CL_{int}) linearly decreased depending on the P420 content, and hence we need to take the P420 content into account to compare the activities among CYP2D6 variants. By detailed analyses using Michaelis-Menten plots, we could find that V_{max} linearly decreased by the increase of P420 content, while K_m value was almost insensitive to the content. Therefore, we could deduce an equation from these kinetic parameters to correct the activity, and the equation could allow us to compare the activities of variants with that of WT CYP2D6. By correcting activity for the P420 content, we could find that combinations of SNP mutations exhibit synergistic effect on the drug metabolism. This finding is very important especially to CYP2D6, because i) it is very unstable and ii) reported to have more than 100 SNPs, many of which consist of combinations of other SNP mutations. Using our equation, we would be able to correct the activity for the P420 content, and hence SNP effects would be evaluated by the combination of data from other SNP variants.

In conclusion, we prepared some SNP variants of CYP2D6, and we could deduce an equation to correct the effect of P420 content. Although the relationship between SNPs and drug metabolism has not been fully revealed, our findings will contribute to the drug development as well as to the personalized therapeutics with drugs.

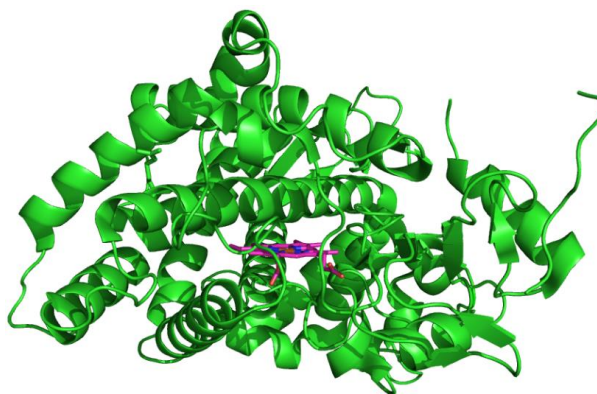


Fig. 1. Crystal structure of CYP2D6 (PDB code 2F9Q).

P-17*

A Proposal for a New Drug Binding Step in CYP1A2

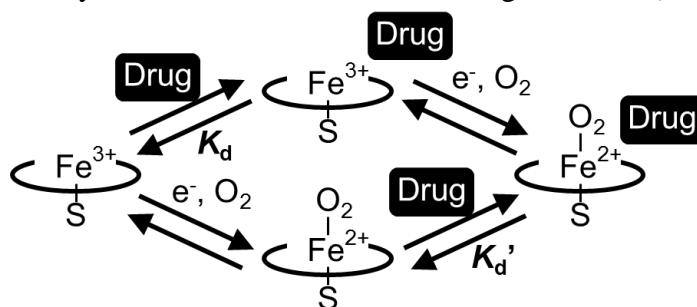
Ryota KAWAGUCHI¹, Ryu NAGAO¹, Junichi NODE¹, Sakiko MORITA¹, Hirofumi TSUJINO¹, Taku YAMASHITA^{1,2}, and Tadayuki UNO¹

¹Graduate School of Pharmaceutical Sciences, Osaka University

²School of Pharmacy and Pharmaceutical Sciences, Mukogawa Women's University

Cytochrome P450s (CYPs) comprise a superfamily of heme-containing enzymes which catalyze mono-oxygenation of various drugs and xenobiotics. CYPs are ubiquitous in nature and occur widely in animals, plants, and bacteria. Human CYP superfamily consists of many isoforms such as CYP1A2, CYP2C9, CYP2C19, CYP2D6, and CYP3A4. These five CYPs are major isoforms in human drug metabolism and contribute to oxidative metabolism of more than 90% of the drugs in current clinical use. One of them, CYP1A2, is mainly a hepatic enzyme, and can metabolize drugs such as caffeine and phenacetin, as well as some aromatic amines such as procarcinogens. Additionally, many single nucleotide polymorphisms (SNPs) have been reported for CYP1A2 gene. The effect of SNPs on the drug metabolism has not been fully studied at molecular level, and hence we investigated metabolic activities of CYP1A2 wild-type (WT) and some SNP variants.

We prepared eight CYP1A2 variants which have SNP mutations (D348N, C406Y, E168Q, F186L, S212C, G299S, T438I, and I314V), and measured their metabolic activities for selected drugs (caffeine, phenacetin, propranolol, amitriptyline, and imipramine) as well as for procarcinogens (IQ, MeIQ, MeIQx, and Trp-P-1). We found that maximum reaction velocity (V_{max}) was almost insensitive to the SNP mutations, while Michaelis constant (K_m) was much affected by SNP mutations. This result suggests strongly that the drug binding step was much influenced by the SNP mutations, and hence we estimated drug dissociation constants (K_d) by equilibrium dialysis method. The K_d values thus obtained were almost similar to the K_m values for propranolol, amitriptyline, imipramine, and Trp-P-1. However, the K_d values were much larger than K_m values for caffeine, phenacetin, IQ, MeIQ, and MeIQx. The large K_d values indicate that those drugs have low affinity to CYP1A2 in the ferric resting state. In order to explain this discrepancy, we propose a hypothesis that "some drugs prefer to bind to the oxygenated enzyme (oxy-form) in CYP1A2." Since oxy-CYP1A2 is unstable, we estimated dissociation constants (hereafter referred to as K_d') of drugs for ferric NO-bound CYP1A2 by visible titration at Soret absorption. The K_d' values thus obtained were similar to the K_m value but not to the K_d value (caffeine, phenacetin, IQ, etc). Therefore, some drugs are suggested to bind to the oxy-form but not to the ferric resting CYP1A2 (Scheme 1).



Scheme 1. A Proposal for the Alternative Drug Binding Step in CYP1A2.

P-18*

Roles of Residues 72 and 241 in Drug Discrimination between CYP2C9 and 2C19

Akinori HAYASAKI¹, Takumi SATO¹, Masayoshi MIYAMOTO¹, Yuki YASUHARA¹, Tamer Z. ATTIA^{1,2}, Mohamed A. HAMMAD^{1,2}, Hirofumi TSUJINO¹, Taku YAMASHITA^{1,3}, and Tadayuki UNO¹

¹ Graduate School of Pharmaceutical Sciences, Osaka University, Japan.

² Faculty of Pharmacy, Minia University, Egypt. ³ School of Pharmacy and Pharmaceutical Sciences, Mukogawa Women's University, Japan.

Cytochrome P450 (CYP) is a generic name of heme enzymes which show a unique absorption band at 450 nm in the ferrous-CO state. CYPs are ubiquitous in nature, and more than 50 isoforms were reported for human CYPs as membrane-anchored proteins. Especially, hepatic CYPs are mainly involved in drug metabolism and each isoform shows wide substrate specificity, producing unique metabolite(s). Because a drug is often metabolized by more than two CYP isoforms having different activities for the drug to give various metabolites, it is essential to understand the mechanism how each isoform recognizes its substrate drugs.

In this work, we focused on human CYP2C9 and CYP2C19, both of which belong to the same 2C subfamily. Although their amino acid sequences are about 91% homologous and hence their X-ray crystal structures are almost the same with each other, their drug specificities are much different. Namely, CYP2C9 preferably metabolizes acidic drugs such as diclofenac and ibuprofen, while CYP2C19 mainly metabolizes basic drugs such as amitriptyline and lansoprazole. The reason why these isoforms can distinguish their substrate drugs is still unclear.

Taking notice of charge of the substrate drugs, we considered that acidic and basic amino acid residues may play key roles in the drug discrimination between CYP2C9 and CYP2C19. Comparing the amino acid sequence, we found that CYP2C9 has basic Lys residues (Fig. 1) while CYP2C19 has acidic Glu residues commonly at positions 72 and 241. In order to reveal their roles in drug discrimination, we prepared some mutant CYPs in which the residues at 72 and 241 are mutually exchanged (2C9 K72E, 2C9 K241E, 2C19 E72K, and 2C19 E241K). Using these mutant and WT proteins, we evaluated their drug binding affinity by UV-vis titration and metabolic activity by HPLC.

For acidic drugs, the affinity of WT CYP2C9 was greatly reduced by K241E mutation, while low affinity of WT CYP2C19 was recovered by E241K mutation. For basic drugs, on the other hand, E72K mutation impaired the affinity in 2C19 while K72E mutation raised the affinity in 2C9. These suggest strongly that positively and negatively charged Lys241 and Glu72 play key roles in discriminating acidic and basic drugs, respectively. Because these residues are far from the drug binding site (Fig. 1), we conclude that these residues are located at the gate to recognize the drug charge, leading drugs to their binding site in the protein.

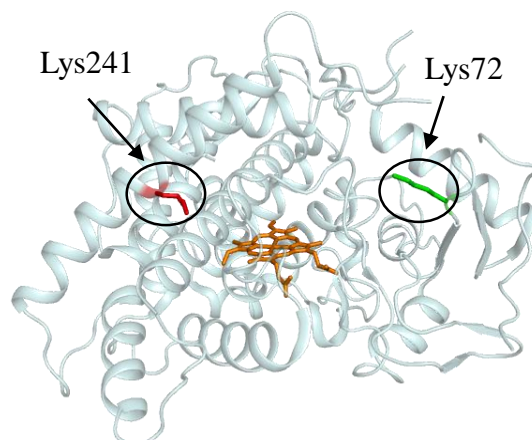


Fig. 1. Crystal structure of CYP2C9 (PDB code: 1R9O).

Effect of Redox-Inactive Metal Ions on the Radical-Scavenging Reaction of Hydroquinones

Tsukasa WAKI^{1,2}, Ikuo NAKANISHI², Kei OHKUBO³, Ken-ichiro MATSUMOTO², Shunichi FUKUZUMI³, Toshihiko OZAWA⁴, and Tadashi KAMADA^{1,2}

¹Graduate School of Medical and Pharmaceutical Sciences, Chiba University, Chiba 260-8670. ²Research Center for Charged Particle Therapy, National Institute of Radiological Sciences (NIRS), Chiba 263-8555. ³Department of Material and Life Science, Graduate School of Engineering, Osaka University, ALCA, Japan Science and Technology Agency (JST), Osaka 565-0871 ⁴Showa Pharmaceutical University, Tokyo 194-8543

Ubiquinol, the reduced form of coenzyme Q10, has a hydroquinone structure as an active center and shows an efficient scavenging activity against reactive oxygen species (ROS). On the other hand, we have recently reported that redox-inactive metal ions, such as Mg²⁺ and Al³⁺, significantly affect the radical-scavenging activity of phenolic antioxidants, such as flavonoids.¹⁾ Thus, in this study, we investigated the effect of redox-inactive metal ions on the radical-scavenging activity of hydroquinone and its methylated derivatives as well as on their one-electron oxidation potentials (E^0_{ox}).

Hydroquinones scavenged 2,2-diphenyl-1-picrylhydrazyl radical (DPPH[•]) as a ROS model. The rates of the DPPH[•]-scavenging reactions of hydroquinones in the presence or absence of 0.1 M Mg(ClO₄)₂ or 0.1 M Al(ClO₄)₃ were determined by monitoring the absorbance change at 517 nm due to DPPH[•] using a stopped flow technique in deaerated ethanol–H₂O (9:1 v/v) at 298 K. The decay of the absorbance at 517 nm obeyed pseudo-first-order kinetics, when the concentration of hydroquinones ([hydroquinones]) was maintained at more than 10-fold excess of the DPPH[•] concentration. The pseudo-first-order rate constants (k_{obs}) increase with increasing [hydroquinones], exhibiting first-order dependence on [hydroquinones]. From the slope of the linear plots of k_{obs} vs. [hydroquinones], the second-order rate constants (k) were determined for the DPPH[•]-scavenging reaction. The k values of hydroquinones were almost unchanged in the presence of Mg²⁺, while they were increased in the presence of Al³⁺. The E^0_{ox} values of hydroquinones were determined by second-harmonic alternating current voltammetry in ethanol–H₂O (9:1 v/v) containing 0.1 M Bu₄NClO₄ as a supporting electrolyte. In the presence of the redox-inactive metal ions, the E^0_{ox} values remained unchanged as compared to the E^0_{ox} values in their absence. On the other hand, the one-electron reduction potential (E^0_{red}) of DPPH[•] determined from a well-defined reversible wave by cyclic voltammetry in ethanol–H₂O (9:1 v/v) was slightly shifted in the presence of 0.1 M Mg²⁺ and largely shifted in the presence of 0.1 M Al³⁺ to the positive direction.

These results indicate that in the presence of Al³⁺, the DPPH[•]-scavenging reaction of hydroquinones occurred via an electron transfer as a rate-determining step, rather than one-step hydrogen atom transfer. Al³⁺ may stabilize DPPH anion (DPPH⁻) produced by one-electron reduction of DPPH[•], leading to the acceleration of the DPPH[•]-scavenging reaction.

1) T. Waki, S. Kobayashi, K. Matsumoto, T. Ozawa, T. Kamada, and I. Nakanishi, *Chem. Commun.* **2013**, 49, 9842

Shigeki KOBAYASHI¹, Mariko SHINAGAWA¹, Hiroki YASUGATA¹, Yuko SUZUKI¹, and Toshiyuki CHIKUMA¹

¹Department of Analytical Medicinal Chemistry, Showa Pharmaceutical University, Tokyo 194-8543

Reactive oxygen species (ROS) such as the hydroxyl radical (HO·), superoxide (O₂^{·-}), and hydrogen peroxide (H₂O₂) have high oxidative strength, abstract electrons and hydrogen radicals from biological targets, and cause oxidative damage *in vitro*. In organelles, excess production of ROS has been implicated in the pathogenesis of diseases such as cancer, inflammation and diabetes mellitus, and neurodegenerative diseases such as Alzheimer's and Parkinson's diseases. ROS also play a critical role in aging. Ohta *et al.* recently proposed molecular hydrogen (H₂) as a new antioxidant with the ability to reduce the oxidative state *in vivo*.¹⁾ Thus, H₂ may be used in treatment and prevention of inflammation, cancer, diabetes, Parkinson's disease, Alzheimer's disease, and cardiovascular diseases.



H₂ is the smallest antioxidant, with a molecular weight of 2. The antioxidative activity of H₂ is considered to be high because it only scavenges the HO· radical, as shown in reaction (1). The antioxidative activities of the deuterium (D₂) isotope of H₂, which has a molecular weight of 4, have not been examined, in part because measurement of these activities of H₂ and D₂ gases is difficult. Here, we used a chemiluminescence assay to evaluate the antioxidative activities of H₂ and D₂ produced from Microcluster® (1), Hydrozin (2) in H₂O and D₂O, and the reaction $\text{Mg} + 2\text{H}_2\text{O} \rightarrow \text{Mg}(\text{OH})_2 + \text{H}_2$ (3).

Antioxidant activities of H₂ and D₂ yielded from methods 1, 2, and 3 were determined through reaction with O₂^{·-} and HO· produced by the hypoxanthine-xanthine oxidase (HPX - XOD) system and Fe(II)²⁺-H₂O₂ system, respectively, as the half maximal inhibitory concentration (IC₅₀) based on changes in chemiluminescence. Reduction of compound 4 to compound 5 by reaction of 4 with 1 (Fig. 1) is important for understanding the measurements of active species in methods 1, 2, and 3. Interestingly, our results suggest that active species in methods 1 and 2 differ from that in 3.

¹⁾ I. Ohsawa, M. Ishikawa, K. Takahashi, M. Watanabe, K. Nishimaki, K. Yamagata, K. Katsura, Y. Katayama, S. Asoh, S. Ohta S., *Nat. Med.*, **2007**, 13, 688.

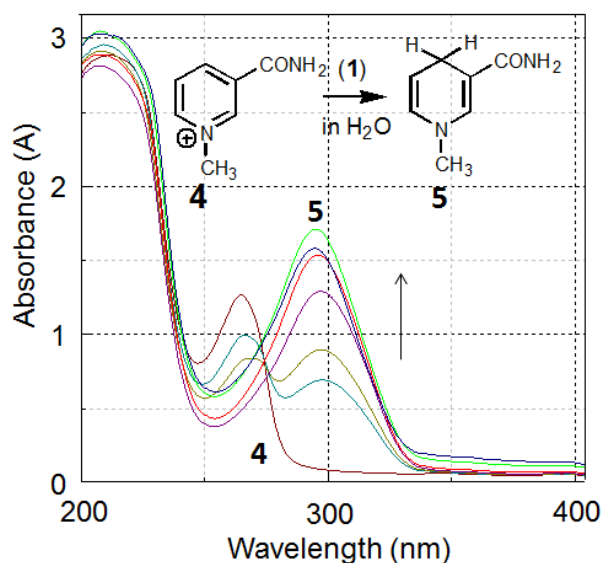


Fig. 1. UV/Vis absorption spectra for reduction of 4 to 5 after addition of 1.

Antioxidant Activities and Mechanism of Production of Hydrogen and Deuterium Molecules Produced from Magnesium-Organic Acid Systems

Shigeki KOBAYASHI¹, Mariko SHINAGAWA¹, Daisuke TUCHIYA², Tomomitsu HIRAI³, and Toshiyuki CHIKUMA¹

¹Department of Analytical Medicinal Chemistry, Showa Pharmaceutical University, Tokyo 194-8543, ²Toppan Forms Co., Ltd., Tokyo 105-8311, ³Nikko-Kasei Co., Ltd., Ibaraki 304-0823.

The reactive oxygen species (ROS) such as the hydroxyl radical (HO·), superoxide (O₂^{·-}), hydrogen peroxide (H₂O₂), and singlet oxygen (¹O₂) have high oxidative abilities, abstract electrons and hydrogen radicals from biological targets, and cause oxidative damage *in vitro*. In organelles, excess production of ROS has been implicated in the pathogenesis of diseases, including cancer, inflammation, diabetes mellitus, and neurodegenerative diseases. ROS also play a critical role in aging. Previous studies have shown that antioxidants are effective scavengers of ROS and free radicals.

The mechanism of production of H₂ in reaction (1) has not been determined in detail, but is thought to involve transfer of two electrons from Mg to H₂O. Production of H₂ has also been shown to be accelerated in the presence of acids, but their role remains unknown. However, reaction (1) differs from the electrode reaction that occurs *via* electrolysis of H₂O with an inactive Pt electrode.



Here, we describe a model for the transition state (TS) [Mg(OH₂)₂]^{*} formed at the saddle point of the reaction between Mg and 2H₂O using the B3LYP method with a 6-311G(d) basis set, as shown in Fig. 1. We found that the accelerated production of H₂ in the presence of acids was linked to a decrease in the activation energy (ΔG_i^{*}) of the TS.

We also measured the antioxidant activities of H₂ and D₂ produced from a Mg-Citric acid system using O₂^{·-} and HO·. We show that Mg-organic acid systems produced H₂ effectively, we describe the

mechanism of production of H₂ in the presence of weak acids, such as H₂O and organic acids, and we discuss the antioxidant activities of H₂ and D₂.

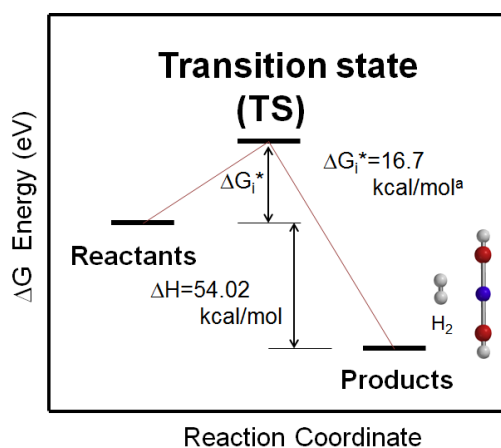


Fig. 1. Activation energy and optimized structure of the TS at the saddle point of the reaction between Mg and 2H₂O for production of H₂. The ΔG_i^{*} and ΔH are corrected for differences in zero point energy.

Takahito KISHIBUCHI, Takao TOBE, Shogo YOSHIDA, Koji UEDA, Yoshinori OKAMOTO, and Nakao KOJIMA

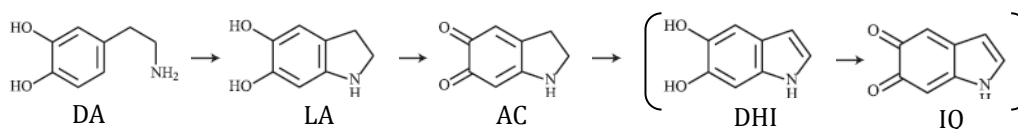
Faculty of Pharmacy, Meijo University, Nagoya 468-8503

Manganese (Mn) overexposure has been observed in recreational drug methcathinone users and mine workers. The overexposure causes dopaminergic neuron dysfunction leading to Parkinson's disease (PD)-like syndrome. Dopamine (DA) loss and iron (Fe) accumulation were reported in the brains of patients with PD. Therefore, we hypothesized that combined actions of Mn and Fe with DA are involved in Mn-induced neural disorder. In the present study, we investigated the involvement of Mn in Fe/DA-mediated cytotoxicity, oxidative DNA damage, and reactive oxygen species generation.

Methods: viability of human neuroblastoma cell line (SH-SY5Y), live-cell specific fluorescence assay; oxidative DNA damage, comet assay or determination of 8-oxo-7,8-dihydro-2'-deoxyguanosine by HPLC with an electrochemical detector; aminochrome (AC) formation, HPLC-DAD.

Mn and Fe in the presence of DA induced nuclear DNA damage, leading to neural cell death. Mn exacerbated the cytotoxicity induced by the DA-Fe reaction, although Mn itself was almost inert. Interestingly, 3,4-dihydroxybenzylamine (a structural DA homologue with an aminomethyl chain) showed no detectable damaging activity, suggesting that aminoethyl moiety of DA plays a key function in oxidative damage induced by Fe and Mn. DA oxidation proceeds with several steps. Initially, DA was notably oxidized by Mn, whereas further oxidation to AC was possible by Mn or Fe. During this oxidation process, an intermediate oxidation product leukoaminochrome (LA) induced intensive DNA damage in the presence of Fe. AC, of course, induced oxidative DNA damage again in the presence of Fe.

These results suggest that Mn initially triggers off the oxidation of catecholamines including DA followed by spontaneous reversion to catechol structures via side chain cyclization of their respective quinones, and then again oxidized to AC via the reaction with Fe (rather than Mn). Furthermore, 5,6-dihydroxyindole (DHI) is generated by the rearrangement of AC followed by oxidization to indolequinone (IQ) by reacting with Fe. This sequential oxidation would effectively produce reactive oxygen species by employing each Mn and Fe characteristics (coordination chemistry and redox potentials) leading to dopaminergic neural cell death. We propose that enhanced AC formation accompanying with Fe-mediated oxidative DNA damage could be involved in Mn-induced PD-like syndrome.



P-23*

Structure and Properties of a Blue Copper Protein, Pseudoazurin Gly39Trp Mutant

Hiroshi OSHITA¹, Takahide YAMAGUCHI¹, Akiko TAKASHINA¹, and Takamitsu KOHZUMA^{1,2}

¹Institute of Applied Beam Science, Ibaraki University, Ibaraki 310-8512.

²Frontier Research Center for Applied Science, Ibaraki University, Ibaraki 319-1106

Pseudoazurin (PAz) is a blue copper protein, which has a Type I copper at the active site. PAz functions as an electron donor to nitrite reductase and nitrous oxide (N₂O) reductase in denitrification process through the redox reaction of Cu⁺²⁺ ion [1, 2]. The Cu atom is coordinated by two imidazole N atoms of His40 and His81, one thiolate S of Cys 78 and one thioether S of Met 81 in the distorted tetrahedral configuration [3]. The uncoordinated Met16 is located at the outer sphere of Cu atom, and the spectroscopic and electrochemical studies of Met16X variants showed the significant contribution of the second sphere in the structure and properties of PAz [4, 5]. The solvent exposed Gly39 is found to be coordinated to His 40. XAS and DFT calculation have suggested the role of Gly39 on the electronic structure of PAz [6].

In the present study, Gly39Trp variant were constructed to know the influence of outer sphere Gly39 on the structure and properties of PAz. The mutation of Gly39Trp was confirmed by MALDI-TOF mass spectrum showing the 132.8 Da larger mass number of the mutant. The electronic absorption spectrum of Gly39Trp showed the absorption maxima at 453 nm and 593 nm in the visible region. The intensity ratio of those absorption bands (A_{450}/A_{600}) was estimated to be 0.40, which is smaller than that of WT PAz (0.46). The smaller A_{450}/A_{600} ratio suggested that the more axial structure is dominated at the active site. The Gly39Trp PAz provided the redox potential at 267 mV vs. NHE, which is almost identical to the reduction potential of WT PAz (260 mV). The X-ray crystal structure of Gly39Trp showed that the newly introduced Trp indole ring was confirmed to direct the outside of protein. The bond distances of Cu-N_{His81} = 2.19 (1.92 for WT), Cu-N_{His40} = 2.04 (1.95 for WT), Cu-S_{Cys78} = 2.21 (2.13 for WT), and Cu-S_{Met86} = 2.61 (2.71 for WT) Å.

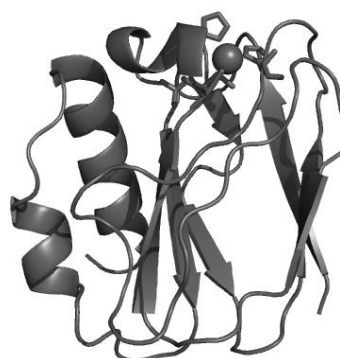


Figure 1. Overall protein structure of *Achromobacter cycloclastes* Pseudoazurin [3].

1. T. Kohzuma, S. Takase, S. Shidara, and S. Suzuki, *Chem. Lett.*, **1993**, 149-152.
2. K. Fujita, M. H.-Fujita, D. E. Brown, Y. Obara, F. Ijima, T. Kohzuma, D. M. Dooley, *J. Inorg. Biochem.*, **2012**, *115*, 163-173.
3. T. Kohzuma, C. Dennison, W. McFarlane, S. Nakashima, T. Kitagawa, T. Inoue, Y. Kai, N. Nishio, S. Shidara, S. Suzuki, A. G. Sykes, *J. Biol. Chem.*, **270**, 25733-25738(1995).
4. R. F. Abdelhamid, Y. Obara, T. Kohzuma, *J. Inorg. Biochem.* **2008**, *102*, 137-1379.
5. B. M. Fitzpatrick, T. Kohzuma, S. R. Czernuszewicz, *J. Biol. Chem.*, **2010**, *104*, 250-260.
6. T. Kohzuma. *et al. unpublished results.*

Structure and Electrochemical Characterization of a Blue Copper Protein, Met16Phe/His6Val Pseudoazurin

Yuki GOTO¹, Akiko TAKASHINA¹, Tsuyoshi SAKAIRI¹, Masaki UNNO^{1,2}, and Takamitsu KOHZUMA^{1,2}

¹*Institute of Applied Beam Science, Ibaraki University, Mito 310-8512.*

²*Frontier Research Center for Applied Atomic Science, Ibaraki University, Tokai 319-1106.*

Pseudoazurin (PAz) is a blue copper protein, which functions as an electron donor to nitrite reductase in the reduction of NO₂⁻ to NO under anaerobic conditions [1]. The crystal structure of PAz revealed that the single copper atom is coordinated by His81, His40, Cys78, and Met86 amino acids with distorted tetrahedral geometry [2]. PAz shows an intense S(Cys) → Cu²⁺ ligand-to-metal charge transfer (LMCT) transition at approximately 600 nm in the visible region with another LMCT band around at 450 nm [3]. Recently, the biological significance of a weak interaction between the metal ion coordinated imidazole ring and the phenyl ring of a phenylalanine residue was elucidated in a blue copper protein, plastocyanin from a fern plant, *Dryopteris crassirhizoma* [4]. Phenylalanine was substituted Met16 in PAz from *Achromobacter cycloclastes* to investigate the π-π interaction between the imidazole ring of the solvent-exposed His81 aromatic ring and benzene ring of newly introduced Phe16. The Met16Phe PAz variant demonstrated the important role of the second coordination sphere of the active site regulating the structure and properties of the active site [5]. The X-ray crystal structure of PAz showed an uncoordinated His6 exists within the distance (~12 Å) from the copper site, and the reduction potential of PAz was shifted in the higher potential region. The higher reduction potential shift has been considered to be induced by the protonation of the uncoordinated His6. The remote His6 site has also been considered to contribute in the regulation of the electron transfer reaction of PAz [6].

In this study, Met16Phe/His6Val double mutant and His6Val were newly constructed and characterized to shed light on the more exact role of the π-π interaction in the vicinity of the active site. The electrochemical properties were investigated by cyclic voltammometry. The redox potentials of PAz and its mutant proteins were evaluated to be 260, 258, 305, and 309 mV for Wild Type, His6Val, Met16Phe, and Met16Phe/His6Val, respectively at pH 7.0. The reason of higher reduction potential shift is clearly concluded by the effect of π-π interaction between the imidazole ring of the coordinated His81 and benzene ring of the newly introduced Phe16.

1. M. Y. Liu, M. C. Liu, W. J. Payne, and J. Legall, *J.Bacteriol.* **1986**, 166, 604-608.
2. R. H. Holm, K. Pierre, E. I. Solomon, *Chem. Rev.* **1996**, 96, 2239-2314.
3. T. Inoue, N. Nishio, S. Suzuki, K. Kataoka, T. Kohzuma, Y. Kai, *J.Biol.Chem.* **1999**, 274, 17845-17852.
4. T. Kohzuma, T. Inoue, F. Yoshizaki, Y. Sasakawa, K. Onodera, S. Nagatomo, T. Kitagawa, S. Uzawa, Y. Isobe, Y. Sugimura, M. Gotowda, and Y. Kai, *J.Biol. Chem.* **1999**, 274, 11817-11823.
5. R. F. Abdelhamid, Y. Obara, Y. Uchida, T. Kohzuma, D. M. Dooley, D. E. Brown, H. Hori, *J.Biol. Inorg. Chem.* **2007**, 12, 165-173.
6. K. Sato, C. Dennison, *Biochem.* **2002**, 41, 120-130.

P-25*

Functional Regulation by Heme-Dependent Oxidative Modification in Iron Regulatory Protein 2 (IRP2)

Yudai NISHITANI¹, Yukiko TAKEDA², Takeshi UCHIDA^{1,3}, Kazuhiro IWAI², and Koichiro ISHIMORI^{1,3}

¹Graduated School of Chemical Sciences and Engineering, Hokkaido University, Hokkaido 060-0810. ²Graduated School of Medicine, Kyoto University, Kyoto 606-8501. ³Department of Chemistry, Faculty of Science, Hokkaido University, Hokkaido 060-0810.

Iron is indispensable metal for living organisms because it functions as an active center for biochemical reactions such as oxygen transport, electron transfer, and enzyme reaction. However, iron can react with molecular oxygen to generate reactive oxygen species (ROS), which is severe toxic for cells. Therefore, iron content in cells must be tightly regulated. Iron Regulatory Protein 2 (IRP2) is the primary regulator of iron metabolism in mammalian cells, controlling the translation of proteins involved in iron metabolism by binding to mRNA of the proteins. In iron-replete conditions, IRP2 loses the RNA binding activity by degradation of the ubiquitin-proteasome system. Previous studies reported that the heme binding to the iron-dependent degradation (IDD) domain is a trigger for the oxidative modification, leading to the degradation of IRP2, and the oxidative modification is promoted by ROS. Although the activation of molecular oxygen to ROS at the heme iron in the IDD domain is the crucial process in the oxidative modification in IRP2, the detail mechanism of ROS generation has not yet been clear. Here, we found the heme degradation in heme-bound IRP2 and identified the oxidative modification sites to propose a novel mechanism for the heme-induced oxidative modification in IPR2.

In previous studies, ROS responsible for the oxidative modification was supposed to be hydroxyl radical ($\cdot\text{OH}$), which would be formed by Fenton's reaction ($\text{Fe}^{2+} + \text{H}_2\text{O}_2 \rightarrow \cdot\text{OH} + \text{Fe}^{3+}$). Although Fenton's reaction requires non-heme iron, heme bound IRP has no endogenous non-heme iron, suggesting the iron release from the degradation of heme. To detect the release of heme, we used PDTS giving the characteristic absorbance at 562 nm in the presence of ferrous ion. The time course of the absorption spectra for heme bound IRP2 with PDTS clearly showed the absorbance at 562 nm concomitant with decrease in the intensity of the Soret band, a characteristic band of hemoprotein, confirming the release of iron from the degradation of heme.

The release of iron from heme suggests that the active center for $\cdot\text{OH}$ would be located around heme binding site in the IDD domain. Considering the short life time of $\cdot\text{OH}$, $\cdot\text{OH}$ would react with amino

acid residues in the IDD domain. To identify the modification site, we measured the mass spectrometry (MS) of intact and oxidized IRP2 and successfully detected a peak showing the specific shift from at m/z 3480 to at m/z 3496 upon the oxidation. This mass peak was attributed to a peptide fragment, ^{186}N - ^{216}K , in the IDD domain of IRP2 as we expected. In conclusion, we confirmed the release of iron from heme in the heme-induced oxidation of IRP2 and the oxidative modification is induced in the IDD domain, which leads to the specific recognition of ubiquitin ligase (E3) for the degradation in the ubiquitin-proteasome system (Fig.1).

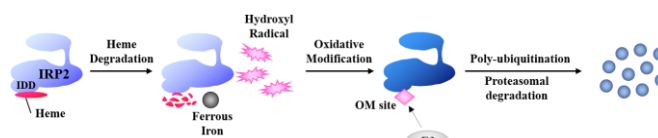


Fig.1. IRP2 OM mechanism

P-26*

Characterization of the Heme Effect on the Interaction between Iron Regulatory Protein (IRP) and the Targeted mRNA by Fluorescence Anisotropy

Yuta WATANABE¹, Yukiko TAKEDA², Takeshi UCHIDA^{1,3}, Kazuhiro IWAI², and Koichiro ISHIMORI^{1,3}

¹Graduate School of Chemical Sciences and Engineering, Hokkaido University, Hokkaido 060-0810. ²Graduate school of Medicine, Kyoto University, Kyoto 606-8501. ³Department of Chemistry, Faculty of Science, Hokkaido University, Hokkaido 060-0810

Iron is vital for almost all organisms because of many activities such as oxygen transport and electron transfer. Iron deficiency results in their decreased activities, causing anemia and immunological deterioration. In contrast, excess iron damages cellular macromolecules because the redox cycling of ferrous and ferric iron activates molecular oxygen to generate reactive oxygen species (ROS) by Fenton reaction. Thus, the iron control mechanism is essential for cells. Iron is delivered to most tissues via an iron transport protein, called transferrin (Tf), and binding to the transferrin receptor (TfR) leads to the receptor-mediated endocytosis. Absorbed iron is, then, carried to mitochondria for heme (iron-porphyrin complex) and iron-sulfur cluster biosynthesis, while the excess iron is stored in an iron storage protein, ferritin (Ft), to avoid the generation of ROS. The expression of TfR and Ft is post-transcriptionally controlled by iron regulatory proteins (IRPs). IRPs bind to the iron-responsive element (IRE) of the target mRNA, depending on the cellular iron content, to inhibit the binding of ribosome or 3'-endnuclease. It is the crucial step that IRPs sense the iron content in cell to regulate the translational activity of target mRNA. Recently, we have shown that two homologues of IRPs, IRP1 and IRP2, share the consensus sequences, heme regulatory motif (HRM), which is found in many heme-regulated proteins, suggesting that heme binding regulates the activity of IRPs.

Using the gel shift assay, we have shown that binding heme to IRP1 inhibits the formation of the complex with IRE. However, this assay was qualitative and the quantitative analysis is required to draw more convincing conclusions. Also, we failed the gel shift assay for IRP2 due to the low stability of the protein in the gel. Here, we used the fluorescence anisotropy to characterize the IRE binding to IRP under the physiological condition. The fluorescence anisotropy of the fluorescent group, 6-FAM, covalently bound to the 5'-end of the Ft IRE was followed in the titration of IRPs to IRE. K_d of the IRP1-IRE complexes was successfully estimated to be 6.85 ± 0.26 (nM) (red dots in Figure), which is comparable to that in other RNA binding proteins. In the presence of heme, formation of the IRP1-IRE complex was significantly suppressed (blue and black dots in Figure), supporting the inhibition of the IRE binding to IRP1 by heme. The specific and direct heme-induced inhibition of the IRE binding in IRP1 suggests a novel heme-dependent regulation mechanism in IRPs, showing that heme is a signaling molecule for the iron metabolism.

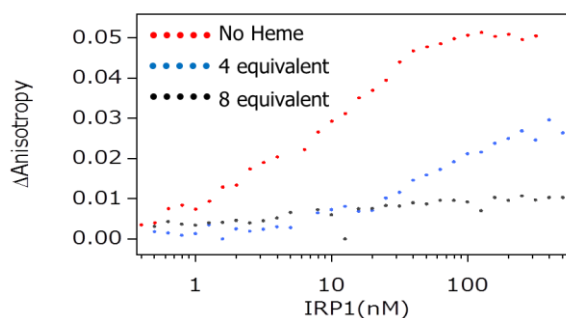


Figure. Heme-dependent regulation of IRP1 by Fluorescence Anisotropy

Structural Characterization of Heme Binding Sites in Iron Regulatory Protein1

Mariko OGURA¹, Yuta WATANABE¹, Yukiko TAKEDA², Takeshi UCHIDA^{1,3}, Kazuhiro IWAI², and Koichiro ISHIMORI^{1,3}

¹Graduate School of Chemical Sciences and Engineering, Hokkaido University, Hokkaido 060-0810. ²Graduate School of Medicine, Kyoto University, Kyoto 606-8501. ³Department of chemistry, Faculty of Science, Hokkaido University, Hokkaido 060-0810.

Iron is an essential element for many organisms. It has the ability to readily accept and donate electrons, allowing it to function as an oxidant or reductant in a large number of biochemical reactions. In mammals, iron is notably required for oxygen transport as a component of hemoglobin, and as an electron acceptor/donor in cytochromes. On the other hands, iron catalyzes the generation of free radicals that damage protein and DNA. Therefore, iron metabolism is tightly regulated. Iron Regulatory Proteins (IRPs) are the regulators of iron metabolism in mammalian cells. IRPs control the translation of proteins involved in iron uptake, storage and utilization by binding to the specific sequences of the mRNA, iron-responsive elements (IREs). IRPs have a typical heme regulatory motif (HRM), a consensus sequence found in heme-regulated proteins⁽¹⁾, suggesting that heme is the signaling molecule for IRPs. However, the ligation of heme in HRM of IRPs has not yet been confirmed spectroscopically. In this study, we report structural characterization of the heme binding to HRM in IRP1, one of the homologues of IRPs, using the absorption, resonance Raman spectroscopies to shed light on the functional significance of heme as the signaling molecule for iron metabolism.

Because the supposed heme binding site, HRM, was reported to have a cysteine residue, we measured the resonance Raman spectra of heme bound IRP1 to detect the Fe-Cys stretching mode. As shown in Fig. 1, a broad Raman line was observed around 330 cm⁻¹, as found for heme-regulated proteins such as Irr, but significantly different from that for conventional Cys-ligated proteins like P450 (~350 cm⁻¹). Although the isotope shift of the peak upon the replacement of ⁵⁶Fe-porphyrin with ⁵⁴Fe-porphyrin was not so clear, the deconvolution of the peak (dotted line in figure) showed that the peak at 331cm⁻¹ is shifted to 333cm⁻¹, confirming that a cysteine residue is one of the axial ligands in heme bound IRP1. To identify the cysteine residues as the axial ligands, we measured the resonance Raman spectra of two heme-bound mutants, C300A and C118A, having the mutations at the cysteine residue in HRM. The intensity of the Fe-Cys stretching mode was lower than that of wild type IRP1, corresponding to the ligation of Cys residues in HRM. Thus, the heme binding site for IRP1 is characteristic of heme-regulated proteins, indicating that heme functions as the signaling molecule for iron metabolism.

1. Chen, et al., *PNAS*, **1991**, 88, 315
2. Champion, et al., *J. Am. Chem. Soc.* **1982**, 104, 5469

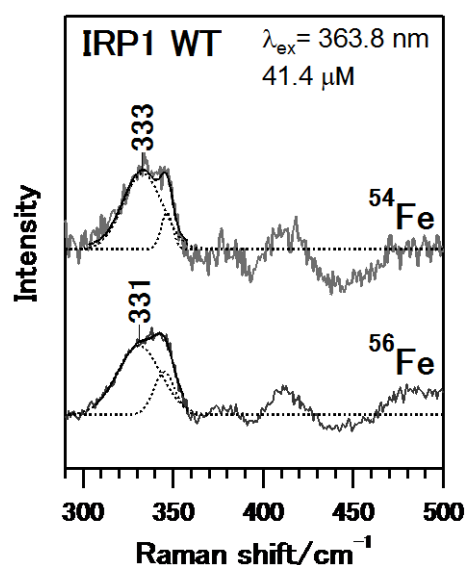


Fig.1 Resonance Raman spectra of the low-frequency region

Study of Radiometal-Octabromoporphyrin Complex as a Tumor Diagnostic Agent

Yoji KITAMURA^{1,2,3}, Kazuma OGAWA², Takashi KOZAKA¹, Miyuki NAKASHIMA¹, Mohammad A. AZIM³, Daisuke MIWA², Risa KUROMIYA⁴, Saya YURUZUME⁴, and Kazuhiro SHIBA^{1,2,3,4}

¹Advanced Science Research Center, Kanazawa University, Kanazawa 920-8640. ²Graduate School of Medical, Pharmaceutical and Health Sciences, Kanazawa University, Kanazawa 920-1192. ³Graduate School of Natural Science and Technology, Kanazawa University, Kanazawa 920-1192. ⁴School of Health Sciences, Kanazawa University, Kanazawa 920-1192.

Porphyrin is composed tetrapyrrole structure compound, and capable of forming stable coordinated complexes with metal ions, and is known to accumulate in a tumor. Among the porphyrin derivatives, the hematoporphyrin derivatives are used as photosensitizers for photodynamic therapy and fluorescence imaging. But the application of hematoporphyrin derivatives fluorescence imaging is limited to surface tumor due to the invasive endoscopy procedure. Radiolabeled porphyrins with short half-life gamma emitters could be better tumor imaging agent. We previously found that octabrominated porphyrin derivatives rapidly form metal complexes, and ¹¹¹In complex of Octabromotetrakis(4-carboxyphenyl)porphine (¹¹¹In-OBTCPP) accumulated in Colon26 and NB2a tumor tissues of tumor-bearing mice. In this study, to examine the possibility of radiometal-octabromoporphyrin complex as a tumor imaging agent, we investigated the accumulation of ¹¹¹In-OBTCPP in another type of tumor, KLN205 (lung squamous cell carcinoma), in vivo.

OBTCPP was synthesized according to the method previously reported¹⁾. The ¹¹¹In complex of OBTCPP (¹¹¹In-OBTCPP) was prepared by using microwave. The radiochemical purity of ¹¹¹In-OBTCPP was 98% in the analysis of TLC. KLN205 cell (mouse cell line derived from lung squamous cell carcinoma) was cultured in a RPMI1640 medium with 10% FBS. Tumor bearing mice was made by s.c. injection of 5×10^6 cells of KLN205 in femoral region and shoulder of BALB/c mice. Biodistribution study of ¹¹¹In-OBTCPP was performed with the tumor bearing mice.

The blood clearance of ¹¹¹In-OBTCPP was relatively low, but 24 h after injection, radioactivity in blood was lower than 0.4% dose/g. ¹¹¹In-OBTCPP was highly accumulated in liver and kidney, but cumulative excretion via urine and feces for 24 h was very low. Further investigation is needed to elucidate the cause of high accumulation in these organs.

¹¹¹In-OBTCPP was accumulated in both KLN205 tumor time dependent manners, and at 24 h after injection, the accumulation of ¹¹¹In-OBTCPP was reached about 5% dose/g, and tumor to muscle ratio was over 10 in the tumor. These results suggest that ¹¹¹In-OBTCPP may be applicable for lung squamous cell carcinoma. On the basis of above results, ¹¹¹In-OBTCPP has possibility for tumor diagnostic agent.

1) M. Mifune, K Kawata, K Tanaka et al., *Chem. Pharm. Bull.* **2006**, 54(1), 94

P-29*

Development of ¹¹¹In-labeled Exendin-4 Derivative Targeting GLP-1 Receptors for Pancreatic Beta-cell Imaging

Kaori KAMBE¹, Hiroyuki KIMURA¹, Kentaro TOYODA², Hiroyuki FUJIMOTO², Masahiro ONO¹, Nobuya INAGAKI², and Hideo SAJI¹

¹Graduate School of Pharmaceutical Science, Kyoto University, Kyoto 606-8501. ²Graduate School of Medicine, Kyoto University, Kyoto 606-8507.

Many metallic compounds have biological activities, but their application for the diagnosis and treatment of diseases has been limited because it is difficult to control the specific localization to target site and biological activity. Thus, it has been interest to the development of a compound containing independent groups with the ability to both deliver into the target site and bind a metallic ion, recently. Under these circumstances, we have a plan to develop the peptide derivative with a radiometallic nuclide for nuclear medical diagnosis of diabetes mellitus.

Pancreatic β -cell mass (BCM) decreases in the type 2 diabetes mellitus (T2DM). Thus, to evaluate BCM *in vivo* with nuclear medical imaging, we selected Exendin-4 (Ex4) as the mother compound, a stable agonist of glucagon-like peptide-1 receptors (GLP-1R) which are selectively expressed on pancreatic β -cells, and bound ¹¹¹In to it using diethylenetriamine pentaacetic acid (DTPA) as a chelating moiety since the chelating reaction is quick and easy and useful for radiolabeling with short-lived radioisotopes. ¹¹¹In-DTPA12-Ex4 produced, showed highly affinity to GLP-1R *in vitro*.

In vivo behavior of these radiometallic compounds is expected to be influenced by the presence of ligand in the solution because it may block the specific uptake. Thus, the decrease of this blocking effect by reducing amount of the ligand is effective on *in vivo* behavior. However, it is difficult to separate the radiolabeled compound from the ligand as the difference between the two evaluate is relatively small. So, optimization of the labeling condition was performed at lower amount of ligand. The biodistribution studies of ¹¹¹In-DTPA12-Ex4 produced were performed in ddY mice. *Ex vivo* autoradiography was conducted in the mouse insulin I promoter-green fluorescent protein (MIP-GFP) transgenic mice to evaluate the specificity for pancreatic β -cells. SPECT imaging studies were performed on the ddY mice. The biodistribution study examined its accumulation in the pancreas and fasting plasma glucose in a mouse model of streptozotocin-induced β -cell loss.

As a result of optimization of the labeling condition, the ¹¹¹In-labeled compound, which has a 4.1-fold higher specific activity (369 GBq/ μ mol) than the previously reported ¹¹¹In-labeled Ex4 derivative (*JNM*,47;2025(2006)), was obtained. In the biodistribution study, high uptake into the pancreas (30.2%ID/g) was observed at 30 min post injection. *Ex vivo* autoradiography showed that the intensity of the fluorescent signals of the pancreatic sections of MIP-GFP mice also correlated with that of the radioactive signals, indicating specific and high level of ¹¹¹In-DTPA12-Ex4 binding in pancreatic β -cells. In SPECT/CT images, the pancreas was clearly visualized. Pancreatic uptake in the diabetic models was decreased by 42% ($P < 0.001$) compared with that in healthy controls. There was an inverse relationship between the accumulation in the pancreas and fasting plasma glucose in individual mice.

These results suggest that ¹¹¹In-DTPA12-Ex4 has a potential to detect decreased pancreatic BCM *in vivo*.

Chelation of Tricarbonyl-^{99m}Tc with Microwave Systems and Its Application of Synthesis of ^{99m}Tc Labeled Prostate Cancer Imaging Agent

Sotaro SAMPEI, Hiroyuki KIMURA, Naoya HARADA, Masahiro ONO, and Hideo SAJI

Department of Pharmaceutical Sciences, Graduate School of Kyoto University

Some radioactive metals are used in the field of nuclear medicine for imaging and radioimmunotherapy. However, when large amount of precursor are used for radiosynthesis, accumulation of radioactive metals on the target are inhibited because of the precursor. So, the methods of effective radiosynthesis are needed to reduce the amount of precursor.

Technetium-99m (^{99m}Tc) is one of the useful radioactive metals in nuclear medicine diagnosis and is a γ -emitter at an appropriate energy (141 keV) for single photon emission computed tomography (SPECT). Various ^{99m}Tc complexes can be prepared via the coordination of ^{99m}Tc species with low oxidation number with ligands. ^{99m}TcO₄.Triaquatricarbonyl ^{99m}Tc cation ([^{99m}Tc(CO)₃(H₂O)₃]⁺), which can be prepared easily using a commercially available kit (IsoLink kit®), forms compact and stable chelates (tricarbonyl-^{99m}Tc chelates) with a variety of tridentate ligands. Furthermore, we previously showed that microwave systems provide early and effective tricarbonyl-^{99m}Tc chelation.⁽¹⁾

Prostate cancer (PCa) is the most commonly diagnosed form of cancer and the second leading cause of cancer-related deaths in men in the world. The prostate specific membrane antigen (PSMA) is a notable PCa imaging target because of its increased expression in PCa.

PSMA exhibits GCP-II (glutamatecarboxy peptidase-II) activity. Previously, several asymmetric urea compounds (X-CO-Glu) were reported to act as GCP-II inhibitors. We also demonstrated the high affinity of asymmetric urea compounds (maleimido-Cys-CO-Glu) for PSMA *in vivo*.⁽²⁾

Given this background, in this study, we designed [^{99m}Tc]-TCMCE ([^{99m}Tc]-Tricarbonyl-chelating-maleimido-L-Cys-CO-L-Glu) and evaluated its early and effective chelation via a microwave systems and its utility as a novel PSMA imaging probe.

For the preparation of the ^{99m}Tc-complex, we investigated the method using microwave, compared with that of conventional oil bath. We found that the radiochemical yield (RCY) of [^{99m}Tc]-TCMCE reached the plateau significantly earlier with microwave heating than with a conventional oil bath. Moreover, we effectively achieved a good RCY of [^{99m}Tc]-TCMCE via microwave (>20%). In contrast, the oil bath yielded a low RCY of [^{99m}Tc]-TCMCE at a precursor concentration of 3.0 mM.

In cell uptake study, the uptake of [^{99m}Tc]-TCMCE by LNCaP cells (PSMA++) was significantly larger than by PC-3 cells (PSMA-). Moreover, SPECT/CT study demonstrated that the LNCaP tumor was clearly visualized with [^{99m}Tc]-TCMCE.

In conclusion, we suggest that the microwave system is an effective tool for the radio synthesis of tricarbonyl-^{99m}Tc chelates and also that the tricarbonyl-^{99m}Tc complex, [^{99m}Tc]-TCMCE, is a potential PSMA-imaging probe for PCa detection.

(1 J. Oreg. Chem. 696, 3745-3749 (2011)

(2 J. Med. Chem. 56, 7890-7901 (2013)

P-31*

Evaluation of the Usability of ^{64}Cu -labeled Antibody Probe for Imaging Cytotoxic T Lymphocyte-associated Antigen-4 in Tumor

Kei HIGASHIKAWA^{1,2}, Keiko WATANABE¹, Shinichiro KAMINO³,
Masashi UEDA¹, Makoto HIROMURA³, and Shuichi ENOMOTO^{1,3}

¹Graduate School of Medicine, Dentistry, and Pharmaceutical Sciences, Okayama University, Okayama 700-8530. ²Japan Society for the Promotion of Science, Okayama 700-8530. ³Next-generation Imaging Team, RIKEN Center for Life Science Technologies, Kobe 650-0047

Cytotoxic T lymphocyte-associated antigen-4 (CTLA-4) blockade therapy by anti-CTLA-4 monoclonal antibody is remarkably effective for patients with cancer. However, this pharmaceutical agent potentially causes autoimmune-related side effects and is extremely expensive. Therefore, development of the evaluation method of CTLA-4 expression before CTLA-4 targeted therapy is expected to open door to evidence-based and cost-efficient medical care, and avoid the side effects by ineffective therapy. Thus, in this study, we developed the antibody probe for visualization of CTLA-4 in the tumor. First, we examined CTLA-4 expression in the normal colon tissues, cultured CT 26 cells, and CT26 tumor tissues from tumor-bearing BALB/c mice and BALB/c nude mice by RT-PCR analysis. Second, we newly synthesized ^{64}Cu -1,4,7,10-tetraazacyclododecane-*N*, *N'*, *N''*, *N'''*-tetra-acetic acid-anti-CTLA-4 monoclonal antibody (^{64}Cu -DOTA-anti-CTLA-4 antibody) for CTLA-4 imaging, and evaluated its usefulness through positron emission tomography (PET) imaging and ex-vivo biodistribution analysis with CT26-bearing BALB/c mice. High CTLA-4 expression was confirmed in the CT26 tumor tissues of tumor-bearing BALB/c mice. However, CTLA-4 expression is extremely low in the cultured CT26 cells and in the CT26 tumor tissues of tumor-bearing BALB/c nude mice. These results suggested this high CTLA-4 expression was responsible for T cells. Furthermore, our ^{64}Cu -DOTA-anti-CTLA-4 antibody displays significantly high uptake in the CT26 tumor, and we succeeded in the non-invasive visualization of CTLA-4 in the tumor. These results showed ^{64}Cu -DOTA-anti-CTLA-4 antibody would be useful for evaluation of CTLA-4 expression in the tumor.

P-32*

Development of Peptide Chelator for ^{64}Cu Focused on ATCUN Motif

Yuta FUKINO¹, Takaaki MIYAMOTO¹, Shinichiro KAMINO¹, Masashi UEDA¹ and Shuichi ENOMOTO^{1,2}

¹Graduate School of Medicine, Dentistry, and Pharmaceutical Sciences, Okayama University ²The RIKEN Center for Life Science Technologies

^{64}Cu has favorable nuclear characteristics ($t_{1/2} = 12.7$ h, β^+ 17.4%) for positron emission tomography/X-ray computed tomography (PET/CT) imaging. Bifunctional chelating agents (BFCs) are often used for radiolabeling of targeting molecules with ^{64}Cu . We focused on peptide-based chelators because peptide chelators were easily obtained by solid phase peptide synthesis on automatic peptide synthesizer. We utilized amino terminal Cu^{2+} - and Ni^{2+} -binding (ATCUN) motif (XXH) as a BFC for ^{64}Cu . The aim of this study was to investigate the effect of the bulky amino acid residues at positions 1 and 2 on the stability of the ^{64}Cu -ATCUN complexes in blood plasma, and select for the compound which is the most suitable for PET/CT imaging study.

In this study, we have prepared the model peptides by conjugating various ATCUN peptides to tumor-targeting octreotide (YYH-Oct **1**, VVH-Oct **2**, NNH-Oct **3**, TTH-Oct **4** and GGH-Oct **5**). The radiolabeling of these peptides with ^{64}Cu was performed in HEPES buffer (pH 7.5) at 37 °C for 30 min. The ^{64}Cu labeled with **1-5** was incubated in rat plasma for 2 h at 37°C, and the plasma stability was analyzed by size-exclusion HPLC, respectively. Competitive binding assay between the Cu labeled with **1-5** and [^{125}I -Tyr³]-Oct for the somatostatin receptor subtype 2 (SSTR-2) was performed by using rat pancreatic AR42J tumor cells. The half maximal inhibitory concentration (IC_{50}) of the compounds was then calculated. Biodistribution study was investigated in BALB/c nude mice bearing subcutaneous SSTR-2 expressing AR42J tumors. Mice were injected via the tail vein with 100 kBq of ^{64}Cu -**1**. Blocking was performed by coinjection of 500 μg of Oct. Mice were dissected at 2 h after the injection and several tissues were removed. The tissue radioactivity was measured by γ -counter. PET-CT images were acquired on Clairvivo PET. Mice bearing AR42J tumors were injected via the tail vein with 1.5 MBq of ^{64}Cu -**1**.

All the radiolabeled ATCUN-Oct derivatives were obtained with radiochemical purity of > 95%. The plasma stability assay revealed the ^{64}Cu -**1** was the most stable in plasma at 2 h ($85.8\% \pm 0.9$), as compared to that of ^{64}Cu -**2**, **3**, **4** and **5** ($79.1 \pm 1.4\%$, $71.5 \pm 0.9\%$, $58.5 \pm 2.2\%$ and $19.6 \pm 1.4\%$). The results indicated that the structural bulkiness of amino acid residues at position 1 and 2 of ATCUN motif contributes to the stability of the compounds in blood plasma. Cu-**1** also had the highest binding affinity ($\text{IC}_{50} = 55.4 \pm 2.4$ nM) followed by Cu-**2** (139 ± 9.5 nM), **4** (188 ± 54 nM), **5** (217 ± 110 nM) and **3** (547 ± 170 nM). From these results, it was anticipated that **1** is promising as a BFC for ^{64}Cu . Therefore, both biodistribution study and PET/CT imaging study were performed by using **1** as a BFC. The uptake of ^{64}Cu -**1** in the target tumors (1.88 ± 0.42 %ID/g) was higher than that in blood (0.47 ± 0.07 %ID/g) and muscle (0.10 ± 0.07 %ID/g). On the blocking study, the tumor-to-blood ratios decreased from 4.02 ± 0.91 to 1.61 ± 0.50 ($p < 0.01$). This demonstrated that the tumor accumulation was specific. ^{64}Cu -**1** visualized SSTR-2-expressing xenografts by PET/CT imaging.

A Comprehensive Investigation of Reactions between a Reduced Metabolite of Selenious Acid and Hepatic Cytosolic Proteins

Eriko HORI¹, Sakura YOSHIDA¹, Mamoru HARATAKE², Takeshi FUCHIGAMI¹ and Morio NAKAYAMA¹

¹Graduate School of Biomedical Sciences, Nagasaki University, Nagasaki 852-8521 Japan, ²Faculty of Pharmaceutical Sciences, Sojo University, Kumamoto 860-0082 Japan.

Selenium is an essential micronutrient for humans and other higher animal species. Selenious acid (SA), an effective selenium source, is non-enzymatically reduced to selenotrisulfide (STS) by glutathione. Subsequently, it is thought to derivatize to hydrogen selenide (H₂Se), selenophosphate (H₃SePO₃) and then incorporate into selenocystein. However, the definitive metabolic pathways from SA to the selenoproteins are not fully understood yet. In general, the methodological difficulties for studying the metabolic fate of SA include: a) trace element, b) diversity of oxidation state accompanying metabolic reduction and c) no effective probe materials responsible for selenium compounds. In this study, we comprehensively investigated the reaction between rat liver cytosolic proteins and the metabolic intermediate, STS by MALDI TOF-mass spectrometry.

Chemically stable L-penicillamine STS (PenSSeSPen) was used as a STS species. After the incubation of PenSSeSPen with the liver cell lysate from 3-week old male Wistar rat, the resulting cell lysates were dialyzed against 5 mM Tris/HCl (pH 7.4) for removal of unreacted PenSSeSPen and low-molecular mass thiols. Subsequently, selenium and protein thiol concentrations in the dialysate were determined. While the amount of selenium bound to proteins increased, protein thiol content decreased, indicating that the cytosolic proteins were reacted with PenSSeSPen. Such reactive proteins in the cell lysate were characterized by MALDI TOF-mass spectrometry. A 14 kDa-protein was alkylated by *N*-ethylmaleimide, thiol-alkylating reagent, and its mass number increased by 125. This protein from the PenSSeSPen-treated cell lysate gave a peak at 14313 *m/z*, resulting in an increase in *m/z* by 226.3 in comparison to that from the non-treated one (Fig. 1). Such an increase in the molecular mass of the 14 kDa-protein corresponded to the selenenyl-Pen moiety (SeSPen), demonstrating the formation of protein–SeSPen species through thiol-exchange. This protein was thought to be liver fatty acid-binding protein (L-FABP) by protein database search. L-FABP contains only free thiol at Cys69 that allows reacting with PenSSeSPen. L-FABP-derived fragments were detected from the trypsin-digested cell lysate. L-FABP was thought to be one of the liver cytosolic proteins that can react with the STS species. In fact, L-FABP has also been identified as the major selenium-binding protein after i.p. administration of radioactive ⁷⁵Se-labeled SA in mouse (*J. Biol. Chem.*, 1989, **264**, 13780). Consequently, our approach using the metabolic intermediate was thought to be an effective methodology for uncovering cytosolic proteins reacting with selenium species.

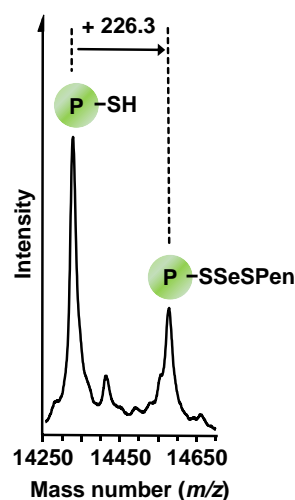


Fig. 1. MALDI TOF-mass spectrum of PenSSeSPen treated-liver cell lysate.

P-34

Thiol-Mediated Sequential Metabolism of Selenium Compounds Leading to Cytotoxicity Against Breast Cancer Cells

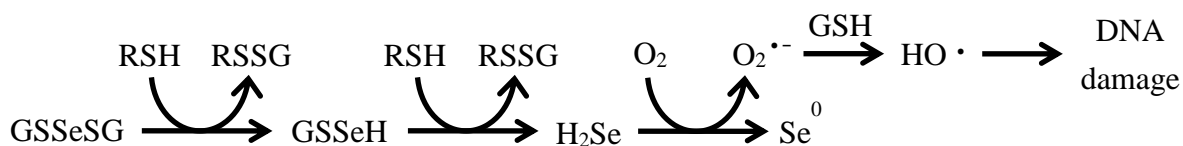
Shino MATSUDA, Takao TOBE, Kazuya TANIGUCHI, Masayuki HAYASHI, Yoshinori OKAMOTO, Koji UEDA, and Nakao KOJIMA

Faculty of Pharmacy, Meijo University, Nagoya 468-8503

Selenium (Se) is an essential micronutrient, and its cancer preventive effects have been reported. Actually, Se exerts selective cytotoxicity against cancer cells above the nutritional levels. Because the pharmacological window is very close to the toxic levels for normal cells, elucidation of the toxicity mechanism is essential for the safe use of Se. We have observed that a primary metabolite of selenite (selenodiglutathione, GSSeSG) induced oxidative DNA damage rather than selenite in the presence of thiols such as glutathione (GSH). In the present study, we have investigated potential roles of thiols in the mechanisms by which Se exerts the cancer-selective cytotoxicity.

GSSeSG was prepared by mixing selenite and 4-fold GSH under acidic condition and purified using preparative HPLC. Cell viability was evaluated by live-cell specific fluorescent reagent in human breast cancer cells MCF-7. Apoptotic cell death was determined by Annexin V assay using a flow cytometer. Amount of 8-oxo-7,8-dihydro-2'-deoxyguanosine in genomic DNA was determined by LC-MS. Nuclear DNA fragmentation was determined by comet assay followed by fluorescence intensity analyses. Single strand breaks in a plasmid pBR322 were measured by agarose gel electrophoresis.

GSSeSG suppressed cell viability and increased apoptotic cell population. Under the same concentrations used for these cell events, GSSeSG induced 8-oxodG formation and nuclear DNA fragmentation. These correlations indicate that GSSeSG induces apoptosis via oxidative stress including DNA damage. Neither NADH, NADPH, FAD, nor oxidized glutathione (GSSG) induced DNA damage together with GSSeSG, whereas all tested thiols such as GSH, cysteine, or homocysteine did. These suggest a thiol-specific mechanism rather than oxido-reductive events for the Se-induced DNA damage. This DNA damage was decreased by the addition of ethanol, indicating the involvement of hydroxyl radicals (HO^\cdot). However, Fenton-based generation mechanisms involving transition metals are not likely due to the absence of metals in the systems. Alternatively, thiol-mediated radical generation would be possible, although its detailed mechanism is unclear. This notion would be supported by the observation that GSH was still needed to induce cytotoxicity for H_2Se , which is a resulting product in the GSH-mediated sequential Se metabolism followed by autooxidation generating superoxide anion radical ($\text{O}_2^{\cdot-}$). In conclusion, thiols induce cytotoxicity of Se via multiple roles including catalyst for HO^\cdot generation as well as the reported sequential metabolism of Se (Scheme 1).



Scheme 1. Proposed pathway of Se metabolism leading to DNA damage.

P-35*

Analysis of Manganese Accumulation Mechanism by TNF α and IL-1 β in SH-SY5Y Cells

Tomoki KITAYAMA, Hitomi FUJISHIRO, and Seiichiro HIMENO

Laboratory of Molecular Nutrition and Toxicology, Faculty of Pharmaceutical Sciences, Tokushima Bunri University

Exposure to an excess amount of manganese (Mn) causes neurological symptoms similar to Parkinson's disease. Zinc transporters such as Zrt, Irt-related protein 8 (ZIP8), and ZIP14 have been shown to have affinities for Mn²⁺ and Cd²⁺ as well as Zn²⁺, but their roles in Mn²⁺ uptake in neuronal cells remain unclear. In a previous study, we found that the pretreatment of human SH-SY5Y neuroblastoma cells with interleukin-6 (IL-6) markedly increased the accumulation of Mn, which could be partly explained by the increased uptake of Mn²⁺ due to the up-regulation of ZIP14 by IL-6¹⁾. The treatment of SH-SY5Y cells with IL-6 decreased the expression levels of ZnT10, which has been shown to be involved in Mn excretion. These results suggest that both the up-regulation of ZIP14 and the down-regulation of ZnT10 by IL-6 might have enhanced the accumulation of Mn in SH-SY5Y cells.

We examined the roles of other inflammatory cytokines such as TNF α and IL-1 β on Mn accumulation in SH-SY5Y cells. The treatment of SH-SY5Y cells with TNF α and IL-1 β increased 24-h Mn accumulation. Also, the treatment of SH-SY5Y cells with TNF α and IL-1 β increased both mRNA and protein levels of ZIP8 and ZIP14, while decreased both mRNA and protein levels of ZnT10. These results are in accordance with the changes caused by treatment with IL-6, suggesting that there is a common mechanism underlying the increased Mn accumulation by the inflammatory cytokines.

To confirm the roles of ZIP8 and ZIP14, we introduced cDNAs of ZIP8 and ZIP14 into SH-SY5Y cells. The over-expression of ZIP8 and ZIP14 each resulted in the increases in the uptake of Mn²⁺ and Cd²⁺, suggesting that both ZIP8 and ZIP14 have the ability for the uptake of Mn²⁺ and Cd²⁺ in SH-SY5Y cells. The mechanism of the down-regulation of ZnT10 by the cytokines, and the role of ZnT10 in Mn accumulation are now under examination.

Extensive evidence has demonstrated that inflammatory cytokines such as IL-6, TNF α , and IL-1 β are deeply associated with the pathogenesis of various neurodegenerative disorders. Here we show that IL-6, TNF α , and IL-1 β have similar characteristics in Mn transport. Our results provide new insight into the roles of zinc transporters in the aberrant Mn accumulation in neuronal cells, particularly in the presence of inflammatory cytokines.

1) Fujishiro et al., *Metallomics*. 2014, 6(4):944-9.

P-36*

Hydrogen Peroxide Triggers a Novel Alternative Splicing of Arsenic (+3 Oxidation State) Methyltransferase Gene

Chieri TAKEDA, Daigo SUMI, and Seiichiro HIMENO

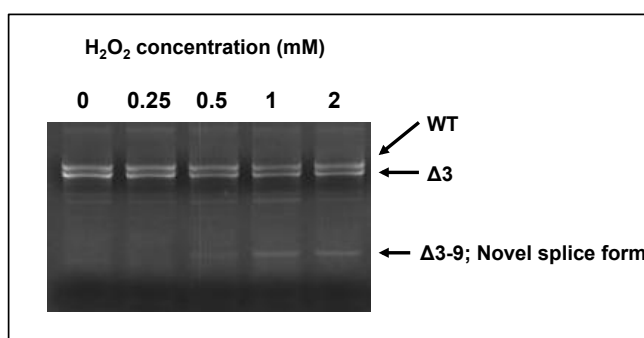
Faculty of Pharmaceutical Sciences, Tokushima Bunri University, Tokushima 770-8514

Arsenic (+3 oxidation state) methyltransferase (AS3MT) catalyzes the methylation of trivalent arsenic (As(III)) to monomethylarsonate and dimethylarsinic acid. Epidemiological studies have suggested that the difference in expression of AS3MT is involved in individual differences in the capacity for arsenic methylation among the people living in arsenic-polluted areas.

We previously reported the identification of two splicing variants of human AS3MT gene, which are exon 3 skipping ($\Delta 3$) and exon 4 and 5 skipping ($\Delta 4,5$), in HepG2 cells¹. The lack of methyltransferase activity of the recombinant $\Delta 4,5$ AS3MT was detected, suggesting that the alternative splicing of AS3MT gene may also be involved in the reduced arsenic methyltransferase activity. Thus, we examined whether exposure of HepG2 cells to As(III) alters the levels of $\Delta 4,5$ AS3MT mRNA. The real-time PCR experiments showed that the levels of $\Delta 4,5$ AS3MT mRNA increased in the HepG2 cells exposed to 10 μM As(III). However, the levels of wild type (WT) AS3MT mRNA also increased.

On the other hand, it has been reported that exposure to arsenic stimulates reactive oxygen species (ROS) generation in various cells. Thus, we examined whether ROS trigger the alternative splicing of AS3MT gene. After exposure of HepG2 cells to hydrogen peroxide (H_2O_2), we performed RT-PCR with the primers located at exon 1 and exon 10 to detect WT, $\Delta 3$ and $\Delta 4,5$ AS3MT mRNAs. The results indicated that H_2O_2 did not affect the levels of WT, or $\Delta 3$ AS3MT mRNA. However, we detected a novel band at 240 bp. The intensities of the bands increased in a H_2O_2 concentration-dependent manner. The results of DNA sequencing revealed that the novel band at 240 bp is derived from the AS3MT mRNA which skipped the exons from 3 to 9 ($\Delta 3-9$) (See right figure). The $\Delta 3-9$ spliced form was not detected in the HepG2 cells exposed to *tert*-butyl hydroperoxide or cumene hydroperoxide. In order to gain insight into how H_2O_2 enhances the alternative splicing of AS3MT gene, we searched the database to analyze putative binding sites of the exons of AS3MT for the splice factors. Several factors such as serine-arginine rich (SR) and heterogeneous nuclear ribonucleoprotein (hnRNP) are found as candidate splice factors that can bind to the exons of AS3MT gene and enhance and suppress the occurrence of alternative splicing.

To our knowledge, this is the first report showing that H_2O_2 triggers alternative splicing of AS3MT gene. We are currently examining whether H_2O_2 affects the levels of these splice factors.



¹ D. Sumi, K. Fukushima, H. Miyataka, and S. Himeno. *Biochem. Biophys. Res. Commun.* **2011**, 48-53.

P-37

Nuclear Trafficking of Zinc Finger Protein and Several Factors

Jun KUWAHARA, Yumi YANAGIHARA, Yuri YOSHIKAWA

*Faculty of Pharmaceutical Sciences, Doshisha Women's University,
Kyotanabe City, Kyoto 610-0395*

Zinc finger motif is one of the most abundant protein motif in eukaryotic genomes. It possesses repeats of zinc-binding module which contains conserved four metal-coordinating amino acids, cysteine and/or histidine residues. We have been intrigued by versatility of these motifs and have been searching a novel role for them, especially protein interaction. One of these functions is nuclear localization signal (NLS).

Bidirectional traffic between the cytoplasm and the nucleus is routed through the nuclear pore complex (NPC) embedded in the nuclear envelope. Nuclear import of globular proteins of greater than approximately 60 kDa in size is an active process that requires the presence of a suitable nuclear localization signal (NLS) and is mediated by a related family of shuttling transport factors, importins, which can recognize NLS. Nuclear trafficking of classical NLS-containing protein is mediated by a specific complex with transport factors such as importin α and importin β , and then the NLS-importin α/β complex is transported into the nucleus. Most of classical NLS can be recognized by an adaptor protein importin α , whereas a few NLS is the target of importin β .

Sp1 is a human ubiquitous transcription factor involved in the early development of an organism. The protein comprises three tandem repeats of C2H2 zinc finger motif at its carboxyl terminus, binds directly to a GC-rich element of DNA (GC box)(1) and activates reasonably large subset of mammalian genes containing GC box upstream promoter elements.

Like other nuclear proteins, Sp1 is supposed to be actively transported into the nucleus due to its molecular mass (95 kDa). We identified that three C2H2 zinc fingers of Sp1 can serve as a 'bona fide' NLS. Then, we analyzed several factors affecting nuclear localization. Overall tertiary structure formed by zinc binding is essential for its NLS function as well as basic amino acids dispersed in the entire zinc finger region (2). Solid-phase binding assay using cytoplasmic extract from HeLa cell suggests that Sp1 zinc fingers can directly interact with at least one of transport factors (3). A series of basic amino acids in zinc finger region play pivotal role for specific DNA recognition (Fig.1). Those may also contribute to the interaction with transport protein because classic NLS has one or two basic clusters which would be important for importin binding. Then, we tried to use specific DNA as a probe to evaluate comprehensively the role of basic amino acids dispersed within the entire zinc finger region on interaction with transport factors. The mode of protein interaction via the zinc finger domain will be discussed. The roles for zinc fingers of Sp1 as a NLS would be compared to those of other zinc finger-type transcription factors.

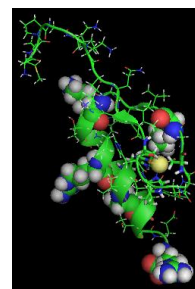


Fig.1 Basic amino acids in the zinc finger motif are displayed as a spherical view.

References:

- (1) J. Kuwahara, J. E. Coleman, *Biochemistry* **29**, 8627-8631 (1990).
- (2) T. Ito, M. Azumano, M. Uwatoko, C. K. Itoh, J. Kuwahara, *Biochem. Biophys. Res. Commun.* **380**, 28-32 (2009).
- (3) T. Ito, H. Kitamura, C. Uwatoko, M. Azumano, K. Itoh, J. Kuwahara, *Biochem. Biophys. Res. Commun.* **403** 161-166 (2010).

Metallomic Study of Zn and First Transition Metals with Anti Life-Style Related Diseases Properties

Yutaka YOSHIKAWA^{1,2}, Chihiro ANDO¹, Chiaki KANAOKA¹, Yoshiki KURIYAMA¹, Sawako SHIOMI¹, Naoko SETA¹, and Hiroyuki YASUI¹

¹*Department of Analytical and Bioinorganic Chemistry, Kyoto Pharmaceutical University, Kyoto, 607-8414.* ²*Department of Health, Sports, and Nutrition, Kobe Women's University, Kobe, 650-0046.*

Diabetes mellitus (DM) is a life-style related disease. DM is one of the most common chronic diseases extensively spread in the world. DM sometimes causes many severe secondary complications, such as atherosclerosis, diabetic retinopathy, and ocular disorders. Thus we try to improve DM and their complications at the same time.

We have previously reported that some metal ions and their complexes show the anti-diabetic effects. Moreover, there are several reports on the relationship between metal ions and enzyme activity; however, studies on the effect of essential metal ions and regulation of *in vivo* enzymes action are quite limited. We thus examined the inhibitory effects of Zn and various first transition metal ions against α -glucosidase, angiotensin converting enzyme (ACE), pancreatic lipase, and saliva amylase which are closely related with DM and life-style related diseases. The α -glucosidase, ACE, lipase, and amylase inhibitory effects were estimated according to the previously reported methods [1-4]. The inhibitory effects of VO, Ni, Cu, and Zn ions against α -glucosidase (from rat small intestine), Cr, Ni, Fe, and Cu ions against ACE (from rat plasma), Fe, Ni, Cu, and Zn ions against pancreatic lipase (from pig), and VO, Fe, Cu, and Zn ions against amylase (from human saliva) were found to be dose-dependent, respectively. The apparent IC₅₀ values, the 50% inhibitory concentration of the compounds on four kinds of enzymes activity, were estimated from the *in vitro* activity curves. The order of α -glucosidase inhibition was Zn < Cu >> VO > Ni. The order of ACE inhibition was Ni > Cu >> Fe > Cr. Moreover, the order of pancreatic lipase and amylase were Fe > Zn >> Cu > Ni and Cu > Fe >> Zn >>> VO respectively. These results indicated that Cu and Zn ions may inhibit α -glucosidase action in the epithelium of the small intestine and reduce disaccharide digestion. Ni, Cr, and Cu ions inhibiting ACE action exhibit the possibility of the anti-hypertensive action. And Fe and Zn ions inhibiting pancreatic lipase action exhibit the possibility of the anti-hyperlipemia. Furthermore, Cu and Fe ions inhibiting amylase action may reduce the starch digestion. We propose that to combine Zn or the first transition metals may improve the DM and their complications.

[1] Anal. Biochem., **7**, 18-25 (1964) [2] J. Chromatogr., **233**, 123-130 (1982) [3] JP patent 56860 (2006) [4] JP patent 27389 (1992)

P-39*

Effect of Zn(bpy)Cl₂ on Osteoblast Activation and an Osteoporosis Mouse Model

Akira ONODERA¹, Takafumi ISHIBASHI¹, Natsumi NEZU¹, Shuji YASUIKE², Hiroshi NAKA³, Masanobu UCHIYAMA⁴, Masahiko SATHO², Toshiyuki KAJI⁵, Norio ITOH⁶, and Yuichi KAWAI¹

¹Faculty of Pharmaceutical Sciences, Kobegakuin University, Kobe 650-8568. ²School of Pharmacy, Aichi Gakuin University, Nagoya 464-8650. ³Department of Chemistry, Research Center for Materials Science, Nagoya University, Nagoya 464-8602. ⁴Graduate School of Pharmaceutical Sciences, Tokyo University, Tokyo 113-0033. ⁵Faculty of Pharmaceutical Sciences, Tokyo University of Science, Chiba 278-8510. ⁶Graduate School of Pharmaceutical Sciences, Osaka University, Osaka 565-0871

Background & Purpose

Chemical compounds are being generated using various metals from the periodic chart through progressive organometallic chemistry. However, there has been a delay in application studies related to biological or drug discovery research using these chemical compounds. Thus, we have been evaluating the efficacy of organozinc complexes and precursors of unknown function in various animal and cellular disease models.

These cellular model analyses have demonstrated that Zn(bpy)Cl₂ and Zn(4,7-di Me Phen)Cl₂ · ½ (H₂O) (hereafter referred to as Z.34 and Z.19, respectively) have little cell cytotoxicity and its inhibited fat cell differentiation from our group's original organometallic complex library. In addition, we have found that Z.34 promotes the activity of osteoblasts. Thus, Z.34 has the potential to promote osteogenesis and prevent obesity.

Here we evaluated the *in vivo* toxicity and osteogenic efficiency of Z.34 and Z.19 using an osteoporosis mouse model.

Materials & Methods

The *in vivo* toxicity test was performed on 5-week-old female ddY mice. Evaluation of toxicity involved analysis of the survival rate and biochemical blood tests for the functions of the kidney, liver and other organs following 3-per-week repeated administration. The osteogenic efficiency test was performed in 12-week-old female ddY mice. An osteoporosis mouse model was produced by removal of ovaries (OVX) and breeding with a continuous low-calcium diet (LowCa). Evaluation of osteogenic efficiency involved analysis of the thigh bone density using the X-ray imaging system IVIS®. The concentration of Z.34 and Z.19 was 3.8–15.2 mg Zn/kg. ZnSO₄ used in pharmaceutical products was employed for comparison.

Results & Discussion

Repeated administration of 15.2 mg Zn/kg Z.34 or Z.19 reduced the survival rate and increased the exacerbation of the biochemical blood marker. However, these toxic effects were not observed with repeated administration of 3.8 mg Zn/kg Z.34 or Z.19. Thus, using the concentration of 3.8 mg Zn/kg, we analysed the effect of Z.34 and Z.19 on the OVX-LowCa mouse model. We observed that the reduced thigh bone density of the OVX-LowCa model was improved by Z.34 but not by Z.19 and ZnSO₄. These results strongly supported our past *in vitro* data and demonstrated the *in vivo* efficiency of Z.34.

P-40*

Morphological Analysis of the Pancreas and Liver in Diabetic KK-A^y Mice Treated with Zinc or Oxovanadium Complexes

Takayasu MOROKI¹, Yutaka YOSHIKAWA^{1,2}, Katsuhiko YOSHIKAWA³, Airo TSUBURA³, and Hiroyuki YASUI¹

¹ Department of Analytical and Bioinorganic Chemistry, Kyoto Pharmaceutical University, Kyoto, 607-8414. ² Department of Health, Sports, and Nutrition, Kobe Women's University, Kobe, 650-0046. ³ Department of Pathology II, Kansai Medical University, Hirakata 573-1010.

Diabetes mellitus (DM), which will be the most significant disease in the 21st century, is generally classified into two types, insulin dependent type 1 DM and non-insulin dependent type 2 DM. The relationship between biometals, such as zinc, vanadium, copper, cobalt, and magnesium ions, and diabetes therapy has been recognized for several years. In particular, the antidiabetic activities of Zn²⁺ and VO²⁺ complexes have been measured by biochemical approaches, but we have not examined the morphological changes in organs. In this study, we checked the antidiabetic effect of bis(1-oxy-2-pyridine-thiolato)Zn²⁺ [Zn(opt)₂] and bis(1-oxy-2-pyridine-thiolato)VO²⁺ [VO(opt)₂] by biochemical analysis and morphological changes in the pancreas and liver after administration for 4 weeks. Additionally, zinc gluconate [Zn(glc)₂] and bis(ethylmaltolato)VO²⁺ [VO(ema)₂] were used as reference compounds. These complexes were orally administered to KK-A^y mice for 4 weeks. VO²⁺ and Zn²⁺ complexes were adjusted to maintain their doses of 0.38 to 3 mg (7 to 59 μmol) V kg⁻¹ body weight/day and 0.75 to 5 mg (11 to 76 μmol) Zn kg⁻¹ body weight/day, respectively. After administration, we examined the morphological and biochemical analysis. Pancreatic islet cell size were smaller, and there was a tendency towards a lower islet cell area ratio in Zn(opt)₂-treated mice compared with nontreated KK-A^y mice. Furthermore, plasma insulin concentrations were significantly reduced. These results suggest that Zn(opt)₂ administration provides morphological and biochemical improvements in hyperinsulinemia. In contrast, islet cell size and islet cell area ratio in received Zn(glc)₂ and VO²⁺ complexes groups did not differ from those in nontreated KK-A^y mice. Zn(opt)₂- and VO(opt)₂-treated mice exhibited significantly lower fat deposition and fat deposition area ratio in the liver compared to those observed in nontreated KK-A^y mice. The difference in morphological improvements of the pancreas and liver owing to Zn(opt)₂ or VO(opt)₂ treatment may be explained by the difference in the sites of actions of Zn²⁺ and VO²⁺ complexes on organs in KK-A^y mice.

In this presentation, we will show the morphological changes in pancreas and liver, using several figures and photographs, and discuss the importance of morphological analysis in the treatment of diabetic mellitus by metal complexes.

P-41*

Enhancement of the Bone Strength in STZ-Induced Diabetic Mice by Supplementation of the Zn²⁺ and First Transition Metal Ions with Anti-Saccharification Action Against the Collagen

Yoshiki NAOE¹, Kanako MICHIGAMI¹, Yutaka YOSHIKAWA^{1,2}, Naemi KAJIWARA², and Hiroyuki YASUI¹

¹ Department of Analytical and Bioinorganic Chemistry, Kyoto Pharmaceutical University, Kyoto, 607-8414. ² Department of Health, Sports, and Nutrition, Kobe Women's University, Kobe, 650-0046.

It has been reported that diabetic patients are at great risk of the bone fracture. Hyperglycemia is induced by the lack of insulin and then deterioration of the bone matrix based on the glycation is also derived from bone morphogenetic drop in the diabetes state. Approximately 50% of bone compositions consist of collagen as volume ratio, and the collagen is required as ingredient to keep the strength of the bone. In this study, we screened whether the Zn²⁺ and first transition metal ions (Ni²⁺, Cu²⁺, Fe²⁺, VO²⁺, and Mn²⁺) might exhibit the anti-saccharification activity against the collagen and act on bone metabolism abnormality in streptozotocin (STZ)-induced diabetic mice with the proposed mechanism.

The anti-saccharification activity was measured with Collagen Glycation Assay Kit, Glyceraldehyde (Cosmo Bio). Female ddy mice at 6 weeks of age were intraperitoneally injected by STZ (100 mg/kg BW), and the STZ-induced diabetic mice were orally given zinc sulfate (ZS) for 8 weeks (ZS administrated diabetic group; 30 mg Zn/kg BW, saline administrated diabetic or non-diabetic groups; 0 mg Zn/kg BW). The bone strength was measured with TK-252C (Muromachi Kikai Co, Ltd.). The alkaline phosphatase (ALP) activity and hydroxyproline level were assayed by the Walter Shutt and the Woessner methods, respectively. The serum osteocalcin (OC) level and urinary type 1 collagen cross-linked N-telopeptide were measured by the ELISA method and OSTEOMARK[®] (Alere medical), respectively. The Ca, P, Mg, and Zn concentrations in bone were determined with ICP-MS.

The *in vitro* results showed that Cu²⁺, VO²⁺, and Zn²⁺ exhibited significantly the anti-saccharification activity against the collagen. Since Zn²⁺ is the safest among these metal elements, we selected Zn²⁺ in *in vivo* experiments. From the *in vivo* results, the bone strength was found to weaken in the STZ diabetic group. The ALP activity and element concentrations in bone decreased, while serum OC level increased in the diabetic group. On the other hand, the bone metabolism significantly increased in the ZS administrated diabetic group, suggesting that Zn²⁺-administration enhanced the bone strength in STZ-induced diabetic mice through the anti-saccharification action against the collagen.

P-42*

The Effects of Feeding Zinc-Deficient Diets on Rats Behavior and Its Relations with the Hematopoietic Function

Miho NAKAMURA¹, Satomi YOSHIOKA¹, Naemi KAJIWARA², Yutaka YOSHIKAWA^{1,2}, and Hiroyuki YASUI¹

¹ *Department of Analytical and Bioinorganic Chemistry, Kyoto Pharmaceutical University, Kyoto, 607-8414.* ² *Department of Health, Sports, and Nutrition, Kobe Women's University, Kobe, 650-0046.*

Zinc is the essential trace element of human and animals, and it is an important nutrient related to the action in organism including the adjustment of the metabolism and maintenance of the appetite. Therefore, it has been reported that various symptoms including anorexia and failure of growth appear when zinc is deficient. However, humans easily fall into zinc-deficiency because of not producing zinc in the body. Then we studied the influence caused by zinc-deficiency in rats. Furthermore, on the assumption that disorder may occur in the hematopoietic system, we investigated what kinds of relation to zinc-deficiency and hematopoietic system, because iron is known to accumulate in spleen by zinc-deficiency.

We divided male Wistar rats at 3 weeks of age into two groups. One is control group (Cont group, intake quantity of Zn: 25 µg/g), and the other is zinc-deficient diets group (ZD group, intake quantity of Zn: 0 µg/g). Both groups took zinc only from a water supply bottle freely and were orally given low zinc liquid diets to take the same calorie quantity and bred for 14 days, where Cont group was given zinc acetate water (Zn: 25 µg/g) and ZD group was given ultrapure water (Zn: 0 µg/g). After euthanasia, we collected the blood and measured the number of the white and red blood cells, and the platelets. In addition, we assayed the various clinical inspection values, using plasma and bone strength. Furthermore, we measured the changes of the reticulocyte, concentration of non-heme iron in the spleen, and indirect bilirubin as an anemia index.

From the results, all groups were given liquid feed of the same quantity by oral gavage, and body weights were maintained constantly in ZD group. The number of white blood cells showed a tendency to increase in ZD group, suggesting that zinc-deficiency caused inflammation. As for the clinical inspection values, the concentrations of the amylase, albumin and alkaline phosphatase showed a tendency to decrease in ZD group, while that of the triglycerides tended to increase. The bone strength of the thighbone was found to be harder in ZD group. Additionally, we will present the results and consideration for the ratio of reticulocyte to normal red blood cells, indirect bilirubin and non-heme iron concentrations in our presentation.